This manuscript is a non-peer-reviewed preprint submitted to EarthArXiv. It has been submitted to Environmental Science & Technology for peer review.

Constructing Prospective Multiregional Input–Output Tables via Scenario-Constrained Optimization for Future Environmental Footprint Assessment

Sidi Peng,[*,†] Vassilis Daioglou,[‡] Konstantin Stadler,[¶] Ramin Roshandel,[§] Martin Bruckner,[‖] and Stephan Pfister[†]

†*Institute of Environmental Engineering, ETH Zürich*

‡*Netherlands Environmental Assessment Agency*

¶*Norwegian University of Science and Technology*

§*Sharif University of Technology*

‖*Vienna University of Economics and Business*

E-mail: sipeng@ethz.ch

Abstract

Prospective multi-regional input–output (MRIO) tables that integrate scenarios from integrated assessment models (IAMs) support forward-looking environmental footprint analysis, but the trade-off between historical structural fidelity and scenario compliance has not been quantified. We constructed 12 prospective MRIO tables from the EXIOBASE 2019 and IMAGE SSP2 scenario for 2035, including a Leontief-based projection and 11 optimization-based projections under different combinations of scenario

constraints on GDP, value added, sector outputs, as well as energy and agriculture consumption. Among the constraints, those on energy and agriculture consumption were satisfied at the highest cost in coefficient deviations from the Leontief-based projection and shifted the corresponding transaction flows most significantly. Regional shares of the global carbon footprint remained stable, but sectoral attribution within each region was substantially reshuffled, and the identification of high-growth consumption hotspots was sensitive to scenario compliance level. Some hotspots persisted at all levels of compliance. The consumption-based carbon footprint driven by China's final energy demand grew the fastest and emerged as a major new hotspot in 2035. The footprint of Livestock-consumption showed persistent high growth in multiple regions and India and the Rest of Asia rose in environmental significance through their industrial sectors.

Keywords

EXIOBASE; IMAGE; integrated assessment model; consumption-based footprint; scenario compliance; structural fidelity; environmental hotspots

Introduction

Today, the global environmental crisis is deeply interconnected with the structure of the world economy, because production and consumption are distributed across international borders and linked through global supply chains that propagate environmental burdens from distant production sites to distant consumers[1,2]. This teleconnected perspective is essential for sustainability governance in a highly globalized economy[3–5]. Multi-regional input–output tables (MRIO table) serve as the main accounting framework to quantify the environmental burdens embodied in international trade, as they trace flows across countries and sectors to link production-based resource use and emissions to final consumption worldwide[1,2,6]. However, standard MRIO tables offer static and historical snapshots of economic structure, which constrains the prospective analysis needed to evaluate long-term climate policy and sustainability transitions that unfold over decades[7,8]. As a consequence, the literature increasingly advocates the integration of MRIO tables with scenario analysis to explore future trajectories and transition pathways[9–12].

To project environmental footprints under different socioeconomic futures, researchers must introduce scenario changes to MRIO tables either endogenously or exogenously. Although endogenous approaches exist, such as the dynamic MRIO table simulation model GINFORS (global inter-industry forecasting system)[13,14], they rely on aggregate econometric relationships calibrated to historical data. As such, they lack the technology-rich and bottom-up physical representation of specific energy and industrial transformation pathways found in IEA (International Energy Agency) Energy Technology Perspectives[15] or integrated assessment models (IAMs)[16], which constitutes a policy-relevant knowledge base for international climate governance. Consequently, most forward-looking MRIO studies adopt exogenous approaches.

Since these technology-rich scenario models typically lack the full cross-sectoral economic granularity of an MRIO table, this creates a fundamental reconciliation problem that has been addressed in two divergent approaches by previous studies. In the first approach, re-

searchers adapt energy-related coefficient matrices and final demands based on exogenous scenario data, while leaving the broader regional industry mix and outputs to be projected via a standard Leontief demand model[10,17,18]. This method prioritizes the structural fidelity of the MRIO table, but risks inconsistency with the scenario regarding macroeconomic variables (GDP, value added, sector outputs), transaction flows such as energy consumption, and ultimately emissions and resource consumption. In the second approach, researchers adapt transaction flows directly to align with predefined scenarios and iteratively scale tables using balancing techniques to ensure that the remaining flows satisfy exogenous macroeconomic constraints under minimal structural changes[19–21]. This approach prioritizes scenario compliance and treats residual changes as indirect effects of exogenously specified changes, but it risks significant coefficient deviations, and thus may produce unrealistic inter-industry relationships.

These two divergent prioritizations, being normative choices, highlight a fundamental methodological tension in prospective environmental analysis. This study systematically examines the trade-off between scenario compliance and structural fidelity by investigating how sensitive prospective MRIO tables are to the progressively expanded enforcement of scenario data. Although previous research has often focused on a narrow set of drivers, such as energy system parameters[17,18] or lifestyle changes[22], we expand the scope of exogenous data coverage from basic macroeconomic variables and energy to include crop production, price fluctuations, and trade dynamics, allowing for a more comprehensive assessment of the trade-offs inherent in the reconciliation process. In general, our goal is to provide a detailed understanding of how different reconciliation strategies influence projected global supply chains and environmental footprints.

Materials and Methods

To evaluate the trade-off between scenario compliance and structural fidelity in the reconciliation process, we integrated scenario information into a historical MRIO table progressively in three stages (see Figure S1). We utilized EXIOBASE version 3.8.2 in 2019[23] as a historical baseline and scenario outputs for the year 2035 of the Integrated Model to Assess the Global Environment (IMAGE)[24] under the Shared Socioeconomic Pathway 2 (SSP2) as a prospective reference. The final prospective MRIO tables were expressed in billions of 2010 USD (10^9 \$2010).

After data harmonization and pre-processing, the integration process began by incorporating future energy and crop coefficients or structure derived from IMAGE into the coefficient matrices of the historical multi-regional supply and use tables (multi-regional SUT). With an updated Leontief inverse and a scaled final demand, a prospective MRIO table was projected. This corresponds to the first reconciliation approach, where the economy is scaled up with the inter-region-sector relations captured by the Leontief inverse, but only structural changes are integrated. We refer to this as the Leontief-based projection.

Gaps exist between the Leontief-based projection and the IMAGE scenario outputs, due to the baseline data discrepancies between EXIOBASE and IMAGE, fundamental differences in modeling logic between the Leontief inverse and IMAGE, and underlying scenario assumptions that are not endogenously captured by a static IO structure. For example, the Leontief-based projection could not endogenously capture the implicit relations between heavy industry production and GDP per capita in IMAGE[25].

Closing these gaps requires non-uniform relative changes on the existing flows, and thus inherently necessitates coefficient deviations from the Leontief-based projection, because preserving the original economic structure only allows for uniform scaling of the economy. To analyze this tension, we developed an optimization framework that enforced the constraints of the IMAGE scenario on the Leontief-based projection, applied both independently and cumulatively. The optimization preserved the remaining economic structure as much as

possible through coefficient deviation minimization, since no further scenario information was available to constrain it directly. We refer to the resulting MRIO tables as optimization-based projections. The enforced constraints included macroeconomic parameters (i.e. GDP and Value Added for agriculture, industry, and service sector), sector outputs for heavy industries and transport, energy outputs, energy consumption, agriculture outputs, and agriculture consumption. Enforcing these constraints independently allowed isolating their individual roles before considering cumulative implementations. This process generated two series of prospective MRIO tables, i.e., one complied with individual scenario constraints and a second representing progressively higher levels of scenario compliance.

We evaluated the structural fidelity of the optimization-based projections by quantifying their coefficient deviations from the Leontief-based projection, revealing which constraints require the largest adaptation of the economic structure. Lastly, we assessed the sensitivity of macroeconomic variables, sector outputs, agriculture and energy flows, and carbon footprints to the level of scenario compliance.

The following sections summarize the methodology, with full details provided in SI1.

Data Harmonization and Pre-processing

We first defined the resolution of the prospective MRIO table by reconciling the region, product, and sector classifications of EXIOBASE with IMAGE scenario outputs. The reconciled resolution encompasses 20 regions, 72 products, and 70 sectors, with the corresponding concordances provided in SI2. To create a consistent starting point, we aggregated the multi-regional SUT in 2019 to this unified resolution (see Section S1.2.2).

The IMAGE scenario data were preprocessed into monetized variables aligned with the MRIO table structure (see Section S1.2.3). We first derived physical use tables for crops, livestock, and energy products based on regional demand and bilateral or net trade data in IMAGE. We then monetized these physical tables using IMAGE-based producer prices to ensure consistency with EXIOBASE transaction flows, yielding energy consumption, energy

output, agriculture consumption, and agriculture output in monetary unit. Finally, we monetized the sector outputs of heavy industries and transports by assuming constant historical prices. Once monetized, these data were aggregated to the defined resolution.

Leontief-based Projection Framework

We implemented structural changes to the multi-regional SUT in 2019 and utilized the Leontief quantity model to project a future economy. To distinguish the resulting matrices from the historical matrices, we denote them with a superscript ($'$).

First, we modified the supply share matrix D to D' by enforcing a one-to-one correspondence between each scenario-relevant product and its primary producing sector, i.e., setting the corresponding supply share to one and all secondary supply shares to zero. This follows the logic of the transfer method for treating secondary production[26]. For example, we mapped the ruminant livestock farming sector exclusively to the ruminant livestock product, even though the original EXIOBASE data record this sector as also co-producing minor amounts of other products. This simplification ensures consistency with the IMAGE outputs, where such co-production is not represented. We did not systematically re-derive the use coefficient matrix under the same assumption. However, the IMAGE outputs used to modify the intermediate coefficient matrices are themselves consistent with this transfer method. For example, in IMAGE the feed crops to livestock production and the N_2O and CH_4 emissions from the sector, are attributed entirely to the livestock product.

We also introduced new sectors and products modeled by IMAGE but not individually represented in the original multi-regional SUT, including hydrogen, electricity from hydrogen, and relevant categories for biofuels. We assigned diagonal entries of 1 in D' for these new sectors and selected proxy sectors for their input structure in B (see Table S5 for proxy sectors).

We further modified the use coefficient matrix B to B' by incorporating the energy and crop coefficients and structure derived from the monetized IMAGE tables. For sectors where

both specific inputs and total sector outputs are available, we calculated and applied coefficients directly, which was the case for energy coefficients in energy sectors, heavy industries, and transport. For sectors whose inputs are reported only for an aggregated purpose or whose sector output is missing (see Table S7), we instead integrated the consumption structure—the relative ratios among region-product suppliers for that purpose.

When integrating new coefficients, we ensured each column sum of intermediate and value-added coefficients (B' and L') remained equal to one through proportional scaling (Eq.1). Where the sum of the integrated coefficients exceeded one, the value-added coefficient was computed as the residual needed to satisfy the column-sum constraint, yielding a negative value that represents a production subsidy. For structural ratios, we assumed energy products are globally substitutable across all consumers. Agriculture products are substitutable for food and feed but not for other purposes, mainly food processing (e.g., rice and livestock processing). For these sectors, we preserved the product structure and integrated only each product's trade structure.

Finally, we updated the final demand matrix Y to Y' using IMAGE scenario data. We assumed that the variation in the region-product final supply follows the variation in the value added of the corresponding broad sector (agriculture, industry, and service), with the mapping provided in SI2. This approach captures shifting consumption patterns, such as the rising share of services in final demand as economies develop. Monetary residential energy demand was also incorporated into Y'.

With the modified matrices B', D', and Y', intermediate coefficient matrix A' and final demand matrix F' were calculated (Eq.2, 3). Sector output g' was then projected via the Leontief inverse (Eq.4). With the new g', we derived the intermediate matrix Z' and the value added matrix V' based on Eq.5.

$$\sum_i B'_{i,j} + L'_j = 1 \tag{1}$$

$$A' = D'B' \tag{2}$$

$$F' = D'Y' \tag{3}$$

$$g' = (I - A')^{-1}F'\mathbf{1} \tag{4}$$

$$Z' = A'\hat{g}', \quad V' = L'\hat{g}' \tag{5}$$

Where:

- D' is the modified supply share matrix (region-sector by region-product).
- B' is the modified use coefficient matrix (region-product by region-sector), with i denoting region-product and j denoting region-sector.
- L' is the modified value added coefficient matrix (value added by region-sector).
- A' is the projected intermediate coefficient matrix (region-sector by region-sector).
- Y' is the modified final use matrix (region-product by region).
- F' is the projected final demand matrix (region-sector by region).
- I is the identity matrix.
- $\mathbf{1}$ is a summation vector of ones that sums F' across the final demand regions.
- g' is the vector of projected region-sector output.
- $\hat{g}'$ represents the diagonalized vector of projected region-sector output.
- Z' is the projected intermediate matrix (region-sector by region-sector).
- V' is the projected value added matrix (value added by region-sector).

Enforcing Scenario Values via Optimization

To achieve higher levels of scenario compliance, we extended the enforcement of scenario data beyond the structural level to the scenario values themselves. We imposed six scenario

constraints on the Leontief-based projection both independently and cumulatively, using optimization to minimize deviations in the intermediate coefficients, A', value-added coefficients L' and expenditure share E' (Eq.6). This approach generated two series of prospective MRIO tables.

$$E'_{j,k} = \frac{F'_{j,k}}{\sum_j F'_{j,k}} \tag{6}$$

Where:

- $E'_{j,k}$ is the entry of the expenditure share matrix E' for region-industry j and final demand region k.
- $F'_{j,k}$ is the entry in the projected final demand matrix F'.
- The denominator $\sum_j F'_{j,k}$ represents the total final demand for region k across all region-industry j.

Technically, we defined scaling factors $m^{Z'}$, $m^{V'}$, and $m^{F'}$ on Z', V', and F' as decision variables in the optimization. The initial values were 1. The standard bounds for these scaling factors were set between 4.6×10^{-4} and 8.8×10^{3}, corresponding to the minimum and maximum ratios between the scenario constraints and the Leontief-based projection. When all constraints were enforced simultaneously, the standard bounds caused numerical difficulties. As a practical adjustment for the agriculture consumption scaling factors, we estimated initial scaling factors from the ratios between the agriculture consumption constraints and the Leontief-based projection, and set bounds as factors of 10^{-4} to 10^{4} around these estimates. Sensitivity tests across factor widths from 10^{2} and 10^{4} yielded the same optimum, indicating that the reported solution is stable within this range. Scaling factors for residential energy demand within F' were fixed at 1, ensuring that this robust scenario input remained unchanged during optimization and preventing the solver from over-adapting F' to satisfy other constraints. Scaling factors for all zero flows were set to zero.

Scenario and balance constraints were enforced by Eq.S18-S28. MRIO table balance was always imposed as a constraint, regardless of whether scenario constraints were enforced independently or cumulatively (see Table 1).

Table 1: Summary of individual and cumulative scenario constraint implementations and their corresponding abbreviations.

Level	Setting of Scenario Constraints	Abbreviations
Individual	IO balance, GDP, Value Added	KpBlGdpVa
	IO balance, Sector Outputs (Heavy Ind. & Trans.)	KpBlSeouit
	IO balance, Energy Output	KpBlSeoue
	IO balance, Energy Consumption	KpBlEnergy
	IO balance, Agriculture Output	KpBlSeouc
	IO balance, Agriculture Consumption	KpBlCrop
Cumulative	IO balance, GDP, Value Added	KpBlGdpVa
	+ Sector Outputs (Heavy Ind&Trans.)	KpBlGdpVaSeouit
	+ Energy Output	KpBlGdpVaSeouitSeoue
	+ Energy Consumption	KpBlGdpVaSeouitSeoueEnergy
	+ Agriculture Output	KpBlGdpVaSeouitSeoueEnergySeouc
	+ Agriculture Consumption	KpBlGdpVaSeouitSeoueEnergySeoucCrop

The optimization problem was formulated as a Quadratically Constrained Program (QCP) under constraints listed in Table 1. The objective function minimizes the sum of squared deviations of non-zero scaling factors from their column mean (Eq.7). This formulation follows the principle that if all scaling factors within a column are identical, A', L', and E' are perfectly preserved. Conceptually, the setting allows for uniform scaling of the matrices and conceptually minimizes structural distortion (coefficient deviations). Each matrix is normalized by its number of non-zero scaling factors so that all three are weighted equally by the solver. Squared deviations for flows exceeding 10^6 \$2010 in Z', V', and F' were assigned a weight of 100 to penalize distortion of larger coefficients.

$$\text{Objective} = \min \left[\frac{1}{N^{Z'}_{\text{non-0}}} \sum_{j_1,j_2} w_{(j_1,j_2)} \left(m^{Z'}_{(j_1,j_2)} - \overline{m}^{Z'\&V'}_{j_2} \right)^2 + \frac{1}{N^{V'}_{\text{non-0}}} \sum_{j_2} w_{(1,j_2)} \left(m^{V'}_{(1,j_2)} - \overline{m}^{Z'\&V'}_{j_2} \right)^2 + \frac{1}{N^{F'}_{\text{non-0}}} \sum_{j_1,k} w_{(j_1,k)} \left(m^{F'}_{(j_1,k)} - \overline{m}^{F'}_{k} \right)^2 \right] \tag{7}$$

Where:

- $m^{Z'}_{(j_1,j_2)}$, $m^{V'}_{(i=1,j_2)}$, and $m^{F'}_{(j_1,k)}$ represent the scaling factors for Z', V' , and F', respectively.
- j_1 and j_2 denote the region-sector indices for rows and columns, while k denotes the region index for final demand.
- $\overline{m}^{Z'V'}_{j_2}$ denotes the mean value of the non-zero scaling factors within column j_2 for both Z' and V'.
- $\overline{m}^{F'}_{k}$ represents the mean value of the non-zero scaling factors within column k for F'.
- w is a weighting factor equal to 100 for transaction flows $> 1 \times 10^6$ \$2010 and 0 otherwise.
- $N_{non\text{-}0}$ indicates the total number of non-zero flow elements in the respective prospective matrices, used to provide equal weighting to Z', V', and F'.

We implemented the optimization using the GAMSpy package in Python with the CPLEX solver to reach the global optimum. To distinguish the new prospective MRIO tables from the Leontief-based projection, we denote them with a double-prime superscript ($''$). Applying the optimal scaling factors yielded the final matrices Z'', V'', and F'' (Eq.8). From these reconstructed flows, we derived g'', A'', and L'' (Eq.9, 10), and E'' following Eq.6.

$$Z''_{j_1,j_2} = m^{Z}_{j_1,j_2} \cdot Z'_{j_1,j_2}, \quad V''_{1,j_2} = m^{V}_{1,j_2} \cdot V'_{1,j_2}, \quad F''_{j_1,k} = m^{F}_{j_1,k} \cdot F'_{j_1,k} \tag{8}$$

$$g''_{j_2} = \sum_{j_1} Z''_{j_1,j_2} + V''_{1,j_2} \tag{9}$$

$$A''_{j_1,j_2} = \frac{Z''_{j_1,j_2}}{g''_{j_2}}, \quad L''_{1,j_2} = \frac{V''_{1,j_2}}{g''_{j_2}} \tag{10}$$

Where:

- Z'', V'', and F'' represent the resulting prospective intermediate, value-added, and final demand matrices, respectively, based on the optimal scaling factors.
- g'' is the vector of final prospective industry output.
- A'' and L'' are the final prospective intermediate and value-added coefficient matrices.
- j_1 and j_2 denote the region-sector indices for rows and columns, while k denotes the region index for final demand.

Measurement of structural fidelity and scenario compliance

To quantify trade-offs among different prospective MRIO and assess the effect of the various scenario constraints, we measured the structural fidelity and scenario compliance of the optimization-based MRIO tables against the Leontief-based projection as a benchmark.

We measured structural fidelity using the relative deviations of the non-zero coefficients (hereafter, coefficient deviations) of the four sector groups (as suppliers) in A'' and E'', and of the non-zero coefficients in L'', from their counterparts in A', L' and E' (Eq.11). The sector groups were heavy industry and transport, energy, and agriculture, each separately targeted by scenario constraints, together with a residual "other" group comprising the remaining sectors. Larger coefficient deviations correspond to lower structural fidelity. We measured

scenario compliance using the relative deviations of a prospective MRIO table from the scenario constraints (hereafter, scenario deviations) (Eq.11). The larger scenario deviations correspond to lower scenario compliance. These deviations were summarized into empirical cumulative distribution functions (ECDFs) as a statistical basis for the following synthesized indicators.

$$d = \frac{x - x^{\mathrm{ref}}}{x^{\mathrm{ref}}} \tag{11}$$

where x is the value being evaluated and x^{ref} is its reference. For structural fidelity, x is an optimization-based coefficient and x^{ref} is the corresponding Leontief-based coefficient. For scenario compliance, x is a projected value, and x^{ref} is the IMAGE scenario constraint.

To synthesize the distributions of coefficient deviations into a single value representing the structural fidelity of a prospective MRIO table, we summed the absolute values of the coefficient deviations within each sector group, normalized each sum by the total number of non-zero coefficients across all matrices (Eq.12), and then summed the resulting normalized values across the four groups into a single indicator C_{struct} (Eq.13). Absolute values were used to prevent positive and negative deviations from canceling in the overall measure. A sector group thus contributes more to the final sum when its coefficient deviations are larger and when it contains more coefficients, so that the final sum reflects the overall state of the entire MRIO table.

$$C_{\mathrm{struct},\,g} = \frac{1}{N_{\mathrm{tot}}} \left(\sum_{j_1 \in g} \left[\sum_{j_2} \left| \frac{a''_{j_1,j_2} - a'_{j_1,j_2}}{a'_{j_1,j_2}} \right| + \sum_{k} \left| \frac{e''_{j_1,k} - e'_{j_1,k}}{e'_{j_1,k}} \right| \right] + \sum_{j_2} \left| \frac{l''_{j_2} - l'_{j_2}}{l'_{j_2}} \right| \right) \tag{12}$$

$$C_{\mathrm{struct}} = \sum_{g \in \mathcal{G}} C_{\mathrm{struct},\,g} \tag{13}$$

where:

- $C_{\text{struct},\,g}$ is the normalized total coefficient deviation per group g.
- C_{struct} is the single indicator for coefficient deviations and structural fidelity.
- $\mathcal{G}$ denotes the four supplier sector groups: heavy industry and transport, energy, agriculture, and other.
- a''_{j_1,j_2} and a'_{j_1,j_2} are the non-zero intermediate coefficients (A) supplied by sector j_1 in group g to consumer j_2, in the optimization-based and Leontief-based projections, respectively.
- $e''_{j_1,k}$ and $e'_{j_1,k}$ are the non-zero expenditure-share coefficients (E) supplied by sector j_1 in group g to final-demand region k, in the optimization-based and Leontief-based projections, respectively.
- l''_{j_2} and l'_{j_2} are the non-zero value-added coefficients (L) in the optimization-based and Leontief-based projections, respectively.
- j_1 and j_2 denote the region-sector indices for rows and columns in the MRIO matrix; k is the region index for final demand.
- N_{tot} is the total number of non-zero coefficients across A'', E'', and L''.

To synthesize the distributions of scenario deviations into a single value representing the scenario compliance of a prospective MRIO table, we averaged the absolute values of relative deviations within each scenario constraint (Eq.14) and summed these per-constraint averages into a single indicator C_{scen} (Eq.15). Instead of normalization as for C_{struct}, summing per-constraint averages treats all constraints equally and keeps every constraint explicit in the total. This prevents constraints with many cells like agriculture and energy consumption conceal constraints with few elements such as GDP&VA. To limit the noise of negligible flows, we excluded monetary values below 1×10^6 \$2010 when computing the relative deviations.

$$C_{\text{scen},\,t} = \left(\frac{1}{N_t} \sum_{(p,q)\in t} \left| \frac{x_{p,q} - x^{\text{scen}}_{p,q}}{x^{\text{scen}}_{p,q}} \right| \right) \tag{14}$$

$$C_{\text{scen}} = \sum_{t=1}^{6} C_{\text{scen},\,t} \tag{15}$$

where:

- $C_{\text{scen},\,t}$ is the remaining deviations from scenario constraint t.
- C_{scen} is the single indicator for remaining scenario deviations and scenario compliance.
- t indexes the six scenario constraints: GDP&VA, sector output of heavy industry and transport, energy output, energy consumption, agriculture output, and agriculture consumption.
- $x_{p,q}$ is a projected value (Leontief-based $x'_{p,q}$ or optimization-based $x''_{p,q}$) and $x^{\text{scen}}_{p,q}$ is the corresponding unimplemented IMAGE scenario constraint. For GDP, $x_{p,q}$ is the GDP of region q; for value added, the value added of sector p in region q; for sector output, the total output of sector p in region q; for consumption flows, the transaction from supplier p to consumer q (both region-sectors).
- N_t is the number of non-zero elements within constraint t.

The Leontief-based projection without any scenario constraint carries the largest scenario deviations, and therefore has the lowest scenario compliance. Each optimization starts from this projection and eliminates a subset of these deviations, determined by the constraints implemented in that run. Scenario deviations tied to the unimplemented constraints remain. A fully scenario-compliant table eliminates all deviations and thus attains the highest compliance, whereas partially constrained tables fall in between. In cumulative implementation, the scenario deviations eliminated at each step are the combined scenario deviations that the corresponding constraints would eliminate individually. As discussed earlier, these devi-

ations being eliminated under different constraint settings are the direct drivers of coefficient deviations. Therefore, we also summarized them in ECDFs.

Sensitivity of global supply chains and environmental footprints

Following this technical evaluation of the trade-off, we assessed the practical implications for global supply chains and environmental footprints under increasing levels of scenario compliance.

We evaluated the sensitivity of global supply chains by examining changes in regional GDP&VA, sector outputs, energy and agriculture consumption flows and the corresponding coefficients across the prospective MRIO tables under cumulative scenario constraints. Relative changes were computed against the Leontief-based projection following Eq.11, revealing how each economic variable responds to increasing levels of scenario compliance. We also calculated relative changes from the 2019 EXIOBASE table to the Leontief-based projection, illustrating the projected shift from 2019 to 2035. Results were aggregated into nine regions (the eight largest economies by GDP in 2019 plus a combined category for the remaining regions) and into ten sector groups that preserve the major energy and crop consumers, with energy and consumption flows and coefficients aggregated from the consumer perspective. Concordances can be found in SI2.

We evaluated environmental sensitivity through the consumption-based carbon footprint, expressed in Mt CO_2-eq (GWP_{100}). The top three contributors to global greenhouse gas emissions, CO_2, CH_4, and N_2O[27], were obtained from the IMAGE scenario data by sector and region for 2020 and 2035, mapped to the resolution of the prospective MRIO tables (concordances in SI2), and characterized with the GWP_{100} factors[28].

For each regional sector, we calculated the gas-specific production-based impact intensities by dividing the sectoral impact in 2020 and 2035 by the sector outputs in 2019 EXIOBASE and the prospective MRIO tables, respectively. The sum of gas-specific GWP intensities was the total carbon intensity. Intensities therefore varied across prospective

MRIO table versions due to differences in sector outputs, while the total impact and emissions for 2035 were preserved. Where sectoral impacts were reported at a coarser resolution than the MRIO table, such as N_2O from total industry, we assumed uniform intensity across the corresponding MRIO subsectors, since these emissions were small relative to the primary emission categories.

Regional consumption-based footprints were then computed for 2019 EXIOBASE, the Leontief-based projection, and the optimization-based projections under cumulative scenario constraints (Eq. 16). Using the Leontief-based projection and the prospective MRIO fully compliant with IMAGE as representative cases, we decomposed their regional footprints by final-supply sector and final-demand region to assess the environmental sensitivity at sector-region level (Eq. 17). To trace the link between consumption activities and climate impacts, we also computed consumption-based footprints of energy and agriculture products, and disaggregated carbon footprints into CO_2 contributions and $N_2O\&CH_4$ contributions. Residential emissions were unconsidered, so as the energy in final demand. All footprint results were aggregated into nine regions and ten sector groups, as previously.

Lastly, we identified robust environmental hot spots in 2035 by averaging the rank of each sector-region consumption-based footprint across all scenario compliance levels under cumulative cases. Sectors and regions that ranked consistently high were treated as the most robust drivers.

$$GWP_d = g^\top (I - A)^{-1} f^{(d)} \tag{16}$$

$$GWP_{sd} = g^\top (I - A)^{-1} \widehat{f^{(d)}} e^{(s)} \tag{17}$$

Where:

- A is the intermediate coefficient matrix (region-sector by region-sector).
- I is the identity matrix.

- $f^{(d)}$ is the final demand vector for region d in final demand matrix F, and $\widehat{f^{(d)}}$ is its diagonalized form.

- g is the vector of impact intensities, which can be about total GWP, GWP from CO_2, or GWP from $N_2O\&CH_4$.

- $e^{(s)}$ is a column vector of zeros with a value of one at the position corresponding to the final supply sector s.

- GWP_d and GWP_{sd} represent total and sectoral consumption-based carbon footprints for final demand region d and final supply sector s.

Results and Discussions

This study generated 12 different versions of prospective MRIO tables, including the Leontief-based projection and 11 optimization-based projections under 6 individual scenario constraints and 5 cumulative implementations, with optimal objective values shown in the Table S10.

Trade-off between structural fidelity and scenario compliance

The dispersion of the coefficient deviation ECDFs in the optimization-based projections increases as the scenario constraints are cumulatively enforced (Figure S3), reflecting both a higher magnitude of the deviations and a higher frequency of significant deviations. This indicates that structural fidelity decreases as scenario compliance increases, quantifying the trade-off between the two. In particular, adding the energy and crop consumption constraints induces the largest marginal increase in deviations.

Under individual scenario constraints, the more variable the scenario deviations that the optimization eliminates (i.e., the greater the ECDF dispersion in Figure 1a), the greater the resulting coefficient deviations (C_{struct} on x-axis in Figure 1c), except for GDP&VA. This indicates that the variability of the eliminated scenario deviations is the dominant driver of coefficient deviations, with the number of directly constrained cells playing a secondary role. For example, the energy consumption constraint directly constrains more cells than the agriculture consumption constraint (see the TableS1), but the latter causes larger coefficient deviations because the scenario deviations it eliminates are more variable. Conversely, enforcing sector outputs eliminates more variable scenario deviations than GDP&VA, yet the latter causes larger coefficient deviations because it constrains more cells directly, leaving fewer available for flexible adjustment for coefficient deviation minimization. Overall, eliminating scenario deviations of higher variability and magnitudes (e.g., agriculture output, energy consumption, agriculture consumption) incurs larger coefficient deviations as

structural cost (C_{struct} on x-axis in Figure 1c), but leaves the remaining scenario deviations smaller and less variable, yielding higher scenario compliance (y-axis in Figure 1c). This relation is not strictly monotonic, due to the inherently different properties of the individual scenario constraints across macroeconomic, sectoral, and flow levels.

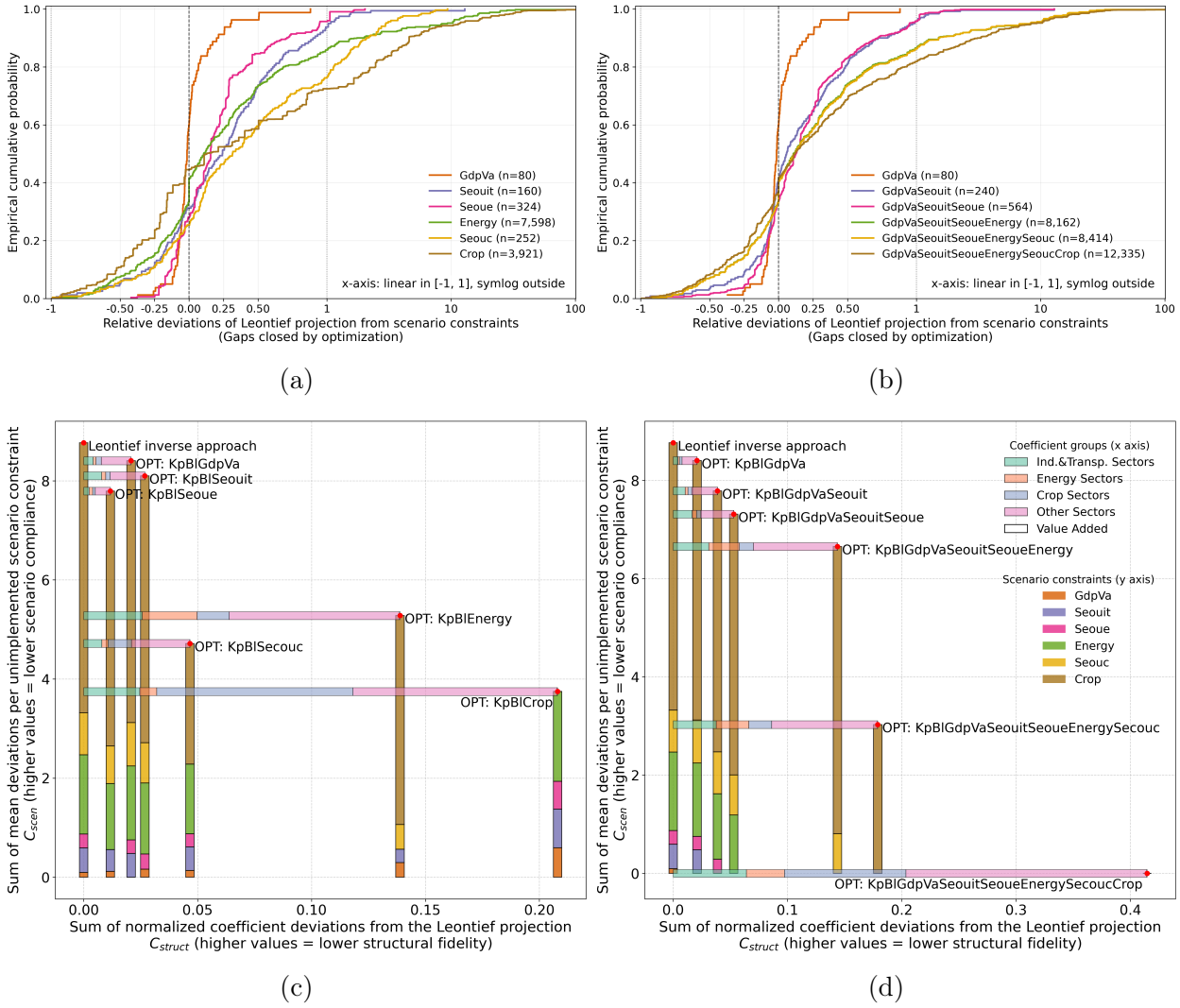

Figure 1: Panels (a) and (b) show the ECDFs of relative deviations between the Leontief-based projection and implemented scenario constraints under individual and cumulative cases, respectively, illustrating the scenario deviations eliminated by optimizations. Panels (c) and (d) sharing the legends summarize the structural fidelity (C_{struct} in Eq.13 based on coefficient deviations) and scenario compliance (C_{scen} in Eq.15 based on scenario deviations) of the Leontief-based projection and of the optimization-based projections, under individual scenario constraints in (c) and cumulative scenario constraints in (d).

Under cumulative scenario constraints, the coefficient deviations (x-axis in Figure 1d)

do not correspond to the overall variability of eliminated scenario deviations (Figure 1b), which can stabilize or even decrease at a given stage depending on the relative variability of the newly eliminated deviations compared to the previous stage. Instead, each newly added constraint increases the number of constrained cells or the number of constraints imposed on each cell, further restricting the solution space and forcing the solver to satisfy preexisting and new constraints simultaneously. Consequently, coefficient deviations increase and structural fidelity decreases monotonically, while the remaining scenario deviations decrease and scenario compliance increases monotonically (y-axis in Figure 1d). The cumulative coefficient deviations are not the linear sum of those induced by individual constraints, since the scenario constraints are not fully independent and the MRIO table is adjusted as a whole to preserve balance. Nevertheless, constraints that individually induced larger deviations also contribute larger marginal deviations in cumulative cases, as observed for energy consumption and agriculture consumption (x-axis in Figure 1c and x-axis in Figure 1d).

In summary, the trade-off between structural fidelity and scenario compliance is evident in both individual and cumulative cases, though the underlying mechanisms differ. Under individual constraints, coefficient deviations are governed primarily by the variability of the eliminated scenario deviations. Under cumulative constraints, they accumulate through the growing number of constrained cells and the layering of multiple constraints on the same cells and therefore increase monotonically (Figure 1d), even when the variability of the eliminated scenario deviations decreases (Figure 1b). However, the two regimes are linked. Scenario constraints that induce larger coefficient deviations individually also contribute larger marginal deviations when added cumulatively. These factors can be assessed in advance to anticipate the resulting coefficient deviations in similar integration tasks, which is particularly useful when computational resources are limited.

In our case, the energy and agriculture consumption constraints eliminate the most variable scenario deviations, which induces the largest total and marginal deviations in the individual and cumulative cases, respectively, concentrated in energy and agriculture coef-

ficients (Figure S2, S3). However, under all constraint settings except the individual crop consumption constraint, coefficients from other sectors contribute the most to total deviations (x-axis in Figures 1c and 1d), due to their larger share in the MRIO table compared to the industry, energy and agriculture sectors (see the number of coefficients within each group in Figure S3).

Sensitivity of economic variables to increasing scenario compliance

From the 2019 EXIOBASE table to the 2035 Leontief-based projection (Figure S4), GDP and VA grow least in the USA, Western Europe (WEU), and Japan (JAP) (below 40%), and most in India (IND), Rest of Asia (RAS), and Rest of Africa (RAF) (above 40%). Once the GDP&VA scenario constraints are enforced, regional GDP deviates from the Leontief projection by less than 10%, whereas VA deviates by up to 40%.

Sector outputs are more sensitive to increasing scenario compliance than GDP&VA (Figure S5). The largest deviations among directly constrained sectors occur for iron and steel in RAS and RAF, with outputs >150% higher than the Leontief benchmark. For all other directly constrained regional sectors, the deviations remain within ±50%. Sector outputs that are not directly constrained are adjusted flexibly to minimize coefficient deviations arising from constraints on other outputs and intermediate flows, and their relative changes can exceed 50%. For example, enforcing the energy consumption constraint in the USA increases food-processing energy use by 230% from the fourth optimization onward, so the solver raises food-processing output by 38%–93% to alleviate the energy coefficient deviations (Figures S6 and S7).

Energy and agriculture consumption flows and their coefficients show higher sensitivity than sector outputs and GDP&VA (Figures S6, S7, S8, S9). In addition to the 230% increase in energy use of food-processing in the USA noted above, enforcing the agriculture consumption constraint raises crop use by livestock production by 1327% in CHN. The response of these flows and their coefficients depends on whether IMAGE-derived coefficients have been

integrated into the Leontief-based projection (see Table S7).

For flows whose coefficients are already taken from IMAGE, including energy consumed by heavy industry, transport, and energy production, and agriculture inputs consumed by energy production (mainly crops for biofuels), the coefficients are largely preserved through the optimization. For the remaining flows, where only energy and agriculture input structure are integrated, the flows fluctuate and then deviate substantially once consumption constraints are enforced, which produces large deviations in the corresponding energy and agriculture coefficients. More details are discussed in Section S2.3.

This high sensitivity is consistent with the previous result that energy and agriculture consumption constraints introduce the largest and most variable scenario deviations eliminated by optimization. The scenario deviations correspond to the large deviations of consumption flows, and their variability results into the largest coefficient deviations, concentrated in energy and agriculture coefficients. Weighted by flow magnitude, the most significant shifts occur in energy consumption by energy production, commercial services, and other industry, and in crop consumption by food processing, residential use, commercial services, and livestock production, with various directions across regions, which can propagate to the environmental footprint outcomes.

Sensitivity of consumption-based carbon footprints to increasing scenario compliance

From 2019 to 2035, IMAGE projects a slight decline in the global carbon footprint, from 44,408 to 44,046 Mt CO_2-eq (-0.82%) (Figure S12). Based on the Leontief-based projection, the largest consumption-based carbon footprint increases occur in RAF (+48.6%), IND (+45.2%), and RAS (+27.6%), and the largest decreases occur in the USA (-26.6%), WEU (-21.4%), and JAP (-20.6%), in line with the relative differences in regional GDP growth (Figure S4). Under increasing scenario compliance, the global total is fixed by the method. Regional shares remain largely stable, with small increases for USA and ME and

corresponding decreases for WEU and JAP in the fully-compliant prospective MRIO (Figure S13). In absolute terms, USA and ME footprints rise by 14.3% and 13.5% above the Leontief level, while WEU and JAP fall by 12.7% and 11.0%.

To identify the drivers of these significant regional shifts and the hotspots within each region, we compared the consumption-based carbon footprint per final-supply-sector and final-demand-region pair (hereafter, sector-region pair) between the Leontief-based projection and the fully-compliant prospective MRIO. We decomposed the total carbon footprint of each pair into a CO_2 component, driven by the energy footprint, and an $N_2O\&CH_4$ component, driven by the agriculture footprint.

Each of these footprints comprises three contributions: direct consumption by the final-supply sector, indirect consumption embedded in its upstream supply chain, and final demand (Eq. S43; decomposed shares in SI3). The sensitivity of direct energy and agriculture consumption flows established in the previous section therefore propagates to each sector-region pair's footprint both directly and indirectly through the supply chain. However, the resulting footprint for a given pair can be dominated by any of these components.

For example, the substantial drop in direct energy use by crop production consumed in CHN (Figure S6) coexists with a sharp rise in its energy footprint (Figure 2a), since 87% of that footprint originates from indirect inputs. In another case, direct agriculture consumption for livestock production consumed by CHN (primarily feed crops) rises by 1327% under full compliance (Figure S8), yet the total agriculture footprint for the pair remains relatively stable (Figure S15a), because direct consumption contributes only 1% to the sector-region pair's footprint while final demand dominates (76%) and rises by just 7%.

Under full compliance, the global energy footprint declines (Figure 2a), as the energy output constraints lower total energy supply (Figure S5), and the global agriculture footprint similarly declines (Figure S15a). For energy, the largest reductions concentrate in commercial services across most regions, driven by both lower direct energy use and reduced upstream inputs. For agriculture, the largest reductions concentrate in food processing. Because the

global CO_2 total is fixed, sector-region pairs whose energy footprints fall most receive a smaller share of the CO_2 attribution under full compliance, while those whose energy footprints fall less or rise receive a larger share (Figure S14). $N_2O\&CH_4$ attribution redistributes analogously with the agriculture footprints (Figure S15b). Since CO_2 dominates the total carbon footprint (Figure 2b), its regional pattern largely mirrors the CO_2 reallocation, with $N_2O\&CH_4$ reinforcing or weakening the CO_2 pattern depending on the sector.

The USA and ME are the only regions whose total footprints rise under full compliance, with increases concentrated in a small set of final supply sectors. In the USA, the rising footprints occur for other industry, food processing, and livestock production — the same sectors where the energy consumption constraint raises direct energy use (Figure S6). For livestock production, the total carbon footprint increase exceeds the CO_2 contribution, with an additional contribution from $N_2O\&CH_4$ (Figure S15b) mainly driven by the increasing livestock consumed in final demand (see residential use in Figrue S8). In ME, the increase is led by transport, other industry, and energy production.

In WEU and JAP, the footprint decline is broadly distributed across final supply sectors — nearly all sectors in WEU, and primarily food processing and commercial services in JAP. In CHN, IND, RAS, RAF, and the "Other" region, the regional totals are stable but the internal attribution shifts. CHN's commercial services footprint falls sharply across all three indicators, while footprint of crop production rises sharply as discussed above. IND shows a contrasting pattern, with rising commercial services and falling livestock production. In RAS and RAF, the substantial growth in iron and steel outputs and their direct energy inputs (Figures S5 and S6) is embedded in the rising energy footprints of other industry, since indirect inputs account for 80% and 77% respectively of these footprints (SI3), while heavy industries themselves rarely appear in final demand.

In summary, the aggregate stability of regional footprint shares across prospective MRIO variants conceals substantial reshuffling of sectoral responsibility within regions, driven by the high sensitivity of energy and agriculture consumption flows propagating through the

supply chain. This shows the relevance of the integration approach chosen in creating the prospective MRIO to identify potential environmental hotspots.

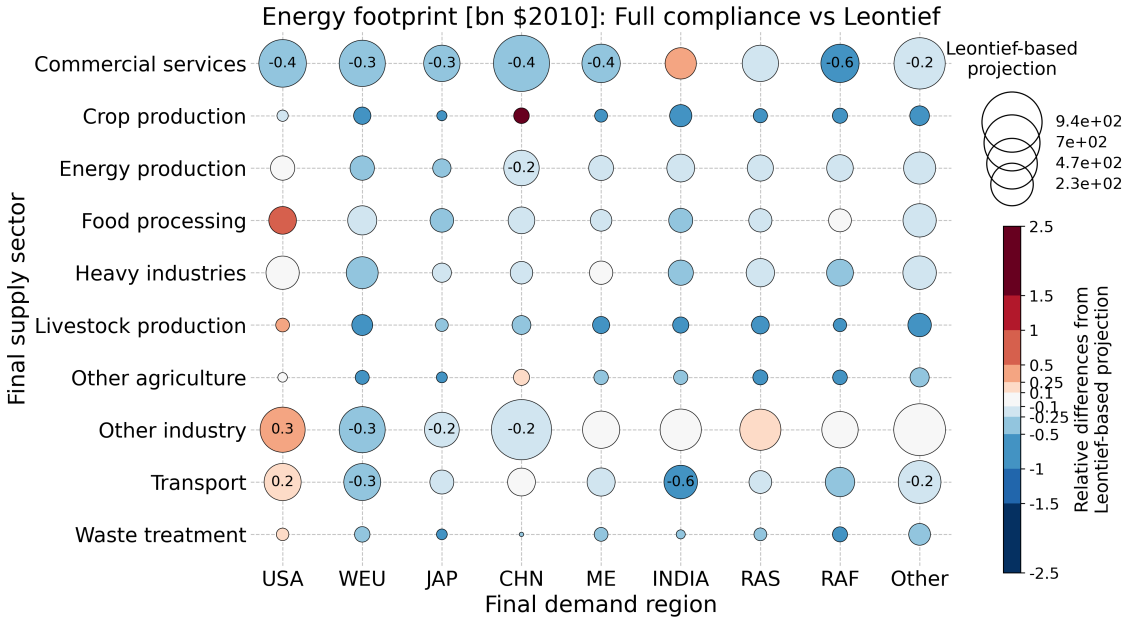

(a)

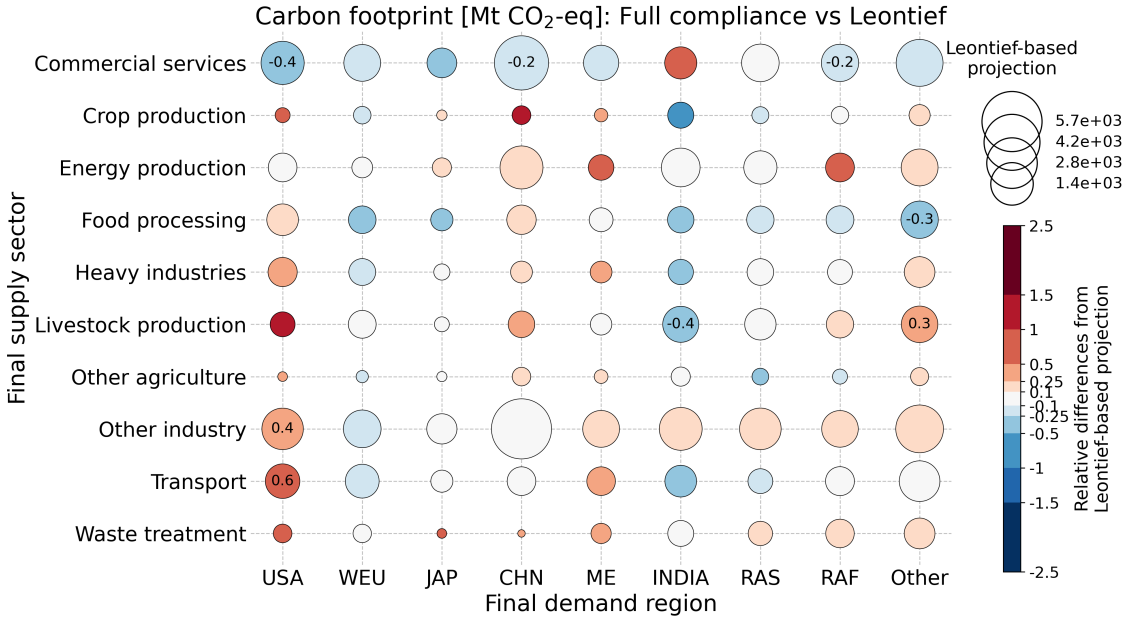

(b)

Figure 2: Energy (a) and carbon (b) footprints induced by consumption for each final supply sector and final demand region, comparing the Leontief-based projection with the fully-constrained prospective MRIO. Circle sizes indicate the footprints from the Leontief-based projection, and colors indicate the relative shifts of the footprints in the fully-constrained prospective MRIO.

Robust environmental hotspots in 2035

Given the significant variability of sectoral footprints within regions shown above, we identified the sector-region pairs that rank consistently high as consumption-based carbon footprint hot spots in 2035 with increasing scenario compliance, both by absolute level in 2035 and by relative growth from 2019. All ranks can be found in SI3.

The top 10 pairs by footprint level in 2035 account for 48.5%–49.8% of the global total (Figure 3a). The four highest — other industry and commercial services consumed in CHN and in Other — hold their positions across all seven versions of MRIO. Energy production consumed in CHN climbs from rank 47 in 2019 to a mean rank of 5.3 in 2035, and other industry consumed in IND and RAS rises from ranks 12 and 9 to mean ranks of about 6 and 8, reflecting emerging industrial activity in these economies. The top 10 set is highly robust, with only one swap across the seven versions: Commercial services consumed in the USA drops from rank 5–8 to 12 under full compliance, and livestock production consumed in Other enters at rank 10 under full compliance.

The top 10 pairs by relative growth form a partly different set (Figure 3b). Energy production consumed in CHN ranks first across all versions except "+Crop", growing by 660%–810% from 2019. Livestock production dominates the remaining high-growth entries, with livestock consumed in USA, JAP, RAS, and ME among the top contributors. Commercial services consumed in IND also increases strongly. Compared with the top by absolute level, this set is more sensitive to scenario compliance. The top five hold their positions across all seven versions, but 16 distinct pairs cycle through the lower half of the top 10 as constraints are added, and a single-version analysis would therefore both miss and misidentify high-growth hot spots. A Leontief-based projection would, for example, place commercial services consumed in RAF (rank 8) and transport consumed in IND (rank 7) in the top 10 and miss that energy production consumed in RAF enters the top 10 (to ranks 6–9) once the energy output constraint is enforced. With the heavy industry and transport output constraints being enforced, transport consumed in IND drops out of the top 10 (to ranks 16–22),

and with the energy output constraint being enforced, commercial services consumed in RAF drop out (to ranks 18–24). Full compliance produces the largest shifts. Livestock production consumed in IND drops from ranks 10–12 to 43, and livestock production consumed in Other rises from ranks 11–14 to 7.

Despite these sensitivities, three robust patterns hold across all seven prospective MRIO versions for 2035. First, energy production consumed in CHN emerges as both a major new high-level hot spot and the fastest-growing one relative to 2019. Second, the increasing carbon footprint of livestock consumption is a persistent high-growth trend across several regions. Third, IND and RAS grow in environmental significance through their industrial sectors. These sector-region pairs should be prioritized for climate change mitigation in future scenario pathways. Additionally, the mean-rank approach provides a summary that does not depend on any single version of the prospective MRIO table and thus can be used to identify further hotspots.

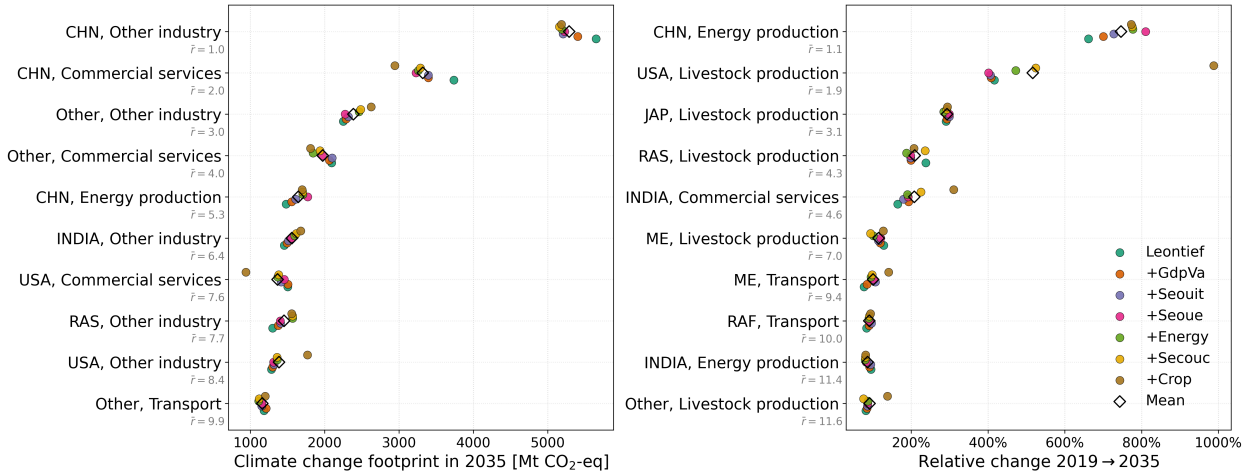

(a) (b)

Figure 3: Top-10 final-demand-region and final-supply-sector pairs (a) ranked by consumption-based carbon footprints in 2035, and (b) ranked by relative growth in carbon footprints from 2019 to 2035. The pairs are ordered by mean rank $\overline{r}$ across seven prospective MRIO versions. Individual colored dots represents one version and hollow diamonds mark the mean across versions.

Limitations and outlook

Several methodological choices and data limitations should be noted.

First, IMAGE and EXIOBASE differ in sectoral and regional resolution, in reporting units, and in their historical base-year values. Concordances bridge these differences but cannot remove inconsistencies in historical accounting, and these inconsistencies propagate into the prospective tables. Part of the movement from the 2019 EXIOBASE baseline to the fully-compliant 2035 table therefore reflects closer alignment with IMAGE's own internal accounting rather than projected structural change alone. Systematic cross-checking between the IAM and MRIO databases, including alignment of base-year sectoral aggregates, would separate these two components[29].

Second, the optimization framework is designed to preserve the intermediate coefficients in columns, which are the technology recipes that the Leontief inverse propagates through the supply chain and directly determine consumption-based footprints. Alternative reconciliation methods, such as biproportional updating in the RAS/GRAS family[30,31] and the KRAS approach with reliability information[32], instead preserve row and column structures jointly, which would distribute the structural deviation differently. The trade-off ranking we report between constraint types and the resulting prospective MRIO tables is therefore conditional on the choice of objective function.

Third, cumulative constraints are enforced in a fixed order from macroeconomic parameters to consumption details. The marginal deviations attributed to each constraint depend on this ordering, although the fully-compliant result does not. A Shapley-style attribution, which averages each constraint's marginal contribution across all possible orderings, would assign each constraint an order-independent share of the total deviation, which might be interesting for further research.

The trade-off between structural fidelity and scenario compliance is inherent to any integration that relies on partial future information from an external scenario model and needs a normative choice regarding what to prioritize. The magnitude of coefficient deviations un-

der each constraint and the identification of environmental hotspots can be sensitive to the choice of scenario model and the baseline MRIO and cannot be generalized. The framework presented here is transferable to alternative IAMs, scenarios, and global MRIO databases (EORA, WIOD, GTAP, OECD-ICIO[33]), as well as to other footprint indicators[34]. Such applications would reveal how hotspots depend on these choices and guide mitigation priorities.

The presented results give insight into the sensitivity of prospective MRIO to integration choices and identify hotspots that are robust across implementations. The final prospective MRIO can serve as a background database representing future supply chains in target years, supporting the evaluation of specific interventions around those years. Future work can add further environmental extensions to also examine synergies and trade-offs among environmental impacts and priorities.

ASSOCIATED CONTENT

Supporting Information 1. Appendix with methodological details (workflow, data harmonization and preprocessing, Leontief-based projection, and optimization formulation) and additional results tables and figures.

Supporting Information 2. Concordances for regions, sectors, and products between IMAGE and EXIOBASE, as well as between the prospective MRIO and the aggregated results.

Supporting Information 3. Shares of the decomposed energy and agriculture footprints (direct consumption by the final-supply sector, indirect consumption embedded in its upstream supply chain, and final demand) in the total footprints. Ranking of final-supply-sector and final-demand-region pairs based on consumption-based carbon footprints, and the relative changes of these footprints from 2019 to 2035.

The 12 versions of the prospective MRIO can be accessed through zenodo (temporarily with restricted access).

AUTHOR INFORMATION

Corresponding Author: Sidi Peng*sipeng@ethz.ch

Present Addresses: Laura-Hezner-Weg 7, 8093 Zürich, Switzerland

Author Contributions: Sidi Peng: conceptualization, data curation, methodology, result analysis, writing. Vassilis Daioglou: data curation (IMAGE), methodology. Konstantin Stadler: conceptualization, data curation (EXIOBASE), methodology, review and editing. Ramin Roshandel: methodology (optimization), review and editing. Martin Bruckner: conceptualization, methodology. Stephan Pfister: conceptualization, methodology, result analysis, review and editing. All authors have given approval to the final version of the manuscript.

Funding Sources: This work was supported by the Swiss State Secretariat for Education, Research and Innovation (SERI) under contract number 22.00188. The work was also part of the BAMBOO (Biodiversity and Trade: mitigating the impacts of nonfood biomass global supply chains) project, which has received funding from the European Union's Horizon Europe research and innovation programme under grant agreement no. 101059379.

ACKNOWLEDGMENT

The authors thank Carlijn Bos, Hermen Luchtenbelt, and Willem Jan van Zeist for providing data and for their help with the IMAGE model, and Kirsten Svenja Wiebe, Lea Ghisalberti, and Yongmin Hu for helpful discussions on the integration method and optimization. This work was supported by the Swiss State Secretariat for Education, Research and Innovation (SERI) under contract number 22.00188. The work was also part of the BAMBOO (Biodiversity and Trade: mitigating the impacts of nonfood biomass global supply chains) project, which has received funding from the European Union's Horizon Europe research and innovation programme under grant agreement no. 101059379.

ABBREVIATIONS

CH_4, methane; CO_2, carbon dioxide; CO_2-eq, carbon dioxide equivalent; N_2O, nitrous oxide; Mt, megatonne; USD, United States dollar; GDP, gross domestic product; VA, value added; IO, input–output; MRIO, multi-regional input–output; SUT, supply and use table; ECDF, empirical cumulative distribution function; GWP, global warming potential; EXIOBASE, Global multiregional environmentally extended input–output database; IAM, integrated assessment model; IMAGE, Integrated Model to Assess the Global Environment; SSP2, Shared Socioeconomic Pathway 2; GINFORS, global inter-industry forecasting system; IEA, International Energy Agency; CHN, China; IND, India; JAP, Japan; ME, Middle East; RAF, Rest of Africa; RAS, Rest of Asia; USA, United States of America; WEU, Western Europe.

References

(1) Hubacek, K.; Feng, K.; Minx, J. C.; Pfister, S.; Zhou, N. Teleconnecting Consumption to Environmental Impacts at Multiple Spatial Scales. *Journal of Industrial Ecology* **2014**, *18*, 7–9.

(2) Tukker, A.; de Koning, A.; Owen, A.; Lutter, S.; Bruckner, M.; Giljum, S.; Wood, R.; Stadler, K.; Merciai, S. Relevance of Global Multi Regional Input Output Databases for Global Environmental Policy: Experiences with EXIOBASE 3. *Journal of Industrial Ecology* **2018**,

(3) Hermans, T.; Oosten, C.; Ingram, V.; Tilborg, E. Telecoupled landscapes for nature inclusive transitions : Conceptual framing and methods. **2023**,

(4) Newig, J.; Challies, E.; Cotta, B.; Lenschow, A.; Schilling-Vacaflor, A. Governing global telecoupling toward environmental sustainability. *Ecology and Society* **2020**, *25*.

(5) Kapsar, K.; Hovis, C.; Silva, R.; Buchholtz, E.; Carlson, A.; Dou, Y.; Du, Y.; Furumo, P.; Li, Y.; Torres, A.; Yang, D.; Wan, H.; Zaehringer, J.; Liu, J. Telecoupling Research: The First Five Years. *Sustainability* **2019**, *11*, 1033.

(6) Hertwich, E. G.; Peters, G. P. Carbon Footprint of Nations: A Global, Trade-Linked Analysis. *Environmental Science & Technology* **2009**, *43*, 6414–6420.

(7) Duchin, F.; Levine, S. H.; Strømman, A. H. Combining Multiregional Input-Output Analysis with a World Trade Model for Evaluating Scenarios for Sustainable Use of Global Resources, Part I: Conceptual Framework. *Journal of Industrial Ecology* **2015**,

(8) Attinasi, M.-G.; Boeckelmann, L.; Meunier, B. The economic costs of supply chain decoupling. *The World Economy* **2025**, *48*, 598–627.

(9) Duchin, F.; Levine, S. H. Combining Multiregional Input-Output Analysis with a World

Trade Model for Evaluating Scenarios for Sustainable Use of Global Resources, Part II: Implementation. *Journal of Industrial Ecology* **2015**,

(10) Gibon, T.; Wood, R.; Arvesen, A.; Bergesen, J. D.; Suh, S.; Hertwich, E. G. A Methodology for Integrated, Multiregional Life Cycle Assessment Scenarios under Large-Scale Technological Change. *Environmental Science & Technology* **2015**,

(11) Li, M.; Wiedmann, T.; Hadjikakou, M. Enabling Full Supply Chain Corporate Responsibility: Scope 3 Emissions Targets for Ambitious Climate Change Mitigation. *Environmental Science & Technology* **2019**,

(12) Wiebe, K. S.; Harsdorff, M.; Montt, G.; Simas, M. S.; Wood, R. Global Circular Economy Scenario in a Multiregional Input-Output Framework. *Environmental Science & Technology* **2019**,

(13) Meyer, B.; Distelkamp, M.; Beringer, T. Contemporary Resource Policy and Decoupling Trends—Lessons Learnt from Integrated Model-Based Assessments. *Sustainability* **2018**, *10*, 1858.

(14) Stocker, A.; Großmann, A.; Madlener, R.; Wolter, M. I. The Socio-Economic Modelling of the ALARM Scenarios with GINFORS: Results and Analysis for Selected European Countries. *Global Ecology and Biogeography* **2011**, *20*, 108–121.

(15) International Energy Agency *Manufacturing and Trade Model Documentation 2026*; Model documentation, 2026; Licence: CC BY 4.0.

(16) Pauliuk, S.; Arvesen, A.; Stadler, K.; Hertwich, E. G. Industrial Ecology in Integrated Assessment Models. *Nature Climate Change* **2017**, *7*, 13–20.

(17) Wiebe, K. S.; Bjelle, E. L.; Többen, J.; Wood, R. Implementing exogenous scenarios in a global MRIO model for the estimation of future environmental footprints. *Journal of Economic Structures* **2018**, *7*.

(18) Dai, N.; Liu, Q.; Li, M.; Malik, A.; Lenzen, M. Coupling an integrated assessment model with an input–output database. *Economic Systems Research* **2024**, *36*, 527–544.

(19) De Koning, A.; Huppes, G.; Deetman, S.; Tukker, A. Scenarios for a 2 °C world: a trade-linked input–output model with high sector detail. *Climate Policy* **2016**, *16*, 301–317.

(20) Beaufils, T.; Wenz, L. A scenario-based method for projecting multi-regional input–output tables. *Economic Systems Research* **2022**, *34*, 440–468.

(21) Cap, S.; De Koning, A.; Tukker, A.; Scherer, L. (In)Sufficiency of industrial decarbonization to reduce household carbon footprints to 1.5°C-compatible levels. *Sustainable Production and Consumption* **2024**, *45*, 216–227.

(22) Vita, G.; Lundström, J. R.; Hertwich, E. G.; Quist, J.; Ivanova, D.; Stadler, K.; Wood, R. The Environmental Impact of Green Consumption and Sufficiency Lifestyles Scenarios in Europe: Connecting Local Sustainability Visions to Global Consequences. *Ecological Economics* **2019**,

(23) Stadler, K. et al. EXIOBASE 3. Zenodo dataset, 2021; `https://zenodo.org/records/5589597`, Version 3.8.2.

(24) Stehfest, Elke; van Vuuren, Detlef; Kram, Tom; Bouwman, Lex; Alkemade, Rob; Bakkenes, Michel; Biemans, Hester; Bouwman, Arno; den Elzen, Michel; Janse, Jan; Lucas, Paul; van Minnen, Jelle; Müller, Christoph; Gerdien Prins,Anne *Integrated Assessment of Global Environmental Change with IMAGE 3.0*; 2014.

(25) Van Sluisveld, M. A.; De Boer, H. S.; Daioglou, V.; Hof, A. F.; Van Vuuren, D. P. A race to zero - Assessing the position of heavy industry in a global net-zero CO2 emissions context. *Energy and Climate Change* **2021**, *2*, 100051.

(26) Miller, R. E.; Blair, P. D. *Input-Output Analysis: Foundations and Extensions*, 2nd ed.; Cambridge University Press: Cambridge, UK, 2009.

(27) IPCC In *Climate Change 2023: Synthesis Report. Contribution of Working Groups I, II and III to the Sixth Assessment Report of the Intergovernmental Panel on Climate Change*; Core Writing Team, Lee, H., Romero, J., Eds.; IPCC: Geneva, Switzerland, 2023; pp 1–184.

(28) Greenhouse Gas Protocol *Global Warming Potential Values*; 2024.

(29) Lefèvre, J. Integrated assessment models and input–output analysis: bridging fields for advancing sustainability scenarios research. *Economic Systems Research* **2023**, *36*, 675–698.

(30) Temursho, U.; Oosterhaven, J.; Cardenete, M. A. A multi-regional generalized RAS updating technique. *Spatial Economic Analysis* **2020**, *16*, 271–286.

(31) Valderas-Jaramillo, J. M.; Rueda-Cantuche, J. M. The multidimensional nD-GRAS method: applications for the projection of multiregional input–output frameworks and valuation matrices. *Papers in Regional Science* **2021**, *100*, 1599–1625.

(32) Lenzen, M.; Gallego, B.; Wood, R. Matrix balancing under conflicting information. *Economic Systems Research* **2009**, *21*, 23–44.

(33) Abd Rahman, M. D.; Los, B.; Owen, A. Multi-level comparisons of input–output tables using cross-entropy indicators. *Economic Systems Research* **2021**, *35*, 75–94.

(34) Malik, A.; McBain, D.; Wiedmann, T. Advancements in input–output models and indicators for consumption-based accounting. *Journal of Industrial Ecology* **2018**, *23*, 300–312.

Supporting Information 1

Contents

S1 Methodological Details

S1.1 Overview of workflow

S1.2 Data harmonization and preprocessing

Inputs. EXIOBASE 2019 multiregional supply and use tables (multi-regional SUT), and IMAGE scenario outputs covering macroeconomic, energy, agriculture, biofuel-crop, and heavy-industry/transport variables.

What this step does. We first reconciled the region, product, and sector classifications of EXIOBASE and the Integrated Model to Assess the Global Environment (IMAGE) into a unified resolution. The preprocessing pipeline then proceeded in three stages: (i) the EXIOBASE multi-regional SUT in 2019 were aggregated to the unified resolution and converted into use, supply-share, and value-added coefficient matrices (B, D, L) for the base year 2019. (ii) IMAGE macroeconomic variables were harmonized to the unified resolution. Energy and agricultural variables were translated into physical use tables, monetized using producer prices (with constant historical prices assumed for heavy industries and transports), and aggregated to the unified resolution. (iii) The resulting tables were checked for input–output consistency and corrected where necessary.

Outputs. Aggregated EXIOBASE base coefficient matrices (B, D, L) and final-use matrix Y, together with the monetized IMAGE energy and agricultural use tables and the heavy-industry/transport sector-output table, all at the unified resolution and expressed in billions of \$2010. These fed into the Leontief-based projection (Section S1.3). Each stage is detailed below.

Scope of preprocessing. All IMAGE-derived preprocessing (macroeconomic, energy, agriculture, biofuel-crop, and heavy-industry/transport tables) was run for every SSP2 scenario year reported by IMAGE rather than only for the target year. This gave a timeline-wide view when screening for inconsistencies in the input–output consistency check (Sec-

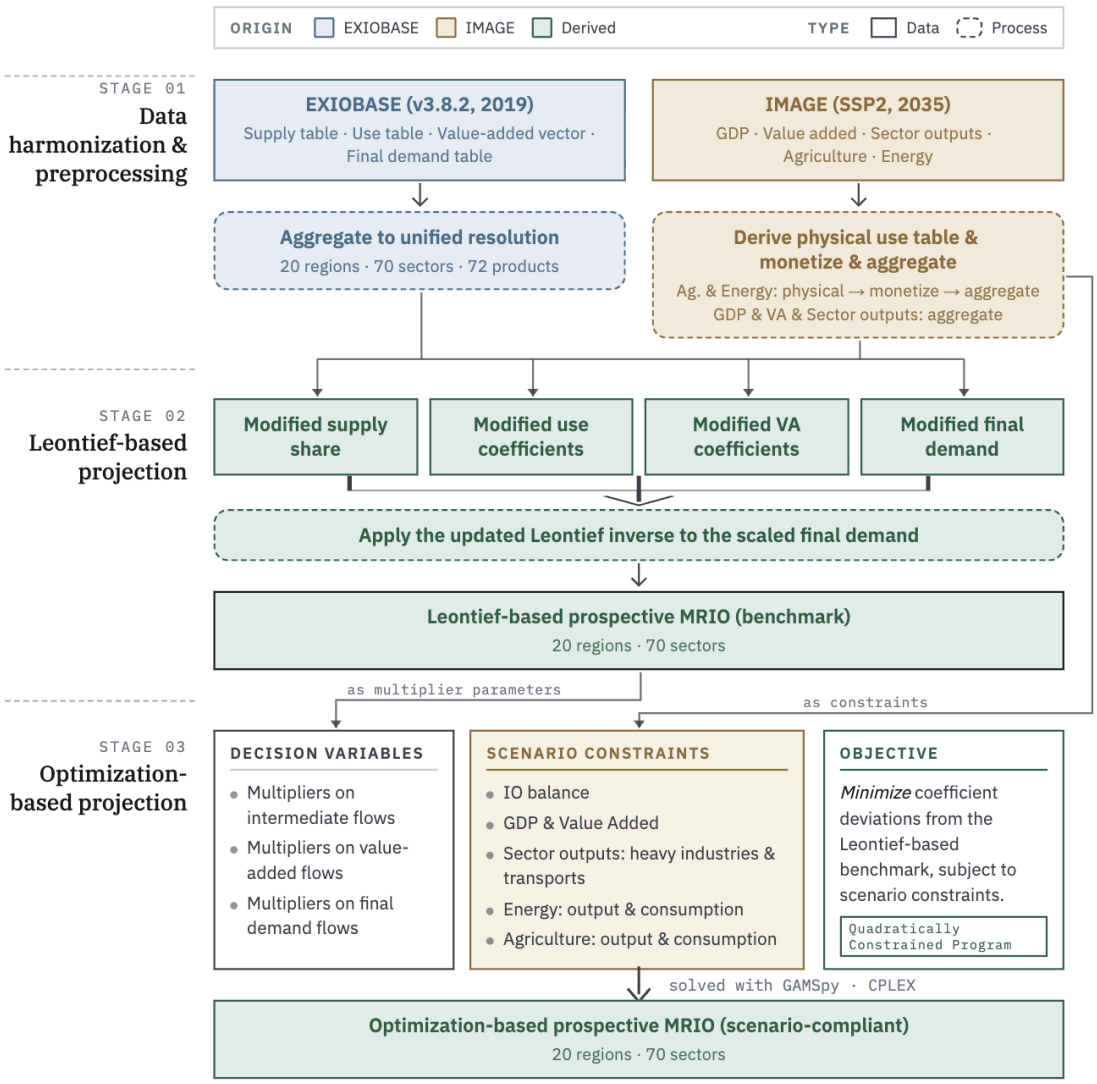

Figure S1: Three-stage construction pipeline for the prospective multi-regional input-output table (pMRIO table). Stage 1 is Data harmonization & preprocessing. The EXIOBASE v3.8.2 (2019) tables are aggregated to a unified resolution of 20 regions, 70 sectors, and 72 products. The IMAGE/SSP2 (2035) scenario data are preprocessed in parallel: GDP, value-added, and sector outputs are aggregated directly, while agriculture and energy variables are first derived into physical use tables, monetized, and then aggregated to the unified resolution. Stage 2 is Leontief-based projection. The preprocessed EXIOBASE and IMAGE inputs jointly populate four updated core matrices. Applying the updated Leontief inverse to the scaled final demand yields a Leontief-based prospective MRIO table that serves as the benchmark. Stage 3 is Optimization-based projection. Decision variables are defined as scaling factors acting on the benchmark flows, while the IMAGE scenario provides the constraints. A quadratically constrained program, solved with GAMSpy/CPLEX, minimizes the coefficient deviations from the benchmark subject to the scenario constraints, yielding the final scenario-compliant prospective MRIO table.

tion S1.2.3.6) and let corrections that arose in any scenario year be traced back to a single root cause. Only the 2035 SSP2 outputs entered the downstream Leontief projection and optimization. For brevity, the equations and variable references below were written for a generic scenario year and were applied year by year. Only where a specific year was essential (e.g., the EXIOBASE 2019 base year, the 2015 implicit-price anchor, or the 2035 target) was it stated explicitly.

S1.2.1 Definition of the unified resolution and classification

We defined the resolution of the prospective multiregional input-output table (pMRIO table) by reconciling the region, product, and sector classifications of EXIOBASE with the scenario outputs from IMAGE. The resulting aligned resolution encompasses 20 regions, 72 products, and 70 sectors. The pMRIO table represents monetary flows expressed in billions of \$2010 (10^9 \$2010).

Sectors and products in EXIOBASE multi-regional SUT follow NACE Rev.2 and CPA2002, respectively. NACE Rev.2 is derived from ISIC Rev.4[1], and CPA is articulated with NACE[2]. EXIOBASE covers 44 countries (28 EU member plus 16 major economies) and five rest-of-the-world regions, with 163 sectors and 200 products[3].

IMAGE employs IEA definitions for energy products and consumers. Though IMAGE models energy production and consumption in various sectors at the technology level, the sectoral energy consumption is calibrated to IEA, where the consuming sectors are defined as ISIC sectors. IMAGE's agriculture products follows GTAP classifications and IMAGE distinguishes three purposes of crop and livestock consumption (food, feed, and other) in addition to biofuel production. IMAGE covers 26 regions.

The concordances of sectors, products, and regions among EXIOBASE, IMAGE, and the unified resolution are provided in SI2.

S1.2.2 Preprocessing of EXIOBASE multi-regional SUT in 2019

The 2019 EXIOBASE multi-regional SUT (supply, use, value added, and final use) were aggregated from the EXIOBASE resolution (49 regions, 200 products, 163 sectors) to the unified resolution based on the region, product, and sector concordances (SI2). All flows are expressed in billions of $2010. The original EXIOBASE flows, reported in euros at 2019 prices, were first converted to 2019 US dollars using the 2019 annual-average euro–dollar reference exchange rate of 1.12 USD/EUR[4], and then deflated from 2019 to 2010 US dollars using a factor of 0.86 derived from the U.S. Bureau of Labor Statistics CPI inflation calculator[5]. The combined conversion factor is thus $1.12 \times 0.86 \approx 0.96$\$2010 per EUR2019. From these aggregated tables we derived the region-sector output g and the region-product output q from Eq. S1 and then the base-year inputs to the Leontief-based projection: the supply-share matrix D, the use coefficient matrix B, and the value-added coefficient matrix L from Eq. S2, while the final use matrix Y taken directly from the aggregated final-use table.

$$g_j = \sum_i U_{ij} + V_j, \qquad q_i = \sum_j S_{ji} \tag{S1}$$

$$B_{ij} = \frac{U_{ij}}{g_j}, \qquad D_{ji} = \frac{S_{ji}}{q_i}, \qquad L_j = \frac{V_j}{g_j} \tag{S2}$$

Where:

- i indexes a region-product and j indexes a region-sector.
- S_{ji} is the supply table (region-sector $\times$ region-product).
- U_{ij} is the use table (region-product $\times$ region-sector).
- V_j is the value-added vector (1$\times$ region-sector).
- Y is the final use table (region-product $\times$ region), taken directly from the aggregated final-use table.

- g_j is the region-sector output, equal to the column sum of intermediate inputs plus value added.

- q_i is the region-product output, equal to the column sum of the supply table over region-sectors.

- D_{ji} is the supply-share matrix (region-sector $\times$ region-product), obtained by dividing the supply table column-wise by q so that each region-product column of D sums to one. Conceptually, D_{ji} is the share of region-product i supplied by region-sector j, i.e., the market share that captures which sectors and regions produce each region-product.

- B_{ij} is the use coefficient matrix, obtained by dividing the use table column-wise by g. Conceptually, B_{ij} is the amount of region-product i used per unit of output of region-sector j, i.e., the input intensity (production recipe) of each region-sector.

- L_j is the value-added coefficient matrix, obtained by dividing the value-added row by g.

S1.2.3 Preprocessing of IMAGE data

Table S1: Resolution of preprocessed IMAGE scenario data at the unified resolution (20 regions, 72 products, 70 sectors)

Preprocessed variable	**Dimensions**	**Role in projection**
GDP (MER)	20 regions	VA/GDP constraint
Value added (MER)	3 macro-sectors × 20 regions (agriculture, industry, services)	VA/GDP constraint
Heavy-industry and transport sector output	8 sectors × 20 regions (Chemicals; Iron and Steel; Pulp and Paper; Non-metallic minerals; Air, Other land, Railway, Water transport)	Sector-output constraint
Energy output	20 energy products × 20 regions (Coal, Oil, Natural gas, Heat, Hydrogen, Modern solid biofuels, Traditional solid biofuels, Liquid biofuels, and 12 electricity technologies: Biomass, Hydrogen, Coal, Oil, Gas, Geothermal, Hydro, Nuclear, Wind, CSP, PV, Other)	Energy-output constraint
Energy consumption (monetary energy MRIO)	20 source regions × 20 energy products × 20 destination regions × 25 consuming sectors (10 non-transport sectors, 8 transport modes, Heat, Hydrogen, and 5 fuel-specific electricity sub-sectors)	Energy-consumption constraint; populates B'
Residential energy demand	20 source regions × 20 energy products × 20 destination regions	Overwritten into Y' (fixed in optimisation)
Agriculture output	∼9 agricultural products × 20 regions (7 crop groups; Ruminant and Non-ruminant livestock)	Agriculture-output constraint
Agriculture consumption (monetary agricultural MRIO)	20 source regions × ∼9 agricultural products × 20 destination regions × 3 consumption purposes (food, feed, other)	Agriculture-consumption constraint; populates B'
Biofuel-crop inputs	20 source regions × ∼6 feedstock crops × 20 destination regions × 2 biofuel pathways (Liquid biofuels, Modern solid biofuels)	Appended to agricultural MRIO; populates B'

S1.2.3.1 Macroeconomic variables GDP and sectoral VA per region under SSP2 were extracted from the IMAGE outputs for every scenario year and harmonized to the unified resolution. The `GDP|MER` variable was taken directly as the regional GDP in Market Exchange Rates (MER) at $2010 and aggregated from the 26 IMAGE regions to the 20 unified regions by summation. Sectoral VA in IMAGE is reported in Purchasing Power Parity (PPP)

at the level of three macro-sectors m (agriculture, industry, and services) based on ISIC classification. To translate it to MER while preserving the sectoral structure, we computed each macro-sector's share of the regional VA total in PPP and rescaled these shares to the regional `GDP|MER`, which is equivalent to multiplying the original VA in PPP by the regional `GDP|MER`/`GDP|PPP` ratio (Eq. S3). The resulting sectoral VA in MER $2010 was aggregated to the 20 unified regions by summation. These regional GDP and three-sector VA provided the scenario data used as the GDP and VA constraints in the optimization step.

$$V_{r,m}^{\mathrm{MER}} = V_{r,m}^{\mathrm{PPP}} \cdot \frac{\mathrm{GDP|MER}_r}{\mathrm{GDP|PPP}_r} \tag{S3}$$

Where:

- $m \in \{\text{agriculture}, \text{industry}, \text{services}\}$ indexes the three IMAGE macro-sectors.
- $V_{r,m}^{\mathrm{PPP}}$ and $V_{r,m}^{\mathrm{MER}}$ are the value added of region r in macro-sector m in PPP and MER respectively.

S1.2.3.2 Energy demand and supply This subsection describes how IMAGE energy outputs were preprocessed into a *monetary energy use table* based on a *physical energy use table*, trade, and prices.

Step 1: Physical energy use table construction. The *physical energy use table* represents, within each region, (i) the direct use of energy carriers by sectoral and residential consumers and (ii) the use of primary fuels by secondary energy production (electricity, heat, hydrogen) that is subsequently delivered to those same consumers. Throughout this section, "sectoral and residential use" refers to consumption within the energy module and only the residential use corresponds to the "final use" block of the multi-regional SUT.

IMAGE reports energy quantities through a structured variable family:

- `Final Energy|*` represents energy carriers directly used by sectoral and residential consumers.

- `Secondary Energy|*` represents secondary energy carriers processed before being delivered to sectoral and residential consumers.
- `Primary Energy|*` represents primary energy carriers used as inputs for secondary-energy production.

All three families quantify regional energy demand at successive stages in physical units, and energy is lost across the primary → secondary → final stages, whether or not the energy carrier type changes. We first extracted the relevant variables from these three families and then assembled a physical energy use table, initially without trade. Specifically, (i) `Final Energy|*` variables populated the energy use table for sectoral and residential consumers (`energy-to-sector`); (ii) `Primary Energy|*` variables populated the energy use table for electricity and hydrogen production; and (iii) because `Primary Energy|*` was unavailable for heat production, inputs to heat were derived from `Secondary Energy|Heat|*` combined with an assumed heat-conversion efficiency.

To respect the physics of conversion losses, the energy carrier at an earlier stage must always exceed the corresponding energy carrier at a later stage. Where this rule was violated, the IMAGE variables were corrected: we scaled up `Secondary Energy|Heat` (and its input breakdown `Secondary Energy|Heat|*`) when it fell below `Final Energy|*` of heat, and we scaled up `PrimaryEnergy|f|Electricity` at flagged points when `SecondaryEnergy|Electricity|f` exceeded it.

Trade was assumed to occur for coal, oil, natural gas, hydrogen, modern solid biofuels, and liquid biofuels at all stages, but not for electricity or heat. Combining the corrected demand and trade data yielded the physical energy use table, from which energy supply was derived. Trade data for hydrogen were missing, so we derived the bilateral trade matrix for hydrogen from the available demand and supply data.

Note that the *physical energy use table* does not reproduce the physical energy flows in IMAGE, because it does not distinguish the same energy carrier across stages (e.g., coal as primary, secondary, or final energy; electricity as secondary or final energy). In the

physical modelling in IMAGE, a same energy carrier carries different energy content at different stages owing to distribution losses. Here since the physical table was used only to construct a monetary energy use table that captures sectoral interlinkages in monetary unit, we collapsed physical stages whenever the energy carrier type was unchanged (i.e., no conversion occurred). In principle, the monetary table could be further disaggregated to mirror the physical stages, but this is rarely done in practice because the corresponding transformations occur within a single economic sector in monetary accounts. Therefore, unlike energy flow in IMAGE, the current *physical energy use table* does not need to reflect the total energy content used by the system or the true energy flows at the various stages. It only needs to capture the interlinkages among energy products and sectors, which are translated to monetary flows once energy-product-specific prices are applied.

Table S2: Simplified structure of physical energy use table. Entries with '1' indicate that flows from the row energy product to the column sector/process are tracked; '0' indicates none, and '-' indicates self-use is not applicable.

Energy Carriers	`energy-to-sector`	`energy-to-elec/heat/h2`		
	Sectors and Residential	Electricity	Heat	Hydrogen
Coal	1	1	1	1
Oil	1	1	1	1
Natural gas	1	1	1	1
Modern solid biofuels	1	1	1	1
Traditional solid biofuels	1	0	0	0
Liquid biofuels	1	0	0	0
Hydrogen	1	1	1	-
Electricity	1	-	0	1
Heat	1	0	-	0

Step 1.1: Construct the energy use table for sectors and residentials (`energy-to-sector`). We extracted `Final Energy|*` variables describing the use of eight energy carriers across the consuming sectors and transport modes listed below. The resulting table `energy-to-sector` has products (energy carriers) as rows and region–sector pairs as columns:

- Ten non-transport sectors: Agriculture, Commercial, Residential, Non-Energy Use (i.e., chemical production), Food Processing, Iron and Steel, Non-Metallic Minerals,

Pulp and Paper, Other Industries, and Other Sector.

- Seven transport modes: Bunkers (i.e., international aviation and shipping), Bus, Light Duty Vehicle, Truck, Rail, Domestic Aviation, and Domestic Shipping.

- Eight energy carriers: Coal, Oil, Natural gas, Solid biofuels, Liquid biofuels, Electricity, Heat, and Hydrogen. The `Solid biofuels` row is later split into `Modern solid biofuels` and `Traditional solid biofuels` (see the "Solid biofuel split" bullet below), so the final `energy-to-sector` table carries nine rows.

The extracted variables were harmonized and disaggregated prior to tabulation:

- **Variable-name harmonization**: variants across IMAGE outputs were mapped to a single convention as follows:
  - `Liquids|Biomass`, `Liquids|Bioenergy`, `Biofuel` → Liquid biofuels;
  - `Liquids|Fossil`, `Liquids|Oil` → Oil;
  - `Solids|Bioenergy`, `Solids|Biomass` → Solid biofuels;
  - `Solids|Coal`, `Solids|Fossil` → Coal;
  - `Gases`, `Gas` → Natural gas;
  - `H2`, `Hydrogen` (with trailing whitespace) → Hydrogen.

- **Reconstruction by subtraction**: any energy carrier missing within a parent aggregate was recovered from the residual according to the following rules:
  - Liquid biofuels = Liquids − Oil (when Oil is present and Liquid biofuels is missing);
  - Solid biofuels = Solids − Coal (when Coal is present and Solid biofuels is missing);
  - Oil = Liquids − Liquid biofuels (when Liquid biofuels is present and Oil is missing).

- **Bunker disaggregation**: `Final Energy|Bunkers` was split into International Aviation and International Shipping using the shares of `Final Energy|Bunkers|International Aviation` and `Final Energy|Bunkers|International Shipping`. The split was applied uniformly across bunker fuels, i.e., the two modes were assumed to have identical bunker fuel mixes.

- **Solid biofuel split**: the `Solid biofuels` row in sectoral and residential demand was split into `Modern solid biofuels` and `Traditional solid biofuels` using a regional modern/traditional share derived from `Primary Energy|Biomass|*`. For each region, we estimated the modern primary-biomass volume routed directly to sectoral and residential use, M, as the residual after subtracting biomass used for secondary energy production:

$$M = \texttt{Primary Energy|Biomass|Solids} - \frac{\texttt{Secondary Energy|Heat|Biomass}}{0.9} - \texttt{Primary Energy|Biomass|Electricity} - \texttt{Primary Energy|Biomass|Hydrogen}. \tag{S4}$$

  where 0.9 is the assumed efficiency for converting biomass into delivered heat. Traditional direct biomass use T was taken as `Primary Energy|Biomass|Traditional`, assumed to flow exclusively to sectoral and residential use rather than secondary energy production. The shares $M/(M+T)$ and $T/(M+T)$ were then applied to split the `Solid biofuels` row. This implicitly assumed that modern and traditional primary biomass converted to their respective solid-biofuel forms with equal efficiency, so that the share computed at the primary-biomass level transferred to the solid-biofuel (secondary) level.

At the end of Step 1.1, `energy-to-sector` was dimensioned as 26 IMAGE regions × 18 consuming sectors and transport modes (10 non-transport sectors plus 8 transport modes, after the Bunkers row was split into International Aviation and International Shipping) ×

9 energy products (Solid biofuels split into Modern and Traditional). The Non-Energy Use sector had no Heat input.

Step 1.2: Construct the energy use table for secondary energy production (`energy-to-elec/heat/h2`). Following IEA accounting, which IMAGE adopts, this step covered only *energy transformation*, i.e., fuel inputs that were converted into a different energy carrier. *Energy industry own use*—energy consumed inside the energy sector for heating, pumping, traction, and lighting, together with non-energy uses such as lubricants and waxes—could be reported by IMAGE under `Final Energy|*` and allocated to the Other Industries aggregate, so it was captured in Step 1.1 rather than here. To represent how fuels were consumed in producing delivered electricity, heat, and hydrogen, we combined (i) primary-energy inputs reported for secondary-energy production with (ii) secondary-energy cross-flows, converted to implied inputs using efficiencies:

- **Primary-energy inputs to electricity and hydrogen**: fuel inputs reported by IMAGE as `PrimaryEnergy|f|Electricity` and `PrimaryEnergy|f|Hydrogen` were taken directly as upstream inputs to delivered electricity and hydrogen production. These series were subsequently *corrected* at flagged points when `SecondaryEnergy|Electricity|f` exceeded `PrimaryEnergy|f|Electricity` (see the electricity balance correction in Step 1.4).

- **Primary biomass reclassified as solid biofuels**: `Primary Energy|Biomass|*` inputs to secondary-energy production were converted into `Modern solid biofuels` inputs to avoid double counting with biomass used for biofuels (detailed in Section S1.2.3.4). The conversion used `Efficiency|Solids|Biomass|Woody` as a region-specific factor.

- **Heat inputs from delivered heat**: because primary inputs to heat production are not reported, they were derived from `Secondary Energy|Heat|*` divided by an assumed heat-conversion efficiency of 0.9.

- **Cross-inputs between electricity and hydrogen**: `SecondaryEnergy|Electric`

ity|Hydrogen and SecondaryEnergy|Hydrogen|Electricity were converted into implied inputs using Efficiency|Electricity|Hydrogen (regional) and Efficiency |Hydrogen|Electricity (reported at the world level).

At the end of Step 1.2, energy-to-elec/heat/h2 was dimensioned as 26 IMAGE regions × 3 producing sectors (Electricity, Heat, Hydrogen) × 5 input energy products (Coal, Oil, Natural gas, Modern solid biofuels, and Hydrogen for Electricity and Heat; Coal, Oil, Natural gas, Modern solid biofuels, and Electricity for Hydrogen).

Step 1.3: Merge the two tables and disaggregate electricity by technology. The tables from Steps 1.1 and 1.2 were merged into a single physical energy use table (without trade). To resolve electricity by generation technology, we extracted the regional electricity production mix from Secondary Energy|Electricity|* and used the resulting regional ratios to (i) split the Electricity *product* row in both energy-to-sector and energy-to-elec/heat/h2 into 12 technology-specific electricity sub-products (Biomass, Hydrogen, Coal, Oil, Gas, Geothermal, Hydro, Nuclear, Wind, CSP, PV, Other), and (ii) split the Electricity *sector* in energy-to-elec/heat/h2 into 5 fuel-specific electricity-production sub-sectors ("Production of electricity by {coal, oil, natural gas, modern solid biofuels, hydrogen}"). The product side and the sub-sector side were intentionally asymmetric here: only the five fuel-burning technologies consumed an energy carrier as a tracked input and therefore appeared as producing sectors in energy-to-elec/heat/h2, whereas the seven non-fuel technologies (Geothermal, Hydro, Nuclear, Wind, CSP, PV, Other) consumed no energy carrier in IMAGE and so had no row of inputs at this stage. Their producing sectors were introduced later when the energy table was layered onto the EXIOBASE economic table.

Step 1.4: Screen inconsistencies and apply corrections. Because energy is lost at each conversion stage, the energy product quantity at an earlier stage must always exceed that at the corresponding later stage. We screened the merged table point-wise across regions and applied the following corrections where this rule was violated:

- **Heat balance**: if the regional sum of sectoral and residential heat demand exceeded `Secondary Energy|Heat`, then `Secondary Energy|Heat` was set to that demand divided by 0.85 (15% assumed loss from delivered heat to sectoral and residential use) and all `Secondary Energy|Heat|*` inputs were scaled by the same ratio. The 0.85 figure was calibrated against IMAGE outputs themselves: from 2035 onwards the implied secondary-to-final heat loss was around 14% in CHN and 18% in WEU, and fell from 40% to 18% in USA. We adopted 15% as a representative central value. (The primary-to-secondary heat-conversion efficiency of 0.9 used in Steps 1.1 and 1.2 is a separate, technology-side parameter taken from the literature, not the same quantity.) If `Secondary Energy|Heat` was zero at a flagged point, the corresponding Heat row in `energy-to-sector` for that region was set to zero (the heat producing block in `energy-to-elec/heat/h2` was already empty in this case, since zero secondary heat output implied zero `Secondary Energy|Heat|*` inputs).

- **Electricity balance**: for each fuel $f \in$ {Biomass, Oil, Gas, Coal}, if `SecondaryEnergy|Electricity|f` exceeded `PrimaryEnergy|f|Electricity`, then `PrimaryEnergy|f|Electricity` was scaled up to match the implied requirement, using an average regional efficiency estimated from "normal" points where `SecondaryEnergy|Electricity|f`$\leq$`PrimaryEnergy|f|Electricity`.

Step 1.5: Add bilateral trade. Trade was assumed to occur for coal, oil, natural gas, hydrogen, modern solid biofuels, and liquid biofuels at all stages, but not for electricity or heat. Bilateral sourcing was constructed in two passes.

First, hydrogen — for which IMAGE reports no trade matrix. Total regional hydrogen demand was computed as the sum of (i) sectoral and residential hydrogen demand, (ii) hydrogen used for heat production (`Secondary Energy|Heat|Hydrogen` / 0.9), and (iii) hydrogen used for electricity production (`SecondaryEnergy|Electricity|Hydrogen / Efficiency|Electricity|Hydrogen`). Every region's `Secondary Energy|Hydrogen` (and `Secondary Energy|Hydrogen|*`) supply was then scaled by the same global ratio of

global hydrogen demand to global hydrogen supply, and `Primary Energy|*|Hydrogen` inputs were scaled by the same ratio. A bilateral hydrogen trade matrix was then built by allocating domestic supply first and distributing residual demand across exporters in proportion to their residual supply.

Second, the remaining traded fuels. For coal, oil, and natural gas (net-trade data) and for modern solid and liquid biofuels (bilateral-trade data), exporter shares were obtained by normalizing the bilateral matrices column-wise (importer-wise) and used to disaggregate each importing region's demand into bilateral sources. Negative entries in the coal, oil, and natural gas trade matrices, which represented net trade in the opposite direction to the positive entries, were clipped to zero before normalization. Products without trade data (electricity, heat, and their sub-products) were assumed to be supplied domestically (identity trade). The resulting physical energy MRIO table was at the IMAGE 26-region resolution and expressed in EJ. In MRIO table form it was dimensioned as 26 source regions $\times$ 20 energy products (the 9 energy products from Step 1.1 with Solid biofuels disaggregated to Modern and Traditional solid biofuels, with the original `Electricity` row replaced by 12 technology-specific electricity sub-products: $9 - 1 + 12 = 20$) by 26 destination regions $\times$ 25 sector columns (10 non-transport sectors + 8 transport modes after the Bunkers split into International Aviation and International Shipping + Heat + Hydrogen + 5 fuel-specific electricity-production sub-sectors).

Step 2: Monetization. Producer prices were obtained from IMAGE and applied to the physical energy MRIO table:

- **Carrier prices from IMAGE**: IMAGE reports two upstream price variables that we drew on. `Price|Primary Energy|*` is the price of a primary fuel at the global or regional spot market, which for the traded fossil fuels (coal, oil, and natural gas) is a close proxy for the producer price at the point of extraction. `Price|Secondary Energy|*` is the price at the regional wholesale market: from a supply-curve perspective, it corresponds to the highest producer price among the regional suppliers plus

transportation, i.e., a *delivery price*. We purposefully avoided `Price|Final Energy|*` variables because they additionally include transmission and distribution costs as well as carbon prices. Our assignment was therefore: `Price|Primary Energy|*` for fossil fuels (coal, oil, and natural gas); `Price|Secondary Energy|*` for electricity and heat, which are largely produced and consumed locally so the delivery price is a close proxy for the producer price; and `Price|Secondary Energy|*` for hydrogen and modern solid and liquid biofuels, which served as a stand-in for the producer price that IMAGE does not report (we accepted the implicit transport mark-up). `Traditional solid biofuels` were assigned a zero price, reflecting the assumption that they were gathered or self-supplied without market exchange. All other prices were expressed in $2010 per GJ.

- **Cross-check against EXIOBASE**: IMAGE prices were compared with the ratio of EXIOBASE 2015 monetary product output to the physical production from the energy MRIO table. The IMAGE values were retained as the more reasonable estimates.

- **Electricity prices by technology**: prices were differentiated by generation technology under the assumption of globally and temporally constant relative cost ratios across technologies, with wind power as the reference (Table S3). For each region and year, the wind-power price was solved such that the production-weighted average of the technology-specific prices equalled the IMAGE `Price|Secondary Energy|Electricity`, and each technology's price was obtained by scaling the wind price by its relative cost ratio.

- **Monetization and aggregation**: the physical energy MRIO table was monetized by applying these region-, energy-product-, and (for electricity) technology-specific prices. The resulting monetary MRIO table was aggregated by summation from the 26 IMAGE regions to the 20-region unified resolution.

Table S3: Literature-based Levelized cost of electricity (LCOE) by generation technology, used to derive the relative cost ratios across electricity technologies in the monetization step. Mean 2019–2021 is taken as a representative pre-shock value. The relative cost ratio is computed as the technology mean divided by the wind-power mean over 2020 (wind = 1).

prospective MRIO product	IMAGE product	Mean 2019–2021 [$/MWh]	Relative cost (wind = 1)
Electricity by nuclear	Secondary Energy|Electricity|Nuclear	161.67†	4.08
Electricity by solar thermal	Secondary Energy|Electricity|Solar|CSP	141.00†	3.55
Electricity by coal	Secondary Energy|Electricity|Coal	109.67†	2.76
Electricity by Geothermal	Secondary Energy|Electricity|Geothermal	82.00†	2.07
Electricity by natural gas	Secondary Energy|Electricity|Gas	58.33†	1.47
Electricity by solar photovoltaic	Secondary Energy|Electricity|Solar|PV	37.67†	0.95
Electricity by wind	Secondary Energy|Electricity|Wind	39.67^{†,a}	1.00
Electricity by hydro	Secondary Energy|Electricity|Hydro	47.67‡	1.20
Electricity by solid biofuels	Secondary Energy|Electricity|Biomass	71.00‡	1.79
Electricity by hydrogen	Secondary Energy|Electricity|Hydrogen	174.17^{‡,b}	4.39
Electricity by other	Secondary Energy|Electricity|Other	83.29^{c}	2.10
Electricity by oil	Secondary Energy|Electricity|Oil	158.33^{d}	3.99

Sources: †Lazard's Levelized Cost of Energy Analysis (US-based). ‡IRENA Renewable Power Generation Costs (global weighted average).
Notes: [Reference to be added]
^{a}Represented by Wind-Onshore, which is more common currently, but offshore wind is growing rapidly.
^{b}\$1.74/kg H_2 in Saudi Arabia and 9.99 kWh of electricity per kg H_2, giving $1.74/9.99 \times 1000 \approx 174.17$ \$/MWh.
^{c}Assumed equal to the geothermal LCOE.
^{d}Oil price is ca. 5 times the natural gas price per MMBtu. Assuming a representative natural-gas fuel cost of ca. \$25/MWh of electricity (consistent with a Combined Cycle Gas Turbine heat rate of ca. 7 MMBtu/MWh at \$3–5/MMBtu gas), the oil-fired equivalent is ca. $5 \times 25 = 125$ \$/MWh, i.e., a fuel-cost increment of ca. \$100/MWh. Fuel cost is only part of LCOE, and we assume the infrastructure part is similar, so we add \$100 on top of the natural-gas LCOE ($58.33 + 100 = 158.33$ \$/MWh). Oil-fired electricity is uncommon, so no literature value is available.

S1.2.3.3 Agriculture demand and supply This subsection describes how IMAGE and MAGNET outputs were preprocessed into a *monetary agricultural use table* based on a *physical agricultural use table*, trade, and prices.

Step 1: Physical agricultural use table construction. The *physical agricultural use table* represents, within each region, the use of agricultural products (crops and livestock) for the three consumption purposes: food, feed, and other (mainly food-processing such as rice and livestock processing). Demand for biofuel production was constructed separately from the physical energy MRIO table and is described in Section S1.2.3.4. Two complementary data sources were used:

- **IMAGE** reports regional physical demand of crops and livestock, disaggregated by consumption purposes (food, feed, and other), in million Dry Matter (DM) tonnes (`Agricultural Demand|*`). It also reports regional price indices for crops and livestock relative to the 2019 base year (`Price|Agriculture|Food Products|Crops|*` and `Price|Agriculture|Food Products|Livestock`), which were used to project base-year producer prices to each scenario year in Step 2.

- **MAGNET**, the agro-economic module of IMAGE, reports bilateral monetary and physical trade of crops and livestock (monetary trade in constant $2017; physical trade in Wet Matter (WM) tonnes), regional production quantities, and crop-specific moisture content used to convert producer prices between WM and DM terms in Step 2.

We first extracted IMAGE demand (Step 1.1), then constructed and harmonized the MAGNET bilateral trade matrices (Steps 1.2–1.3), and finally disaggregated IMAGE regional demand into bilateral flows based on the trade matrices to construct the physical agricultural MRIO table (Step 1.4). Producer prices were addressed in Step 2.

Step 1.1: Extract IMAGE demand. Regional crop and livestock demand under SSP2 across the three IMAGE consumption purposes was extracted in million DM tonnes for every scenario year from the following `Agricultural Demand|*` variables:

- **Crop demand by purpose**: `Agricultural Demand|Crops|Food|*`, `Agricultural Demand|Crops|Feed|*`, and `Agricultural Demand|Crops|Other|*`, where `*` enumerates the IMAGE crop categories.

- **Livestock demand by purpose**: `Agricultural Demand|Livestock|Food`, `Agricultural Demand|Livestock|Feed`, and `Agricultural Demand|Livestock|Other`. These were reported at the aggregated livestock level and were further split into ruminant and non-ruminant species using the regional shares derived from `AgriculturalDemand|Livestock|Food|*` (where `*` enumerates Ruminant and Non-ruminant), under the assumption that the species mix was consistent across purposes.

The extracted demand was aggregated from the IMAGE region–product resolution to the 20-region unified resolution by summation through the concordances (SI2).

Step 1.2: Construct the full bilateral physical trade matrix in MAGNET. MAGNET reports bilateral physical trade between exporters and importers but does not directly fill the diagonal of each trade matrix (a region's domestic supply of its own production). Following the MAGNET modelling assumption that produced commodities are either supplied to domestic markets to satisfy demand by private households and governments or exported, and that demand is met by national producers or by imports, we computed the diagonal as production minus total exports (Eq. S5)[6]. This construction implicitly assumed that all imports were for domestic use and all exports came from local production (i.e., no re-exports), consistent with the MAGNET modelling assumption but not necessarily with raw observed trade. In our processed MAGNET data, no region–product cell yielded a negative diagonal. Spot checks of the resulting diagonals matched expectation: for example, Western Europe imported a substantial share of wheat from Ukraine, while cattle was mostly domestically supplied across regions because livestock itself is rarely traded internationally (meat trade is not reported in MAGNET). The diagonal of the bilateral monetary trade matrix was left empty.

$$Q^{\mathrm{MAGNET}}_{r,r,p} = Q^{\mathrm{prod}}_{r,p} - \sum_{r' \neq r} Q^{\mathrm{MAGNET}}_{r,r',p} \tag{S5}$$

Where:

- r is the producing region and r' is any other region.
- p indexes the agricultural product.
- $Q^{\mathrm{prod}}_{r,p}$ is the MAGNET production of product p in region r.
- $Q^{\mathrm{MAGNET}}_{r,r',p}$ is the MAGNET physical export flow of product p from region r to region r', so $Q^{\mathrm{MAGNET}}_{r,r,p}$ is the imputed domestic supply on the diagonal.

Step 1.3: Harmonize the bilateral trade matrices to the unified resolution. The bilateral physical trade matrix with diagonal filling, the bilateral physical trade matrix without diagonal filling, and the bilateral monetary trade matrix were aggregated from the native MAGNET region–product resolution to the 20-region unified resolution by summing across exporter and importer regions and aggregating products through the concordances (SI2). Within MAGNET, producer prices are assumed identical across purchasers within the same product. After aggregation this no longer held at the unified resolution, because the aggregated price was essentially a quantity-weighted average over MAGNET subregions and subproducts.

Step 1.4: Construct the physical agricultural MRIO table. The physical agricultural MRIO table was constructed by disaggregating, for each product, the unified-resolution regional demand from Step 1.1 into bilateral flows using the MAGNET physical-trade import ratios derived from the harmonized trade matrix with diagonal filling (Step 1.3). The diagonal entries of the import-ratio matrix represented domestic supply. The resulting physical agricultural MRIO table was at the 20-region unified resolution and expressed in million DM tonnes. It spanned 3 consumption purposes (food, feed, other).

Step 2: Monetization. Producer prices were estimated from the MAGNET 2019 trade data (Step 2.1) and projected to each scenario year using IMAGE price indices (Step 2.2), then applied to the physical agricultural MRIO (Step 2.3).

Step 2.1: Derive base-year producer prices. Base-year (2019) producer prices in WM terms were derived from the 2019 MAGNET aggregated physical and monetary trade matrices without diagonal entries (Eq. S6). The aggregated trade was preferred over the native MAGNET trade because it directly yielded an effective producer price for each (region, product) pair at the unified resolution.

$$\pi_{r,p}^{\text{base,WM}} = \frac{\sum_{r' \neq r} M_{r,r',p}^{\text{MAGNET,2019}}}{\sum_{r' \neq r} Q_{r,r',p}^{\text{MAGNET,2019}}} \tag{S6}$$

Where:

- r is the exporting region (producer), $r' \neq r$ indexes other importing regions.
- p indexes the agricultural product at the unified resolution.
- $M_{r,r',p}^{\mathrm{MAGNET,2019}}$ is the bilateral monetary MAGNET trade flow in 2019 (in million \$2017).
- $Q_{r,r',p}^{\mathrm{MAGNET,2019}}$ is the bilateral physical MAGNET trade flow in 2019 (in WM tonnes).
- $\pi_{r,p}^{\mathrm{base,WM}}$ is the base-year producer price of product p in region r (in \$2017 per WM tonne).

Manual price corrections were applied at a small number of region–product cells where the MAGNET-derived prices were inconsistent with the downstream input–output checks of biofuel production (Section S1.2.3.6):

- The prices of sugar cane and sugar beet in CHN, RAM, and RAS were unreasonably high, which would otherwise drive the monetary biofuel output below the cost of crop inputs. These prices were replaced by the average of structurally comparable regions where the price was reasonable: BRA and MEX for RAM; INDIA, INDO, ME, TUR, and RUS for CHN and RAS.

The corrected base prices were converted from WM to DM tonnes using crop-specific moisture-content data from MAGNET, harmonized from the MAGNET crop resolution to the unified product resolution by averaging across MAGNET subcategories within each unified product.

There were still outliers in the resulting base prices at regions with negligibly small production for a given product. We did not further revise these because we could not reliably distinguish real product differences across regions from MAGNET data noise.

Step 2.2: Compute future producer prices. Future producer prices under SSP2 were computed for every scenario year by combining the base-year DM prices with regional price indices reported by MAGNET in IMAGE:

- For each unified region and unified product, the IMAGE price index (relative to the 2019 base year) was aggregated from the IMAGE region–product resolution to the

unified resolution as an average over IMAGE subregions mapped to the unified region and over IMAGE subproducts mapped to the unified product (subproduct grouping is defined entirely by the product concordance, SI2).

- IMAGE reports a single livestock price index that is not differentiated by species. We applied this same index to both the ruminant and non-ruminant unified products.
- The future producer price was then computed as base price multiplied by price index (Eq. S7).

$$\pi_{r,p}^{\text{fut}} = \pi_{r,p}^{\text{base,DM}} \cdot I_{r,p}^{\text{IMAGE}} \tag{S7}$$

Where:

- r is the producing region and p indexes the agricultural product at the unified resolution.
- $\pi_{r,p}^{\text{base,DM}}$ is the 2019 producer price in DM terms (in \$2017 per DM tonne).
- $I_{r,p}^{\text{IMAGE}}$ is the scenario-year IMAGE price index for product p in region r under SSP2 (relative to the 2019 base year).
- $\pi_{r,p}^{\text{fut}}$ is the resulting scenario-year producer price (in \$2017 per DM tonne).

Step 2.3: Monetize the physical agricultural MRIO. The physical agricultural MRIO from Step 1.4 was monetized row-by-row by the corresponding scenario-year producer prices from Step 2.2 and converted from \$2017 to \$2010 using a constant deflator of 0.89 [U.S. Bureau of Labor Statistics inflation calculator]. The result was the monetary agricultural MRIO in million \$2010 at the 20-region unified resolution and across the three food/feed/other purposes.

S1.2.3.4 Crops for biofuel production This subsection describes how the fourth crop-consumption purpose – crop inputs for biofuel production – was constructed separately from the IMAGE crop and livestock demand variables (which cover only food, feed, and other) and integrated into the agricultural MRIO. The construction proceeded in three steps: we derived biofuel production from the physical energy MRIO and translated it into crop inputs by biofuel pathway (Step 1), monetized these inputs with a crop price (Step 2), and concatenated the result with the food/feed/other agricultural MRIO (Step 3). Only Liquid biofuels and Modern solid biofuels carried biofuel-crop inputs in this pipeline: Traditional solid biofuels were assumed to be gathered or self-supplied without market exchange (and already carried a zero price in the energy monetization), so they were not represented as a biofuel feedstock in either the physical or the monetary biofuel-crop matrix here.

Step 1: Physical biofuel-crop use table construction.

Step 1.1: Extract regional biofuel production from the physical energy MRIO. Regional production of Liquid biofuels and Modern solid biofuels (in EJ) at the IMAGE 26-region resolution was extracted from the physical energy MRIO by summing the bilateral physical flows along the row of each regional biofuel product. This yielded a regional biofuel production that was internally consistent with the regional demand for biofuels and the IMAGE bilateral biofuel trade in the energy MRIO. The same regional biofuel production could in principle be read directly from IMAGE `Secondary Energy|Production|*` variables (covering ethanol, biodiesel, biomass-to-liquid, and charcoal-type pathways). The two were not identical at the regional level but agreed within the same order of magnitude. Here, we used the production consistent with the energy MRIO.

Step 1.2: Disaggregate by pathway and convert to crop inputs. Each regional biofuel total was disaggregated into specific biofuel pathways using the regional shares of various pathways (`Secondary Energy|Production|*`) from IMAGE, with CCS and non-CCS variants of each pathway aggregated together (the CCS variants are tracked separately in IMAGE for emissions accounting and use the same upstream feedstock). The crop input

required by each pathway b in region r was then computed as biofuel production divided by the corresponding pathway-specific conversion efficiency (Eq. S8):

- Liquid-biofuel pathways used `Efficiency|Liquids|*`, covering Maize-to-ethanol, Sugar-crops-to-ethanol (sugar cane and sugar beet), and Oil-crops-to-biodiesel, Woody/Non-woody (Grassy)-to-ethanol/FT-diesel/Methanol.

- Solid-biofuel pathways used `Efficiency|Solids|*`, covering Woody, Non-woody (Grassy), and Residues. The residue-pathway efficiency was set to the regional mean of the reported Woody and Non-woody (Grassy) efficiencies for that region, because IMAGE does not report a residue-specific efficiency.

The crop inputs in EJ were then converted to million DM tonnes using crop-specific lower heating values from the literature (Table S4).

$$Q^{\text{crop}}_{r,c,b} = \frac{Q^{\text{biofuel}}_{r,b}}{\eta^{\text{IMAGE}}_{r,b}} \cdot \frac{1}{\text{LHV}_c} \tag{S8}$$

Where:

- r is the producing region, b indexes the biofuel pathway, and c indexes the crop feedstock used by pathway b (uniquely determined by the pathway).

- $Q^{\text{biofuel}}_{r,b}$ is the production of biofuel pathway b in region r (in EJ).

- $\eta^{\text{IMAGE}}_{r,b}$ is the IMAGE conversion efficiency from feedstock to biofuel.

- LHV_c is the literature lower heating value of crop c (in EJ per million DM tonnes).

- $Q^{\text{crop}}_{r,c,b}$ is the resulting crop-input demand (in million DM tonnes).

Table S4: Literature-based Energy content and 2010 world prices (in dry-matter terms) used to monetize biofuel-crop inputs.

Crop (prospective MRIO)	Energy content [GJ/t DM]	World price 2010 [$2010/t DM]
Non-woody solid biomass[a]	18.40[7,8]	63.70[9]
Woody solid biomass[b]	18.60[7,8]	46.50[10]
Sugar cane, sugar beet[c]	16.50	-
Oil seeds[d]	32.35	-
Cereal grains n.e.c.[e]	18.60	-
Residue for solid biofuels[f]	15.25	38.00

Notes:
[a]Represented by switchgrass. $2011 to $2010 deflator 0.98.
[b]Represented by hybrid willow (2014). $2014 to $2010 deflator 0.93.
[c]Energy content derived from sugarcane[11] and sugar-beet pulp[12].
[d]Energy content averaged from rapeseed (41.4 MJ/kg DM)[13] and soybean (23.3 MJ/kg DM) [14].
[e]Represented by maize[15].
[f]Energy content averaged from wood[16] and crop residue[17]. Price represented by corn stover ($28.49–$48.14/t[18], dry-mass content 77.5%[19]). $2022 to $2010 deflator 0.77.

Step 1.3: Harmonize to the unified resolution. The pathway-resolved crop inputs were aggregated from the IMAGE 26-region and pathway resolution to the 20-region unified resolution by summing across IMAGE regions within each unified region, summing across pathways that drew from the same crop, and aggregating crops through the concordances (SI2). The aggregation was performed before monetization so that the unified-resolution prices from Section S1.2.3.3 could be applied directly.

Step 2: Monetization with crop-specific price regimes. The aggregated physical crop inputs for biofuel production were monetized using different price regime per crop class.

- **Food-grade feedstocks** (sugar cane and sugar beet, oil crops, maize): the scenario-year SSP2 producer prices derived in the agricultural preprocessing (Step 2.2 of Section S1.2.3.3) were reused, after applying the same $2017–$2010 deflator of 0.89 used in agricultural Step 2.3. We assumed biofuel-grade crops were at the same price as food-grade.

- **Woody and non-woody (grassy) solid biomass**: a single global, constant literature price in $2010 per DM tonne was applied (Table S4) – one value per crop class, identical across regions and across years. We considered using `Price|Primary`

`Energy|Biomass` from IMAGE but rejected it on rationality grounds. Conceptually, woody and grassy biomass should remain cheaper than food crops because (i) the management required is simpler than for food crops, and (ii) under demand-driven price increases, farmers would shift from food crops to biofuel crops, raising food prices in tandem – so biomass prices alone cannot persistently exceed food prices in equilibrium. With `Price|Primary Energy|Biomass`, biomass for biofuel became more expensive than the cheapest food crop (sugar crops) as early as 2030, and the gap widened over time as IMAGE projected food-crop prices to fall and biomass prices to rise. Crop and biomass prices are modelled separately in IMAGE and this potential inconsistency is not reconciled there. With a constant literature anchor, biomass started cheaper than food crops in the base year. We acknowledged that for a few region–year combinations the modelled food-crop price fell below the constant literature biomass price. We accepted this minor inversion rather than tracking food-crop prices dynamically for biomass.

- **Residues**: a single global, constant literature price was applied (Table S4). In principle residues (a byproduct of other agricultural activities) can be cheaper than dedicated woody and grassy biomass. With future demand increases their price could rise toward the woody and grassy level but should still remain below the food-crop price.

Step 3: Combination with the food, feed, and other agricultural demand. The monetary biofuel crop-input matrix in million $2010 was concatenated with the monetary agricultural MRIO from Section S1.2.3.3 (which covers the food, feed, and other purposes) to form the complete agricultural MRIO supplied to the projection framework. The same concatenation was also performed on the physical side, yielding the complete physical agricultural MRIO. One manual override was applied at this step in both the physical and the monetary matrices: `Agricultural Demand|Crops|Other|Sugar crops` for BRA was set to zero, because the IMAGE estimate for this cell was implausibly large, while the large consumption of Sugar crops in BRA used for liquid biofuel production consistent with reality[20]

had already been reflected in energy use.

S1.2.3.5 Heavy industry and transport This subsection describes how the prospective physical and monetary outputs of the four heavy industries (Chemicals, Iron and Steel, Pulp and Paper, Non-metallic Minerals) and the four transport modes (Air, Other land, Railway, Water transport) were obtained. IMAGE reports physical production for these sectors but no monetary output, so monetization relied on a single historical price anchor from EXIOBASE 2015. We chose 2015 rather than 2019 because IMAGE reports outputs only on a five-year time grid (. . . , 2015, 2020, 2025, . . .), and the 2020 step coincides with the COVID-19 pandemic, which would have distorted the implicit price anchor.

Step 1: Physical output extraction from IMAGE. Sectoral physical outputs were extracted as `Production|*` (in Mt) for the four heavy industries and `EnergyService|Transportation|*` (in billion tonne-km) for the four transport modes, then aggregated from the 26 IMAGE regions to the 20-region unified resolution and from IMAGE-specific products to the unified product list through the concordances (SI2).

Step 2: Monetization using EXIOBASE-derived implicit prices.

- **Implicit price from a single historical anchor**: for each region–product pair, the implicit price was set as the ratio of EXIOBASE 2015 monetary product output to the corresponding IMAGE 2015 physical production (Eq. S9). This was equivalent to assuming constant historical prices that were carried forward unchanged.

- **Filling missing prices**: region–product pairs for which IMAGE reported zero physical production in 2015 (so that the implicit price was undefined) were filled with the mean implicit price of the same product across regions where production was non-zero.

- **Manual corrections**: a small number of implicit prices were then manually corrected because the underlying EXIOBASE monetary output appeared underestimated, which would otherwise drive the prospective monetary output below the cost of energy inputs in the input–output check (Section S1.2.3.6):

- Water and railway transport services in MEX: replaced by the average of RAM and BRA.
- Water transport services in CEU: set to half the price of WEU.

- **Price application**: the corrected implicit prices were applied to the IMAGE physical production under SSP2 for every scenario year to obtain the prospective monetary outputs in $2010.

$$\pi_{r,p}^{\text{impl}} = \frac{M_{r,p}^{\text{EXIO,2015}}}{Q_{r,p}^{\text{IMAGE,2015}}} \tag{S9}$$

Where:

- r is the producing region and p indexes the heavy industry or transport product at the unified resolution.
- $M_{r,p}^{\text{EXIO,2015}}$ is the EXIOBASE 2015 monetary product output (in billions of $2010 after deflator conversion).
- $Q_{r,p}^{\text{IMAGE,2015}}$ is the corresponding IMAGE 2015 physical production (in Mt for industries or billion tonne-km for transports).
- $\pi_{r,p}^{\text{impl}}$ is the resulting implicit producer price.

S1.2.3.6 Input–output consistency check Once the prospective physical and monetary tables had been assembled for all sectors, we ran a battery of input–output consistency checks at the unified 20-region resolution to detect potential inconsistencies and conduct corrections. Consistent with the scope of the IMAGE preprocessing described above, the checks were run for SSP2 only but across all scenario years from 2025 onwards, so that any inconsistency observed at any point along the SSP2 timeline was recorded and traced back to its source, rather than only diagnosing the target year 2035. Only the 2035 SSP2 outputs

were retained for the downstream Leontief projection and optimization. We separated *physical* checks (in EJ, on the physical energy use table) from *monetary* checks (in $2010, on the monetized outputs of the previous subsections), then summarized all corrections that were introduced earlier as a consequence of these checks plus the inconsistency screening in the energy preprocessing.

Physical checks (in EJ, on the physical energy use table).

- **Secondary energy product balance**: physical inputs vs. physical output for each secondary energy product, per region. The check was run on Heat, Hydrogen, and the five fuel-specific electricity sub-products (Electricity by coal, by natural gas, by oil, by solid biofuels, and by hydrogen). For each product, the physical output was calculated by summing demand across all consuming sectors, then compared against the physical input from the corresponding upstream energy carriers.

Monetary checks (in $2010, on the monetized outputs of the previous subsections). For each producing sector, the monetary cost of inputs was compared with the monetary output, per region:

- **Heavy industry and transport**: monetary energy inputs vs. monetary output of each heavy-industry sector (Chemicals, Iron and Steel, Pulp and Paper, Non-metallic Minerals) and transport mode (Air, Other land, Railway, Water transport).
- **Biofuel production**: monetary crop inputs vs. monetary output of Liquid biofuels and Modern solid biofuels production. Traditional solid biofuels were excluded because they carried a zero price by construction (Section S1.2.3.4).
- **Secondary energy production**: monetary energy inputs vs. monetary output of electricity (aggregate Electricity), heat, and hydrogen production.
- **Zero-input / zero-output screening**: non-zero monetary output with zero monetary input, and non-zero monetary input with zero monetary output, both flagged as inconsistencies in the scenario data.

Summary of abnormalities and corrections introduced earlier. The abnormalities flagged by the checks above and by the inconsistency screening in the energy preprocessing were resolved by the following corrections, all already described in the relevant earlier subsection:

- **Energy demand and supply, Step 1.4 (heat balance)**: for many regions and years, the flagged imbalance was that `Final Energy|*|Heat` exceeded the primary-energy inputs derived from `Secondary Energy|Heat` divided by the conversion efficiency. Tracing the chain, the secondary-to-primary link was consistent, while `Final Energy|*|Heat` already exceeded `Secondary Energy|Heat` in IMAGE itself, contradicting the expected energy-loss direction. Where this occurred, `Secondary Energy|Heat` (and its `|*` input breakdown) was scaled up to (regional sum of sectoral and residential heat demand) / 0.85. Where `Secondary Energy|Heat` was zero at a flagged point, the corresponding Heat row in `energy-to-sector` was set to zero for that region.

- **Energy demand and supply, Step 1.4 (electricity balance)**: for several electricity sub-products in specific regions and years, the inferred output (`FinalEnergy|*|Electricity` disaggregated by `Secondary Energy|Electricity|*` ratios) exceeded the input from `Primary Energy|*|Electricity`, which would imply impossible conversion efficiencies. The link from final to secondary energy was consistent. The source was where `Primary Energy|*|Electricity` was underestimated relative to `SecondaryEnergy|Electricity|*` in the affected years while remaining consistent in other years. Accordingly, for $f \in$ {Biomass, Oil, Gas, Coal}, where `SecondaryEnergy|Electricity|f` exceeded `PrimaryEnergy|f|Electricity`, the latter was scaled up to match using the average regional efficiency from non-flagged years. The specific cases corrected are:

  - BRA, electricity by solid biofuels, 2025–2050: `Primary Energy|Biomass|Electricity` estimated from the average efficiency in other years.

  - CHN, electricity by oil, 2030: `Primary Energy|Oil|Electricity` estimated from the average efficiency in other years.
  - CEU, electricity by natural gas, 2035–2040: `Primary Energy|Gas|Electricity` estimated from the average efficiency in other years.

- **Agriculture demand and supply, Step 2.1 (sugar prices)**: the base prices of sugar cane and sugar beet in CHN, RAM, and RAS were replaced by the average of structurally comparable regions (BRA and MEX for RAM; INDIA, INDO, ME, TUR, RUS for CHN and RAS), to avoid monetary biofuel output being much higher than the cost of crop inputs.

- **Heavy industry and transport, Step 2 (transport prices)**: the implicit prices of water and railway transport services in MEX were replaced by the average of RAM and BRA, and the implicit price of water transport services in CEU was set to half the price of WEU. Both corrections targeted the energy-versus-sector-output monetary check.

After applying the corrections above, no abnormalities remained in any of the physical or monetary checks across all SSP2 scenario years.

S1.3 Leontief-based projection framework

Inputs. The aggregated EXIOBASE 2019 base coefficient matrices (B, D, L) and final-use matrix Y, together with the monetized IMAGE energy and agricultural use tables and the heavy-industry/transport sector-output table at the unified resolution, all from the preprocessing step (Section S1.2).

What this step does. Three matrix modifications $D \to D'$, $\{B, L\} \to \{B', L'\}$, and $Y \to Y'$ integrated the IMAGE-derived energy, agriculture, and heavy-industry/transport information into the EXIOBASE 2019 base. The Leontief equations were then applied to obtain the projected flows, followed by a post-projection cleaning step that narrowed the

magnitude range fed to the downstream optimization. All values were expressed in billions of $2010, consistent with the unified MRIO unit.

Outputs. The Leontief-based projected matrices A', L', Z', V', and F' at the unified resolution, and Z', V', and F' served as the base flows for the optimization step (Section S1.4.1).

S1.3.1 Construction of D'

The supply-share matrix D was modified to D' by zeroing the entire product-column and sector-row of every IMAGE-relevant product–sector pair, and then setting the entry at the intersection of the pair's principal sector and principal product to one. (Strictly speaking this is not a diagonal entry, since the rows of D index region–sectors and the columns index region–products. The operation pinned the supply share of the principal product to its principal sector and broke any secondary supply links.) This enforced a one-to-one product–sector mapping consistent with the physical modelling of IMAGE. The same construction was applied to newly created sectors and products that did not exist in EXIOBASE (hydrogen, electricity from hydrogen, woody-biomass, non-woody biomass, residue, liquid biofuels, and modern solid biofuels): their sector-row and product-column in D' were populated only at the principal sector–product entry with a value of one, so that they entered the projection with a fully specified supply share. For regional products without any supply in the base D (manure, traditional solid biofuels, and biogas in certain regions), the principal sector–product entry was likewise set to one, so that any downstream use of these products in B' had a defined source sector. After these modifications, every product column of D' was renormalized to sum to one. This step was needed because zeroing the sector-row of an IMAGE-relevant pair also removed that sector's secondary supply of other products, leaving those product columns summing to less than one. Table S5 lists the IMAGE-relevant product–sector pairs used for this construction.

Table S5. IMAGE-relevant product–sector pairs and agent-sector assignments at unified resolution. The agent sectors are proxies for sectors available in IMAGE but newly added in EXIOBASE.

Product	**Sector**	**Agent sector (for B', L')**
Wheat	Cultivation of wheat	–
Woody solid biomass for biofuels	Production of woody solid biomass	Forestry, logging and related service activities (02)
Non-woody solid biomass for biofuels	Production of non-woody solid biomass	Cultivation of plant-based fibers
Paddy rice	Cultivation of paddy rice	–
Sugar cane, sugar beet	Cultivation of sugar cane, sugar beet	–
Oil seeds	Cultivation of oil seeds	–
Cereal grains n.e.c.	Cultivation of cereal grains n.e.c.	–
Vegetables, fruit, nuts	Cultivation of vegetables, fruit, nuts	–
Plant-based fibers	Cultivation of plant-based fibers	–
Crops n.e.c.	Cultivation of crops n.e.c.	–
Residue for solid biofuels	Production of residue	Cultivation of cereal grains n.e.c.
Heat	Steam and hot water supply	–
Electricity by coal	Production of electricity by coal	–
Electricity by hydro	Production of electricity by hydro	–
Electricity by natural gas	Production of electricity by natural gas	–
Electricity by solar photovoltaic	Production of electricity by solar photovoltaic	–
Electricity by Geothermal	Production of electricity by Geothermal	–
Electricity by solar thermal	Production of electricity by solar thermal	–
Electricity by hydrogen	Production of electricity by hydrogen	Production of electricity by natural gas
Electricity by nuclear	Production of electricity by nuclear	–
Electricity by other	Production of electricity by other	–
Electricity by wind	Production of electricity by wind	–
Electricity by solid biofuels	Production of electricity by solid biofuels	–
Electricity by oil	Production of electricity by oil	–
Hydrogen	Production of hydrogen	Chemical production

Continued on next page

Product	Sector	Agent sector
Modern solid biofuels	Production of solid biofuels	Production of paper, pulp and print
Liquid biofuels	Production of liquid biofuels	Chemical production
Coal	Production of coal	–
Natural gas	Production of natural gas	–
Oil	Production of oil	–
Non-metallic minerals	Manufacture of Non-metallic minerals	–
Air transport services	Air transport	–
Chemicals	Chemical production	–
Iron and steel	Production of iron and steel	–
Other land transportation services	Other land transport	–
Paper, pulp and print	Production of paper, pulp and print	–
Railway transportation services	Transport via railways	–
Water transportation services	Water transport	–
Ruminant livestock	Ruminant livestock farming	–
Non-ruminant livestock	Non-ruminant livestock farming	–
Manure (conventional treatment)	Manure treatment (conventional), storage and land application	–
Manure (biogas treatment)	Manure treatment (biogas), storage and land application	–

S1.3.2 Construction of B' and L'

The base B and L coefficients were first prepared by filling the empty columns produced by EXIOBASE for sectors with zero output and by the newly created sectors:

- Before the peer/agent fill, columns where every B entry was zero but the L entry was non-zero (an EXIOBASE rounding artefact for sectors with effectively zero throughput) were detected, and the L entry was forced to zero so that the subsequent fill operated on consistently empty columns.

- For a regional sector with zero output in EXIOBASE, both the B column and the L entry of the same column were filled with the peer mean across other regions for the same sector.

- For a sector that did not exist in EXIOBASE (the newly created sectors, including production of hydrogen, electricity from hydrogen, woody-biomass, non-woody biomass, residue, liquid biofuels, and modern solid biofuels), both the B column and the L entry of the same column were filled by copying the column of a designated agent sector in the same region. The agent-sector mapping is listed in Table S5. The use coefficients of these new sectors therefore entered the projection as a copy of the agent-sector pattern, before being overwritten where IMAGE energy and agriculture information was integrated (as below).

- Sectors with neither a peer nor an agent (manure in our preprocessing) were left as zero columns.

IMAGE energy and agriculture information was then integrated through two pathways. The first pathway applied to sectors where IMAGE provides both energy or crop inputs and the corresponding sector output (the heavy industries, transport modes, and secondary energy production sectors—biofuels, electricity by coal/oil/gas/biofuels/hydrogen, heat, and hydrogen production): coefficients were calculated for the IMAGE energy or crop rows and substituted into B as a complete block, including zero entries. The residual B rows together with the L entry of the same column were then adjusted to preserve the column-sum constraint (Eq. S10). For the secondary energy production sectors, this block substitution enforced the IMAGE accounting convention that the column contained only fuel inputs for energy transformation: the energy-industry own use that EXIOBASE attributed to these sectors (e.g., own electricity or non-energy carriers consumed inside electricity-from-coal) sat on the substituted rows and was therefore zeroed out in B', while the corresponding own-use volumes were captured under the Other Industries aggregate, integrated through the second

pathway. Four cases were distinguished by the new IMAGE coefficient sum (the column sum of the substituted IMAGE rows) and the original column sum of the same rows in the base coefficient:

- **Zero IMAGE output** (new sum = 0): the entire column of B' and L' was set to zero, since the sector was inactive in the scenario.
- **Negative-VA case** (new sum > 1 and original sum < 1): the residual B rows were left unchanged and L' was assigned a negative value to absorb the excess, representing a production subsidy.
- **Existing negative VA preserved** (new sum < 1 and original sum > 1): L' was kept at its base negative value, and the residual B rows were proportionally scaled so that the column sum returned to one.
- **Standard case** (new sum and original sum on the same side of 1, i.e., both < 1 or both > 1): the residual B rows and L' were proportionally scaled together by a single factor to preserve their relative composition, regardless of whether L' was negative or positive.

$$\sum_i B'_{i,j} + L'_j = 1 \quad \text{for all active region-sectors } j. \tag{S10}$$

The second pathway applied to sectors where IMAGE provides only aggregated-sector inputs without a sector-specific output, namely the IMAGE aggregated sectors Agriculture, Food Processing, Other Industries, and Other Sector for energy consumption, together with the Food, Feed, and Other agricultural consumption purposes (covering both crop and livestock products). Treatment depended on the IMAGE aggregated-sector output and on the type of input:

- **Zero IMAGE aggregated-sector output.** If the IMAGE structural-share column

summed to zero (the corresponding aggregated IMAGE sector had zero scenario production), the entire pMRIO sector column of B' and L' was set to zero.

- **Energy products, and agricultural products for the Food and Feed purposes.** The existing total energy or agricultural input of each pMRIO sector was preserved and reallocated across supplier products and regions in proportion to the IMAGE structural shares.

- **Agricultural products for the Other purpose** (mainly food processing such as livestock processing and rice processing). Agricultural products were assumed not substitutable across products, so for each product separately the input of the pMRIO sector was preserved and reallocated across supplier regions only, in proportion to the IMAGE structural shares. Two sub-rules applied:

  - If the EXIOBASE input of a given agricultural product in the pMRIO sector was already zero, no reallocation was performed for that product even when the IMAGE shares were positive: introducing a non-substitutable agricultural input that did not exist in EXIOBASE was treated as out of scope for this step.

  - If the IMAGE shares for an agricultural product were uniformly zero across all suppliers, the column entries for that product were zeroed and the remaining B' entries together with L' were rescaled so that the column sum stayed at one.

Table S7 summarizes which sectors use coefficients versus structural ratios.

Table S7: Availability of IMAGE scenario data for inputs and sectoral outputs. Blue checkmarks (✓) indicate cells where both input data and total sector output were available, enabling coefficients to be calculated directly. Brown checkmarks (✓) indicate cells where input data were available but total sector output was not. Text entries indicate cells where input data were unavailable, and the text names the broader IMAGE consumption purpose that covers the consuming sector and has inputs available.

Consuming Sector	**Energy Products**	**Agricultural Products**	**Total Sector Output**
Energy production	✓	✓	✓
Heavy industries	✓	Other	✓
Transport	✓	Other	✓
Crop production	Agriculture	Other	✓
Livestock production	Agriculture	Feed	✓
Other industry	Other Industries	Other	-
Other agriculture	Agriculture	Other	-
Commercial services	✓	Food	-
Food processing	✓	Other	-
Final demand	✓	Food	-

S1.3.3 Construction of Y' and Leontief solve

The final-use matrix Y was modified to Y' in two stages:

- Each region-product was mapped to one of the three IMAGE major VA sectors (agriculture, industry, services) through the product-to-major-VA-sector concordance (SI2), and the corresponding region-product entry of Y was scaled by the ratio of IMAGE 2035 SSP2 VA to EXIOBASE 2019 VA in that major sector for that region (Eq. S11).

- The energy rows of Y' were then directly overwritten with the monetary residential energy demand from IMAGE, and the agriculture rows were reallocated across agricultural products and supplier regions in proportion to the IMAGE structural shares of agricultural products for the Food purpose, while preserving each demand region's total final expenditure on agricultural products.

$$Y'_{(r,p),d} = Y_{(r,p),d} \cdot \frac{V^{\text{IMAGE},2035}_{r,m(p)}}{V^{\text{EXIO},2019}_{r,m(p)}} \tag{S11}$$

Where:

- r is the supplying region.
- p is the supplying product.
- d is the final-demand region.
- $m(p)$ is the IMAGE major VA sector (agriculture, industry, or services) to which product p is mapped through the product-to-major-VA-sector concordance (SI2).
- $Y_{(r,p),d}$ and $Y'_{(r,p),d}$ are the base-year and modified final-use entries.
- $V^{\text{EXIO},2019}_{r,m(p)}$ is the EXIOBASE 2019 value added of region r aggregated to major VA sector $m(p)$.
- $V^{\text{IMAGE},2035}_{r,m(p)}$ is the IMAGE 2035 SSP2 value added of region r in major VA sector $m(p)$.

Rationale for the value-added-based scaling of Y. The structure of value added and the structure of final demand are positively correlated through two mutually reinforcing mechanisms, which together motivated using the regional VA ratio as the scaling factor for Y. First, a price effect[21]: in agriculture and parts of industry, productivity gains over the projection horizon outpace the increase in labour costs (and hence value added), so the producer price falls while the producer price for services rises. Since the direct and indirect demand for these products also grows more slowly than for services, sector output and the corresponding final expenditure on agricultural and industrial products grow more slowly than on services. Second, an income effect[22]: as regional incomes rise, household preferences shift toward services, raising the services share of consumption expenditure. Scaling Y by the regional VA ratio at the IMAGE major-sector level therefore reflected the structural shift of the regional economy implied by the scenario. The direction of this shift depends on the region's stage of development—in lower-income regions consumption reallocates from agriculture toward industry, while in higher-income regions it reallocates from both agriculture and industry toward services.

With the modified matrices in place, the pMRIO table was projected through the Leontief equations:

$$A' = D'B' \tag{S12}$$

$$F' = D'Y' \tag{S13}$$

$$g' = (I - A')^{-1}F' \tag{S14}$$

$$Z' = A'\hat{g}', \quad V' = L'\hat{g}' \tag{S15}$$

Where:

- D', B', L' are the modified supply-share, use coefficient, and value-added coefficient matrices constructed in the previous subsubsections.
- Y' is the modified final-use matrix and F' is the corresponding sector-side final demand obtained as $D'Y'$.
- A' is the projected intermediate-coefficient matrix.
- g' is the vector of projected region-sector output, obtained by summing $(I - A')^{-1}F'$ across demand regions, and $\hat{g}'$ is its diagonalised form.
- I is the identity matrix.
- Z' is the projected intermediate matrix and V' is the projected value-added row vector ($1\times$ region-sector), distinct from the raw EXIOBASE value-added vector V in Eq. S1.

Post-projection cleaning. The purpose of the post-projection cleaning was to narrow the magnitude range of the data fed into the QCP optimization, which reduced numerical difficulty in the downstream solve. The magnitude threshold 10^{-6} in scaled units (i.e. 10^3 \$2010, or \$1,000) was chosen low enough that (i) the input–output balance of the projection was preserved within the solver's feasibility tolerance (10^{-3} in scaled units), and (ii) the

cleaned zero/non-zero pattern remained consistent with the IMAGE-derived energy and agriculture tables. The latter consistency mattered because in the QCP optimization the prior values from the projection entered as fixed parameters multiplied by scaling-factor variables, and to reduce numerical difficulty these scaling-factor variables were locked at zero where the projected flow was zero and bounded strictly positive otherwise. As a consequence, the optimization could rescale the magnitude of any retained flow but could not turn an existing zero into a non-zero, or vice versa, so any zero/non-zero disagreement between the cleaned projection and the IMAGE inputs would have left the IMAGE constraint unsatisfiable.

- **Magnitude cleaning of intermediate flows and value added.** Any element of F', Z', or V' with absolute value below 10^{-6} in scaled units was set to zero. The coefficient matrix A' itself was not cleaned, because A' was not consumed by the downstream optimization. Only the cleaned flow matrices and their product-side counterparts (recomputed below) were passed forward. As a residual safeguard, in the rare case where this magnitude cleaning zeroed a sector's input side (its column in Z' together with its entry in V') while its output side (its row in Z' together with its row in F') still carried non-zero entries, or vice versa, both sides of that sector were then forced to zero so the sector was consistently inactive.

- **Sign-consistency reconciliation against IMAGE.** The cleaned $Z' + F'$ was aggregated to the IMAGE agriculture, energy, and heavy-industry / transport resolution and compared cell-by-cell against the corresponding IMAGE-derived inputs (the agricultural use table, the energy use table, and the heavy-industry / transport sector-output table). Where the cleaned projection was zero but the corresponding IMAGE input was non-zero, the IMAGE-side input was forcibly set to zero. The reverse case—non-zero in the cleaned projection where IMAGE was zero—did not arise: the projection inherited IMAGE's zero pattern through both integration pathways, the Leontief solve preserved that pattern, and magnitude cleaning could only add zeros.

S1.4 Enforcement of scenario data through optimization

Inputs. The Leontief-based projected matrices Z', V', and F' from Section S1.3, together with the IMAGE 2035 SSP2 scenario constraints for GDP, sectoral value added, sector outputs of heavy industries and transports, energy output and consumption, and agricultural output and consumption.

What this step does. A convex quadratic-constraint program (QCP) perturbed the projected flows multiplicatively through cell-specific scaling factors so that the IMAGE scenario data were met as equality constraints, while the deviations of the scaling factors from their column means were minimized. The bound design, the stepwise activation of constraint families, the objective weighting and solver settings, and the post-optimization derivation of the final coefficients and shares are detailed in the following subsubsections.

Outputs. The post-optimization flow matrices Z'', V'', and F'', the derived intermediate-coefficient and value-added-coefficient matrices A'' and L'', and the final-expenditure share matrix E'', all consistent with the IMAGE 2035 SSP2 scenario data and used for the downstream characterization step (Section S1.5).

S1.4.1 Multiplicative scaling-factor formulation and bound design

The optimization perturbed the Leontief-based projection multiplicatively: each entry of Z', V', and F' was multiplied by a cell-specific scaling factor (Eq. S30), and the scaling factors – rather than the transaction flows themselves – were the decision variables. This formulation had two motivations. First, it preserved the zero/non-zero pattern of the Leontief-based projection by construction: zero flows remained zero and could not be activated by the solver, so the structural sparsity inherited from the priori-information integration step (and ultimately from EXIOBASE 2019) was retained as a hard property of every pMRIO table. Second, in combination with the column-mean objective (Eq. S29) it yielded a convex QCP to minimize the coefficient and expenditure share changes, for which CPLEX returned a global optimum whenever feasible. The convexity proof is given in Section S1.4.6. If transaction

flows themselves had been used as decision variables, such a convex QCP could not have been formulated.

Cell-level scaling factor. The bounds on the scaling factors were derived from the magnitudes of the active scenario data themselves rather than chosen arbitrarily. For each scenario constraint family $f \in \{\text{sector outputs, value added, energy consumption, agriculture consumption}\}$, we computed a cell-level closing factor

$$\mathrm{m}_{p,q}^{f} \;=\; \frac{x_{p,q}^{\mathrm{scen},f}}{x_{p,q}^{\mathrm{proj},f}}, \tag{S16}$$

where $x_{p,q}^{\mathrm{scen},f}$ is the IMAGE scenario data for cell (p,q) under family f, and $x_{p,q}^{\mathrm{proj},f}$ is the corresponding Leontief-projected aggregate at the resolution at which family f's constraint applies (e.g., aggregated energy- or crop-consumer resolution for the energy and agriculture consumption constraints, respectively, and region-sector resolution for sector outputs and value added). Conceptually, $\mathrm{m}_{p,q}^{f}$ is the cell-level scaling factor that would be required to close the gap between the Leontief-based projection and the scenario constraints for family f in isolation. Because $\mathrm{m}_{p,q}^{f}$ was grounded in the active scenario data, the resulting bounds were scenario-specific and adapted to the magnitude of the gap actually being closed in each run.

Initial level and standard bounds. The initial level and bounds of each scaling factor depended on its base flow:

- **Cells with zero base flow.** The initial level and both bounds were hard-locked to 0. This substantially shrank the active dimensionality of the QCP – the solver did not explore values for cells whose flow was zero.
- **Cells with non-zero base flow.** The initial level was set to 1 (i.e., the Leontief-based projection itself was the starting point of the optimization), and the bounds were

specified as [min_m, max_m], derived from the cell-level closing factors as

$$\text{min\_m} = \min_{f,(p,q):\, x^{\text{proj},f}_{p,q} \neq 0} \text{m}^f_{p,q}, \qquad \text{max\_m} = \max_{f,(p,q):\, x^{\text{proj},f}_{p,q} \neq 0} \text{m}^f_{p,q}, \tag{S17}$$

taken across all scenario constraint families active in the run. For the SSP2-M 2035 run reported in this paper, this gave min_m $\approx 4.6 \times 10^{-4}$ and max_m $\approx 8.8 \times 10^{3}$ – a sufficiently broad range that the optimum returned was global rather than local. Because the scaling factor was strictly positive, the post-optimization flow inherited the sign and non-zero status of the projected flow.

Exceptions to the standard bounds. Two cell groups departed from the standard [min_m, max_m] rule. First, when all scenario constraints were applied at the same time, applying the standard bounds uniformly produced numerical difficulties. The bounds for cells of agricultural consumption were instead adjusted to $[\text{m}^{\text{crop}}_{p,q} \cdot 10^{-4},\ \text{m}^{\text{crop}}_{p,q} \cdot 10^{4}]$ around the cell-specific closing factor, which aided convergence without sensitizing the global optimum. Second, residential-energy entries within F' were fixed to a scaling factor of 1 in level, lower, and upper bound, so that the IMAGE residential energy demand already plugged into F' during the priori-information integration passed through the optimization unchanged. Table S8 restates these bound conventions in the GAMSpy notation.

S1.4.2 Stepwise enforcement of scenario constraints

The series of pMRIO tables corresponding to individual and cumulative scenario constraints (Table 1 of the main text) was generated by manually toggling which equality equations were active in the GAMSpy script for each run. Each scenario constraint – on GDP, sectoral VA, sector outputs of heavy industries and transports, energy output, energy consumption, agricultural output, and agricultural consumption – was pre-coded as a separate equality equation between the IMAGE target and the corresponding sum of scaled projected flows. To produce a given run, the relevant equations were activated and the others were

commented out, while the input–output balance equation was kept active in every run.

1. Macroeconomic constraints

GDP for each region k under the expenditure approach (equivalently, total output of region k minus intermediate inputs absorbed by region k):

$$\mathrm{GDP}_k \;=\; \sum_{j_1 \in \mathcal{J}(k)} \left(\sum_{j_2} Z'_{j_1,j_2}\, m^{Z'}_{j_1,j_2} \;+\; \sum_{k'} F'_{j_1,k'}\, m^{F'}_{j_1,k'} \right) - \sum_{j_2 \in \mathcal{J}(k)} \sum_{j_1} Z'_{j_1,j_2}\, m^{Z'}_{j_1,j_2}, \qquad \forall k \in \mathcal{R} \tag{S18}$$

Value added aggregated to agriculture, industry, and services for each region k:

$$\mathrm{VA}^{g}_{k} \;=\; \sum_{j_2 \in \mathcal{J}(k) \cap \mathcal{J}(\mathcal{S}_g)} V'_{j_2}\, m^{V'}_{j_2}, \qquad g \in \{\text{agr, ind, ser}\},\ \forall k \in \mathcal{R} \tag{S19}$$

2. Sectoral output constraints

For sectors with exogenous output trajectories (heavy industry and transport, energy, and agriculture), the row sum equals the scenario output:

$$X_{j_1} \;=\; \sum_{j_2} Z'_{j_1,j_2}\, m^{Z'}_{j_1,j_2} \;+\; \sum_{k} F'_{j_1,k}\, m^{F'}_{j_1,k}, \qquad j_1 \in \mathcal{J}(\mathcal{S}_{\text{ind\&tr}} \cup \mathcal{S}_{\text{en}} \cup \mathcal{S}_{\text{ag}}) \tag{S20}$$

3. Energy consumption constraints

For consumer groups defined at an aggregated level in the scenario data, the constraint sums across the corresponding MRIO table sectors:

$$E^{g}_{j_1,k} \;=\; \sum_{j_2 \in \mathcal{J}(k) \cap \mathcal{J}(\mathcal{S}^{g}_{\text{4en}})} Z'_{j_1,j_2}\, m^{Z'}_{j_1,j_2}, \qquad j_1 \in \mathcal{J}(\mathcal{S}_{\text{en}}),\ \forall k \in \mathcal{R} \tag{S21}$$

For consuming sectors that map one-to-one between the scenario data and the MRIO, the constraint is imposed cell-by-cell:

$$E^{\text{single}}_{j_1,j_2} \;=\; Z'_{j_1,j_2}\, m^{Z'}_{j_1,j_2}, \qquad j_1 \in \mathcal{J}(\mathcal{S}_{\text{en}}),\ j_2 \in \mathcal{J}(\mathcal{S}^{\text{single}}_{\text{4en}}) \tag{S22}$$

Residential energy consumption is matched through the final-demand block:

$$E^{\mathrm{res}}_{j_1,k} \;=\; F'_{j_1,k}\, m^{F'}_{j_1,k}, \qquad j_1 \in \mathcal{J}(\mathcal{S}_{\mathrm{en}}),\ \forall k \in \mathcal{R} \tag{S23}$$

4. Agricultural consumption constraints

Feed use aggregates deliveries to livestock and related sectors:

$$C^{\mathrm{feed}}_{j_1,k} \;=\; \sum_{j_2 \in \mathcal{J}(k) \cap \mathcal{J}(\mathcal{S}_{\mathrm{feed}})} Z'_{j_1,j_2}\, m^{Z'}_{j_1,j_2}, \qquad j_1 \in \mathcal{J}(\mathcal{S}_{\mathrm{cr}}),\ \forall k \in \mathcal{R} \tag{S24}$$

Other (industrial) use:

$$C^{\mathrm{other}}_{j_1,k} \;=\; \sum_{j_2 \in \mathcal{J}(k) \cap \mathcal{J}(\mathcal{S}_{\mathrm{other}})} Z'_{j_1,j_2}\, m^{Z'}_{j_1,j_2}, \qquad j_1 \in \mathcal{J}(\mathcal{S}_{\mathrm{cr}}),\ \forall k \in \mathcal{R} \tag{S25}$$

Food use combines intermediate use by food-processing sectors with household final demand:

$$C^{\mathrm{food}}_{j_1,k} \;=\; \sum_{j_2 \in \mathcal{J}(k) \cap \mathcal{J}(\mathcal{S}_{\mathrm{food}})} Z'_{j_1,j_2}\, m^{Z'}_{j_1,j_2} \;+\; F'_{j_1,k}\, m^{F'}_{j_1,k}, \qquad j_1 \in \mathcal{J}(\mathcal{S}_{\mathrm{cr}}),\ \forall k \in \mathcal{R} \tag{S26}$$

Biofuel use is resolved at the cell level:

$$C^{\mathrm{biof}}_{j_1,j_2} \;=\; Z'_{j_1,j_2}\, m^{Z'}_{j_1,j_2}, \qquad j_1 \in \mathcal{J}(\mathcal{S}_{\mathrm{cr}}),\ j_2 \in \mathcal{J}(\mathcal{S}_{\mathrm{biof}}) \tag{S27}$$

5. Input–output balance

For every region-sector, total output equals total input:

$$\sum_{j_2} Z'_{j_1,j_2}\, m^{Z'}_{j_1,j_2} \;+\; \sum_{k} F'_{j_1,k}\, m^{F'}_{j_1,k} \;=\; \sum_{j'_1} Z'_{j'_1,j_1}\, m^{Z'}_{j'_1,j_1} \;+\; V'_{j_1}\, m^{V'}_{j_1}, \qquad \forall j_1 \tag{S28}$$

Notation

Indices and sets:

- $k \in \mathcal{R}$: region
- j_1: supplying region-sector (row index of Z' and F')
- j_2: consuming region-sector (column index of Z'; index of V')
- $\mathcal{S}$: set of sectors; $\mathcal{S}_g$: sectors in group g
- $\mathcal{J}(k)$: region-sectors located in region k
- $\mathcal{J}(\mathcal{S}_g)$: region-sectors belonging to sector group g
- $g \in \{\text{agr, ind, ser}\}$: aggregated sector groups (agriculture, industry, services)

Sector groups:

- $\mathcal{S}_{\text{en}}$: energy sectors
- $\mathcal{S}_{\text{ag}}$: agriculture sectors
- $\mathcal{S}_{\text{ind\&tr}}$: heavy industry and transport sectors
- $\mathcal{S}_{\text{4en}}^{g}$: MRIO sectors in consumer group g that consume energy
- $\mathcal{S}_{\text{4en}}^{\text{single}}$: MRIO sectors that map one-to-one to scenario energy-consuming sectors
- $\mathcal{S}_{\text{feed}}$, $\mathcal{S}_{\text{food}}$, $\mathcal{S}_{\text{other}}$, $\mathcal{S}_{\text{biof}}$: MRIO sectors that consume agriculture products for feed, food, other (industrial), and biofuel use, respectively

Matrices (Leontief-based projection):

- Z': intermediate transaction matrix
- V': value-added vector
- F': final-demand matrix

Scaling factors (decision variables):

- $m^{Z'}$, $m^{V'}$, $m^{F'}$: element-wise scaling factors applied to Z', V', F', respectively

Scenario constraints:

- GDP_k: regional gross domestic product
- VA_k^g: value added in sector group g in region k
- X_{j_1}: total output of region-sector j_1
- $E_{j_1,k}^{g}$, $E_{j_1,j_2}^{\text{single}}$, $E_{j_1,k}^{\text{res}}$: energy consumption by aggregated consumer group, one-to-one consumer, and residential, respectively
- $C_{j_1,k}^{\text{feed}}$, $C_{j_1,k}^{\text{food}}$, $C_{j_1,k}^{\text{other}}$, $C_{j_1,j_2}^{\text{biof}}$: agriculture consumption by use category

S1.4.3 Objective weighting and solver configuration

The objective function used in the optimization (also given in the main text) is restated here:

$$\begin{aligned}\text{Objective} = \min \Bigg[& \frac{1}{N_{\text{non-0}}^{Z'}} \sum_{j_1,j_2} w_{(j_1,j_2)} \left(m_{(j_1,j_2)}^{Z'} - \overline{m}_{j_2}^{Z'\&V'} \right)^2 \\ & + \frac{1}{N_{\text{non-0}}^{V'}} \sum_{j_2} w_{(1,j_2)} \left(m_{(1,j_2)}^{V'} - \overline{m}_{j_2}^{Z'\&V'} \right)^2 \\ & + \frac{1}{N_{\text{non-0}}^{F'}} \sum_{j_1,k} w_{(j_1,k)} \left(m_{(j_1,k)}^{F'} - \overline{m}_{k}^{F'} \right)^2 \Bigg]\end{aligned} \tag{S29}$$

Implementation-level details:

- The flow-magnitude weight w was implemented as a parameter taking the value 100 for cells whose absolute Leontief-projected flow exceeded 10^6 \$2010 and 1 otherwise, and applied element-wise inside the squared-deviation sums for Z', V', and F'. Therefore, the optimization penalized coefficient deviations more heavily for cells with larger projected flows.

- The squared deviations and the column-mean denominator were both restricted to only non-zero scaling factors, so that zero cells did not contribute to the objective. Therefore, the solver only saw, and only penalized deviations among, scaling factors that actually multiplied non-zero flows.

The optimization was solved with the CPLEX QCP solver via the GAMSpy interface, under the following non-default options:

- `quality = 1`: request the highest solution quality.
- `scaind = 1`: enable aggressive scaling.
- `numericalemphasis = 1`: prioritize numerical stability over speed.
- `eprhs` = 10^{-3}: relative feasibility tolerance for the equality constraints.

These settings were necessary to handle the wide range of magnitudes in the pMRIO table and to avoid early termination when many scenario constraints were simultaneously active.

S1.4.4 Post-optimization derivation

Once the optimization returned the optimal scaling factors $m^{Z'}$, $m^{V'}$, and $m^{F'}$, the final prospective matrices were derived following the equations of the main text, restated here:

$$Z''_{j_1,j_2} = m^{Z'}_{j_1,j_2} \cdot Z'_{j_1,j_2}, \quad V''_{1,j_2} = m^{V'}_{1,j_2} \cdot V'_{1,j_2}, \quad F''_{j_1,k} = m^{F'}_{j_1,k} \cdot F'_{j_1,k} \tag{S30}$$

$$g''_{j_2} = \sum_{j_1} Z''_{j_1,j_2} + V''_{1,j_2} \tag{S31}$$

$$A''_{j_1,j_2} = \frac{Z''_{j_1,j_2}}{g''_{j_2}}, \quad L''_{1,j_2} = \frac{V''_{1,j_2}}{g''_{j_2}} \tag{S32}$$

$$E''_{j_1,k} = \frac{F''_{j_1,k}}{\sum_{j_1} F''_{j_1,k}} \tag{S33}$$

Where:

- j_1 and j_2 are region-sector indices and k is the final-demand region index.
- $F''_{j_1,k}$ is the post-optimization final demand entry from Eq. S30.
- $E''_{j_1,k}$ is the final-expenditure share matrix at the post-optimization stage.

S1.4.5 Technical summary of the optimization in GAMSpy

Table S8 summarizes the decision variables, parameters, equality constraints, and objective of the QCP optimization, with names matching the GAMSpy implementation. The scaling-factor variables (`Z_m`, `V_m`, `F_m`) follow the initial-level and bound design described in Section S1.4.1. The table only states their domain and the residential-energy exception specific to `F_m`. Each scenario run activates only a subset of the equality constraints. `io_bal_cons` is active in every run, while the remaining scenario constraints are toggled on per Table 1 of the main text. Index conventions: r, s index the supplying region-sector and r', s' the consuming region-sector, and k indexes the final-demand region.

Table S8. Technical summary of the QCP optimization.

GAMSpy symbol	**Meaning**
Decision variables and bounds	
`Z_m`	Cell-specific scaling factor $m^{Z'}$ for the projected Z' flow over (r, s, r', s'). Initial level and bounds per Section S1.4.1.
`V_m`	Cell-specific scaling factor $m^{V'}$ for the projected V' over (r', s'). Initial level and bounds analogous to `Z_m` per Section S1.4.1.

Continued on next page

GAMSpy symbol	Meaning
`F_m`	Cell-specific scaling factor $m^{F'}$ for the projected F' over (r, s, r'). Initial level and bounds analogous to `Z_m` per Section S1.4.1, except residential-energy entries are fixed to 1 in level, lower, and upper bound and therefore pass through the optimization unchanged.
`m_col_mean`	Column mean $\overline{m}_{j_2}^{Z'\&V'}$ of `Z_m` and `V_m` per region-sector (r', s'), restricted to non-zero scaling factors. Free variable.
`m_col_fd_mean`	Column mean $\overline{m}_{k}^{F'}$ of `F_m` per final-demand region r', restricted to non-zero scaling factors. Free variable.
Parameters	
`Z_start_param`, `F_start_param`, `V_start_param`	Leontief-projected Z', F', and V' entries (in billions of \$2010) that the scaling factors multiply to produce the post-optimization flows.
`Z_wt_param`, `F_wt_param`, `V_wt_param`	Flow-magnitude weights w in the objective: 100 for cells whose absolute base flow exceeds 10^6 \$2010, 1 otherwise.
`GDP_new_param`	Regional GDP target in 2035 under SSP2.
`VA_agr_new_param`, `VA_ind_new_param`, `VA_ser_new_param`	Regional value-added targets for the three IMAGE major sectors (agriculture, industry, services).
`SecOut_IndTransp_new_param`, `SecOut_Energy_new_param`, `SecOut_Crop_new_param`	Sector-output targets for heavy-industry/transport sectors, energy-producing sectors, and crop sectors.
`Crop4Feed_new_param`, `Crop4Food_new_param`, `Crop4Other_new_param`	Crop and livestock consumption targets per (region-product, consumer region) at the IMAGE aggregated-consumer resolution for the feed, food, and other purposes.

Continued on next page

GAMSpy symbol	Meaning
`Crop4Biof_new_param`	Crop consumption targets per cell for the biofuel-producing sectors.
`Energy4Other_new_param`, `Energy4OtherInd_new_param`, `Energy4FoodPro_new_param`, `Energy4Agr_new_param`	Energy consumption targets at the IMAGE aggregated-sector resolution (Other Sector, Other Industries, Food Processing, Agriculture).
`Energy4SingSec_new_param`	Energy consumption targets per cell for individual scenario-relevant sectors (heavy industry, transport, biofuel production).
`Energy4Resid_new_param`	Residential energy consumption targets, applied to F'.
`N_non0_per_col_param`, `N_non0_per_col_fd_param`	Number of non-zero scaling factors per region-sector column and per final-demand region column, used as denominators when computing column means.
Equality constraints	
`io_bal_cons`	Input–output balance per region-sector after scaling: total inputs (intermediate + value added) equal total outputs (intermediate + final demand). Active in every run.
`gdp_exp_cons`	Regional GDP expression matches `GDP_new_param`.
`va_cons_agr`, `va_cons_ind`, `va_cons_ser`	Sum of scaled V' flows over each major-VA sector matches the corresponding IMAGE VA target.
`sec_out_ind_transp_cons`, `sec_out_energy_cons`, `sec_out_crop_cons`	Total scaled output of each region-sector matches the IMAGE sector-output target for the three sector groups.
`crop4feed_cons`, `crop4food_cons`, `crop4other_cons`	Sum of scaled A' (and, for food, F') flows over the relevant consumer group matches the corresponding crop-consumption target per (region-product, consumer region).

Continued on next page

GAMSpy symbol	Meaning
`crop4biofuel_cons`	Cell-level equality of scaled A' flows for biofuel-producing sectors against their crop-input targets.
`energy4other_cons`, `energy4otherind_cons`, `energy4foodpro_cons`, `energy4agr_cons`	Sum of scaled A' flows over each IMAGE aggregated consumer matches the corresponding energy-consumption target.
`energy4singsec_cons`	Cell-level equality for energy inputs to scenario-relevant single sectors.
`energy4residential_cons`	Cell-level equality for residential energy in F'.
`m_col_mean_cons`, `m_col_fd_mean_cons`	Define $\overline{m}_{j_2}^{Z'\&V'}$ and $\overline{m}_k^{F'}$ as the average of the non-zero scaling factors in their respective columns.
`obj_def`	Defines obj_val as the right-hand side of Eq. S29.
Objective	
min obj_val	Weighted sum of squared deviations of the scaling factors from their column means (Eq. S29), normalized by the number of non-zero scaling factors in each of Z', V', and F'.

S1.4.6 Proof of convexity of the QCP objective function

The QCP objective (Eq. S29) is a weighted sum of squared deviations of the scaling factors from their column means. Below we show that, after eliminating the column-mean variables through their defining linear equalities, this objective is a convex quadratic form in the scaling factors. Together with the linear equality constraints (input–output balance, scenario constraints, and the column-mean definitions) and the box bounds from Section S1.4.1, the optimization is therefore a convex QCP, and CPLEX returns a global optimum whenever the problem is feasible.

Elimination of the column-mean variables. The column means $\overline{m}_{j_2}^{Z'\&V'}$ and $\overline{m}_k^{F'}$

are free variables tied to the scaling factors by the linear equalities `m_col_mean_cons` and `m_col_fd_mean_cons` (Table S8). Because these equalities are linear, each column-mean variable can be replaced by an affine function of the scaling factors. Substituting an affine expression into a quadratic objective preserves convexity, so it suffices to prove convexity of the resulting objective in the scaling factors alone.

Convexity of one column's contribution. Fix a column index j and let $\mathbf{m}_j \in \mathbb{R}^{N_j}$ collect the scaling factors belonging to that column – the joint vector of non-zero `Z_m` and `V_m` entries in region-sector column j_2, or the non-zero `F_m` entries in final-demand region column k – where N_j is the count of non-zero base-flow cells in that column. After substitution, the column mean is the linear functional

$$\overline{m}_j = \frac{1}{N_j}\,\mathbf{1}^\top \mathbf{m}_j, \tag{S34}$$

with $\mathbf{1} \in \mathbb{R}^{N_j}$ the all-ones vector. The deviation vector therefore writes as

$$\mathbf{m}_j - \overline{m}_j\,\mathbf{1} \;=\; P_j\,\mathbf{m}_j, \qquad P_j \;=\; I_{N_j} - \tfrac{1}{N_j}\,\mathbf{1}\mathbf{1}^\top, \tag{S35}$$

where P_j is the centering projection: symmetric ($P_j^\top = P_j$) and idempotent ($P_j^2 = P_j$). Let $W_j = \mathrm{diag}(\tilde{w}_{1,j}, \ldots, \tilde{w}_{N_j,j})$, where each diagonal entry $\tilde{w}_{i,j}$ is the product of the cell's flow-magnitude weight (1 or 100, Section S1.4.3) and the per-matrix normalizer of the matrix to which the cell belongs ($1/N^{Z'}_{\text{non-0}}$ for Z' entries, $1/N^{V'}_{\text{non-0}}$ for V' entries in the joint $Z'\&V'$ column, $1/N^{F'}_{\text{non-0}}$ for F' entries). All $\tilde{w}_{i,j} > 0$, so $W_j \succeq 0$. The column-j contribution to the objective is

$$\Phi_j(\mathbf{m}_j) \;=\; (P_j\mathbf{m}_j)^\top W_j (P_j\mathbf{m}_j) \;=\; \mathbf{m}_j^\top\,(P_j W_j P_j)\,\mathbf{m}_j, \tag{S36}$$

a quadratic form with Hessian $H_j = 2\,P_j W_j P_j$. For any $\mathbf{x} \in \mathbb{R}^{N_j}$,

$$\mathbf{x}^\top H_j \mathbf{x} \;=\; 2\,(P_j\mathbf{x})^\top W_j (P_j\mathbf{x}) \;\geq\; 0, \tag{S37}$$

since $W_j \succeq 0$. Hence H_j is positive semidefinite and Φ_j is convex on $\mathbb{R}^{N_j}$.

Convexity of the full objective. With the per-matrix normalizers already absorbed into the per-cell coefficients in W_j, the full objective in Eq. S29 is the sum of the column contributions Φ_j over all columns of Z', V', and F'. Different columns share no scaling-factor variables, so the Hessian of the full objective is block diagonal with one block H_j per column. A block-diagonal matrix whose blocks are positive semidefinite is itself positive semidefinite, so the full Hessian is positive semidefinite and the full objective is convex.

Conclusion. The bound design of Section S1.4.1 – the hard-locking of zero-flow cells (level and both bounds set to 0), the standard $[\min\_\mathrm{m}, \max\_\mathrm{m}]$ box on non-zero cells, the crop-narrowing rule, and the fix of residential-energy entries to 1 – reduces to box bounds on the scaling factors, which together with the linear equalities yields a polyhedral feasible set. Combined with the convex quadratic objective established above, the box bounds and linear equalities make the optimization a convex QCP, and CPLEX returns a global optimum whenever the problem is feasible. The optimum value is unique. The optimizer need not be, since H_j is positive semidefinite (the all-ones direction $\mathbf{1} \in \ker P_j$ leaves the column-deviation term unchanged) rather than positive definite.

S1.5 Characterization and impact calculations

Inputs. Region- and sector-resolved GHG emissions from IMAGE `Emissions|*` variables (CO_2, CH_4, N_2O) under SSP2 for 2035, the corresponding 2020 anchor for EXIOBASE 2019, and the monetary sector outputs of every psMRIO version under study (EXIOBASE 2019, the Leontief-based projection of Section S1.3, and the optimization-based pMRIO tables of Section S1.4.1).

What this step does. Gas-specific emissions were extracted, gap-filled, mapped to the 20-region unified resolution, aggregated to gas-specific sector groupings, and characterized to GWP_{100} using AR6 100-year factors. Sectoral GWP intensities (Mt CO_2-eq per billion \$2010) were then computed at the gas-specific aggregated-sector resolution and broadcast

to the fine-sector resolution of each MRIO version.

Outputs. A fine-resolution GWP_{100} intensity field $\text{Intensity}_{r,s}^{\text{GWP100}}$ per MRIO version, used downstream in the consumption-based footprint calculations.

S1.5.1 GHG emissions extraction and characterization

We extracted emissions for the three principal greenhouse gases (CO_2, CH_4, and N_2O) from the IMAGE `Emissions|*` variables under SSP2 for the reference year 2035, plus 2020 for the historical EXIOBASE 2019 anchor. Emissions from the final-demand-side residential combustion were out of scope and excluded, which accounted for approximately 1% - 3% of the total global CO_2, CH_4, and N_2O in 2020 and 2035 in IMAGE. Emissions from land fires, land-use change, harvested wood products, and wetlands were excluded because no consistent assignment to producing sectors was available. The set of emission categories pulled per gas reflected the sources actually reported in IMAGE for that gas:

- **CO_2**: energy demand (industries, transports, commercial, and other sectors), energy supply (production of primary and secondary energy carriers), and industrial processes. CO_2 from crop and livestock production was excluded because its magnitude in IMAGE is negligible.

- **CH_4**: energy demand and supply; industrial processes; agriculture (livestock, paddy rice); waste.

- **N_2O**: energy demand and supply; industrial processes; agriculture (managed soils which was assigned to crop cultivation rather than livestock pasture to avoid additional allocation; livestock); waste.

Several preprocessing rules were applied to fill gaps in the IMAGE outputs:

- **Bunkers**: when only international-aviation emissions were reported, international-shipping emissions were derived by scaling aviation emissions with the regional ratio of

`Final Energy|Bunkers|International Shipping` to `Final Energy|Bunkers|International Aviation`.

- **Industrial processes**: Non-Metallic Minerals process emissions were computed as `Industrial Processes` total minus `Industrial Processes|Chemicals` (clipped at zero) when the Non-Metallic Minerals item was not directly reported.
- **Commercial energy demand**: when the Commercial item was missing, it was derived as `Residential and Commercial` minus `Residential`.
- **Liquids energy supply**: detailed liquids variants were used when available. Otherwise the aggregated `Liquids` variable indicated Oil.

The extracted emissions were then mapped from the IMAGE regional resolution to the 20 unified regions through the regional concordance (the IMAGE `World` aggregate was dropped) (SI2), and aggregated within each region to a gas-specific sector resolution through gas-specific concordance columns (`Agg_co2_prod`, `Agg_ch4_prod`, `Agg_n2o_prod` in SI2). Separate concordances were used because CO_2, CH_4, and N_2O originate from different sets of sectors and therefore admit different levels of aggregation.

Each gas was characterized to Mt CO_2-eq using AR6 GWP_{100} characterization factors (consistent with the IPCC Sixth Assessment Report and the GHG Protocol's August 2024 update):

- CO_2: 1.0.
- CH_4 (fossil): 29.8.
- CH_4 (non-fossil, applied to Livestock farming and Cultivation of paddy rice): 27.0.
- N_2O: 273.0 (with unit conversion kt N_2O $\rightarrow$ Mt CO_2-eq).

S1.5.2 Sectoral GWP intensity calculation

We computed sectoral GWP intensity (Mt CO_2-eq per billion \$2010 of sectoral output) for every MRIO version under study — EXIOBASE 2019 (historical), the Leontief-based projection, and the optimization-based pMRIO tables. The reference year was 2020 for EXIOBASE 2019 and 2035 for all prospective versions.

For each gas g and each (region, emission sector) pair (r, a), the gas-specific intensity was computed as the characterized GWP_{100} emission divided by the aggregated monetary output of the corresponding MRIO sectors in the same MRIO version (Eq. S38). The mapping between emission sectors and MRIO sectors was either one-to-one, in which case the output was that of the single matched MRIO sector, or one-to-many, in which case the output was obtained by summing the fine-sector outputs across the gas-specific concordance. Intensities were set to zero where this aggregated output was zero. To produce a single fine-resolution intensity field used downstream in the consumption-based footprint, each fine sector s inherited the intensity of its corresponding emission sector $a(s)$ (Eq. S39); in the one-to-one case, $a(s) = s$. The three gas contributions were summed to obtain the total GWP_{100} intensity (Eq. S40).

$$\text{Intensity}^{g}_{r,a} = \frac{\text{GWP}^{g}_{r,a}}{\sum_{s \in a} x_{r,s}} \tag{S38}$$

$$\text{Intensity}^{g}_{r,s} = \text{Intensity}^{g}_{r,\,a(s)} \tag{S39}$$

$$\text{Intensity}^{\text{GWP100}}_{r,s} = \sum_{g \in \{\text{CO}_2, \text{CH}_4, \text{N}_2\text{O}\}} \text{Intensity}^{g}_{r,s} \tag{S40}$$

Where:

- $g \in \{CO_2, CH_4, N_2O\}$ denotes the gas.
- r is the region. s is a fine-resolution sector and $a(s)$ is its parent in the gas-specific

aggregated emission concordance (`Agg_co2_prod`, `Agg_ch4_prod`, or `Agg_n2o_prod`).

- $\text{GWP}^{g}_{r,a}$ is the GWP_{100}-characterized emission of gas g at (r, a) (Mt CO_2-eq).
- $x_{r,s}$ is the monetary output of fine-resolution region-sector (r, s) (billion \$2010).
- $\text{Intensity}^{g}_{r,a}$ and $\text{Intensity}^{g}_{r,s}$ are the gas-specific intensities at aggregated- and fine-sector resolution. $\text{Intensity}^{\text{GWP100}}_{r,s}$ is the total GWP_{100} intensity at fine resolution.

S1.5.3 Consumption-based footprints calculation

Regional consumption-based carbon footprints were calculated based on EXIOBASE 2019, Leontief-based projection, and the prospective MRIOs under cumulative scenario constraints (Eq.S41). To trace these results back to shifts in sectoral outputs and consumption flows driven by varing level of scenario compliance, we selected Leontief-based projection and the prospective MRIO fully complied with IMAGE as samples, and decomposed their regional footprints into sectoral consumption footprints (Eq.S42). To differentiate between impacts driven by energy and agricultural products, we further disaggregated the total footprints into parts resulting from CO_2 emissions and those from N_2O and CH_4 emissions. This disaggregation was supported by IMAGE data showing that approximately 70% of global CO_2 emissions in 2020 and 2035 resulted from energy consumption, electricity production, and heat production. Consequently, changes in the CO_2-related carbon footprint were primarily driven by the energy footprint (excluding final demand of energy since residential emissions are excluded). Similarly, since agricultural production accounted for the majority of global N_2O and CH_4 emissions, changes in the corresponding carbon footprints were largely driven by the agriculture footprint. Accordingly, energy and agriculture footprints were calculated for each region and decomposed into final demand, direct consumption, and indirect consumption using Equation S43. This decomposition facilitated the mapping of shifts in intermediate flows (Z) and coefficient deviations (A) to these footprints, and ultimately, to environmental outcomes. All footprint data were aggregated into nine regions

and ten sectors to ensure consistency across the analysis.

$$GWP_d = g^\top (I - A)^{-1} f^{(d)} \tag{S41}$$

$$GWP_{sd} = g^\top (I - A)^{-1} \widehat{f^{(d)}} e^{(s)} \tag{S42}$$

$$\begin{aligned} EN_{sd} &= \underbrace{(u^{en})^\top A \widehat{f^{(d)}} e^{(s)}}_{EN_{sd}^{DIR}} + \underbrace{(u^{en})^\top (L - I - A) \widehat{f^{(d)}} e^{(s)}}_{EN_{sd}^{IND}} \\ AG_{sd} &= \underbrace{(u^{ag})^\top I \widehat{f^{(d)}} e^{(s)}}_{AG_{sd}^{FD}} + \underbrace{(u^{ag})^\top A \widehat{f^{(d)}} e^{(s)}}_{AG_{sd}^{DIR}} + \underbrace{(u^{ag})^\top (L - I - A) \widehat{f^{(d)}} e^{(s)}}_{AG_{sd}^{IND}} \end{aligned} \tag{S43}$$

Where:

- A is the intermediate coefficient matrix (region-sector by region-sector); I is the identity matrix.
- $f^{(d)}$ is the final demand vector for region d in final demand matrix F, and $\widehat{f^{(d)}}$ is its diagonalized form.
- g is the vector of impact intensities, which can be about total GWP, GWP from CO_2, or GWP from $N_2O\&CH_4$.
- $e^{(s)}$ is a column vector of zeros with a value of one at the position corresponding to the final supply sector s.
- GWP_d and GWP_{sd} represent total and sectoral consumption-based carbon footprints for final demand region d and final supply sector s.
- u^{en} and u^{ag} are binary sector-selection vectors equal to one for energy and agriculture sectors, respectively.
- EN_{sd} and AG_{sd} represent the sectoral consumption-based energy and agriculture footprints.

- FD, DIR, and IND denote the final demand, direct consumption, and indirect consumption derived from the decomposition $L = I + A + (L - I - A)$.

S2 Results and discussion

S2.1 Technical results from optimization

Table S10 reports the optimization objective and the mean column-wise variance of scaling factors for each constraint setting. Constraint-setting abbreviations follow Table 1.

Table S10: Technical optimization results by constraint setting.

Constraints setting	**Objective result**	**Mean variance (A+V)**	**Mean variance (F)**
KpBlGdpVa	0.02	1.39e-4	3.87e-5
KpBlSeouit	1.89	0.05	2.84e-3
KpBlSeoue	0.02	3.12e-4	2.51e-5
KpBlEnergy	1.27	0.06	1.02e-3
KpBlSeouc	2.97	0.49	8.53e-4
KpBlCrop	838.44	814.39	0.13
KpBlGdpVaSeouit	1.94	0.05	2.71e-3
+Seoue[a]	6.85	0.20	0.02
+Energy[b]	7.81	0.26	0.02
+Seouc[c]	15.07	6.76	0.02
+Crop[d]	902.51	844.75	0.11

Notes: [a]KpBlGdpVaSeouitSeoue. [b]KpBlGdpVaSeouitSeoueEnergy. [c]KpBlGdpVaSeouitSeoueEnergySeouc. [d]KpBlGdpVaSeouitSeoueEnergySeoucCrop.

S2.2 ECDF of coefficient deviations from Leontief based projection

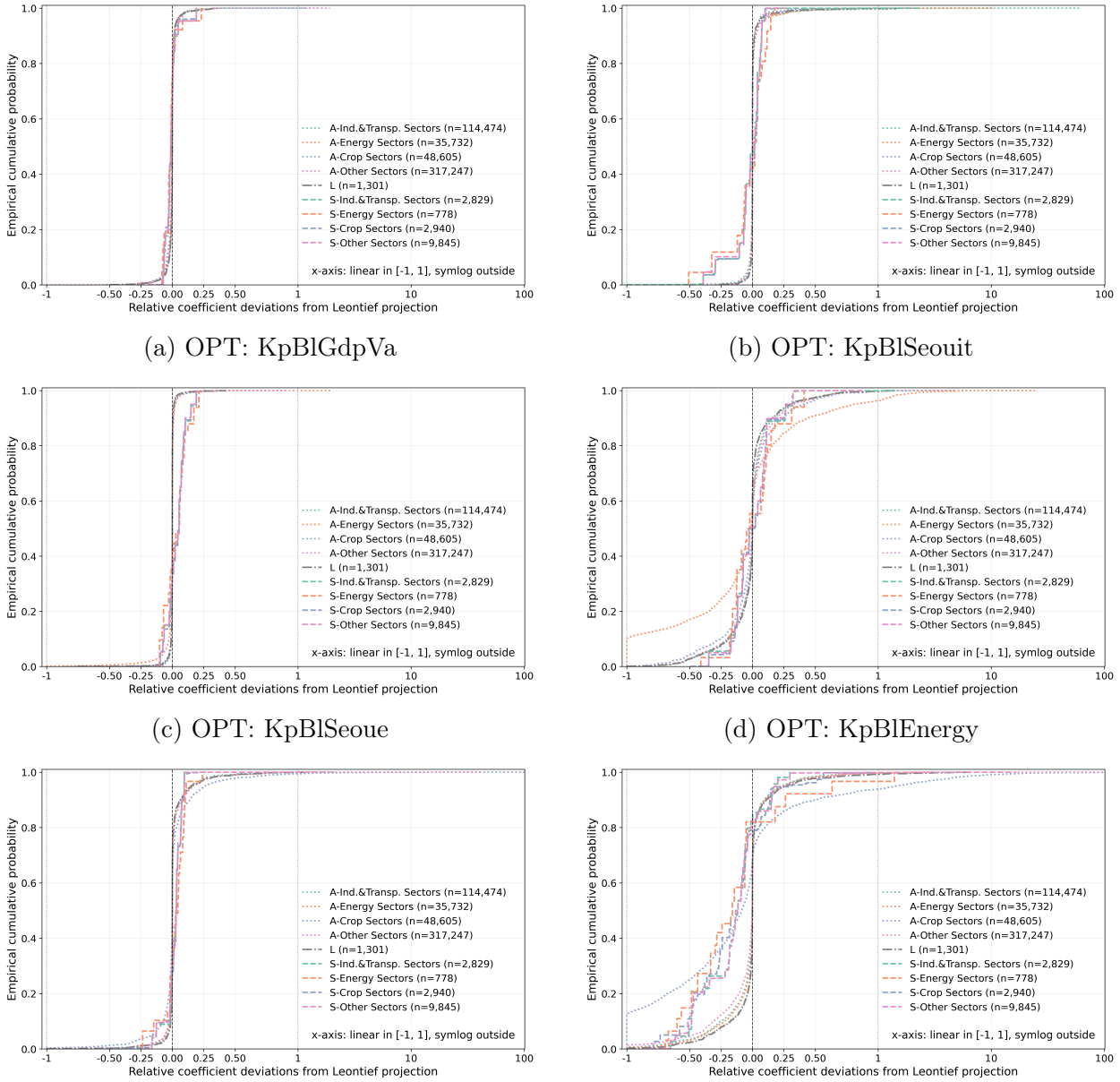

(a) OPT: KpBlGdpVa

(b) OPT: KpBlSeouit

(c) OPT: KpBlSeoue

(d) OPT: KpBlEnergy

(e) OPT: KpBlSecouc

(f) OPT: KpBlCrop

Figure S2: ECDF of relative coefficient deviations in the optimization-based projections under individual constraints from the Leontief-based projection.Coefficients are grouped into four sector groups in intermediate matrix A, four sector groups in expenditure share matrix E, and value added coefficeints V. n is the number of coefficients within each groups.

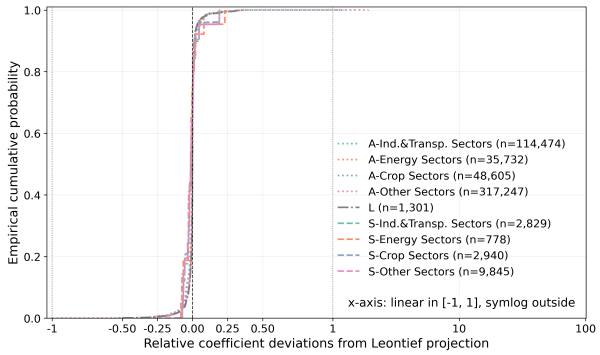

(a) OPT: KpBlGdpVa

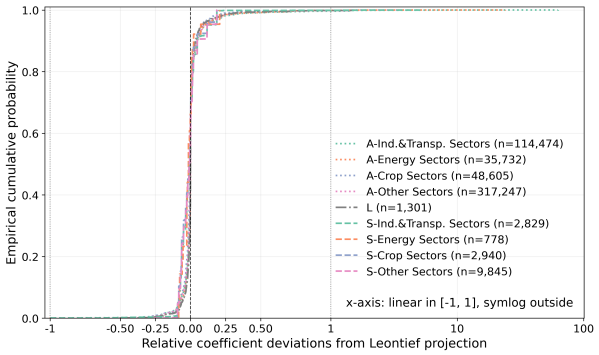

(b) OPT: KpBlGdpVaSeouit

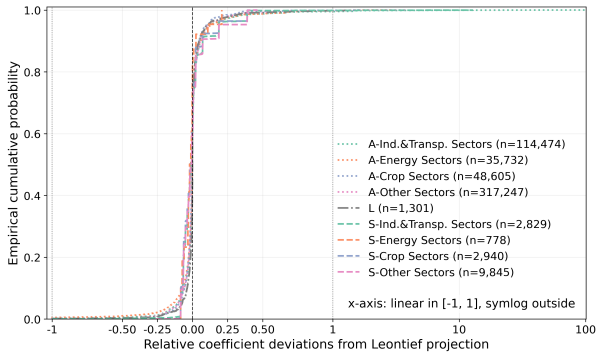

(c) OPT: KpBlGdpVaSeouitSeoue

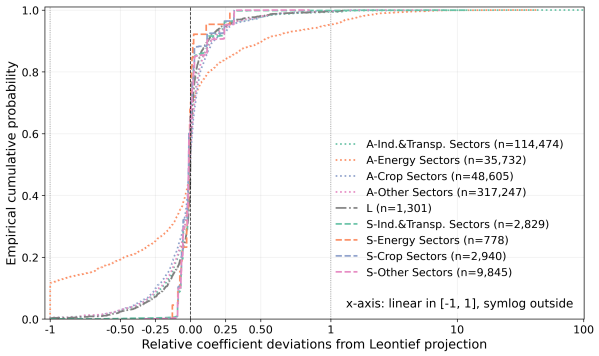

(d) OPT: KpBlGdpVaSeouitSeoueEnergy

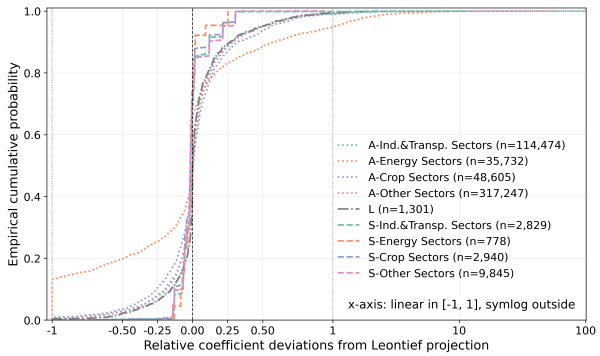

(e) OPT: KpBlGdpVaSeouitSeoueEnergySecouc

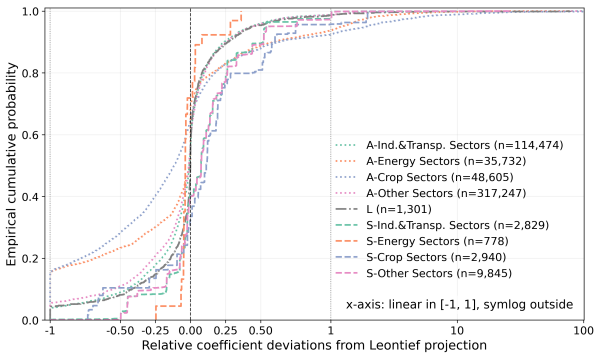

(f) OPT: KpBlGdpVaSeouitSeoueEnergySecoucCrop

Figure S3: ECDF of relative coefficient deviations in the optimization-based projections under cumulative constraints from the Leontief-based projection. Coefficients are grouped into four sector groups in intermediate matrix A, four sector groups in expenditure share matrix E, and value added coefficeints V. n is the number of coefficients within each groups.

S2.3 Changes of economic variables under cumulative scenario constraints

Once the GDP&VA scenario constraints were enforced, regional GDP deviated from the Leontief projection by less than 10%, whereas VA deviated by up to 40%.

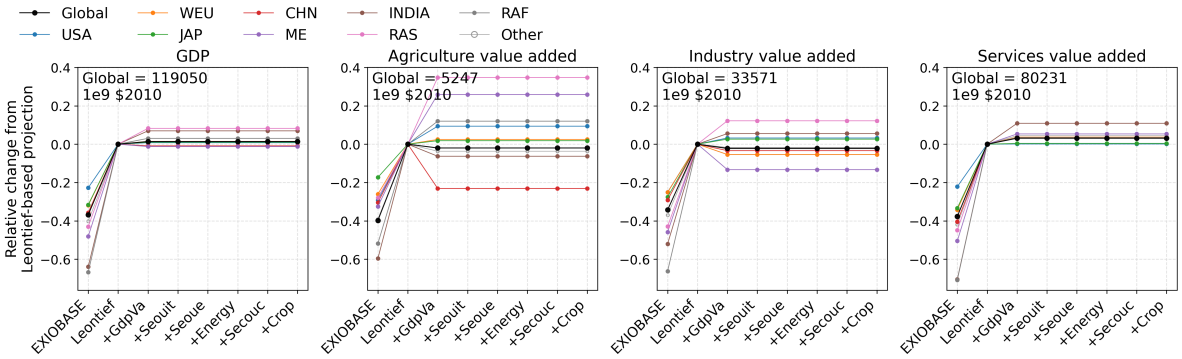

Figure S4: Relative changes of regional GDP and value added (VA) in EXIOBASE 2019 and prospective MRIOs under cumulative scenario constraints from the Leontief-based projection. On the x-axis, the remaining tick labels after the tick of "Leontief" represent the progressively added scenario constraints; the order corresponds to Table 1.

The VA enforcement also led to fluctuations in sectoral outputs, which stayed within ±40% (Figure S5). For instance, crop and livestock outputs in RAS followed the growth of agriculture VA in the same region .

Sectoral outputs were more sensitive to increasing scenario compliance than GDP&VA. Heavy industry and transport outputs were enforced from the second optimization-based projection onward, energy outputs from the third, and agriculture outputs from the fifth (Table 1). The largest deviations among directly constrained sectors occurred for iron and steel in RAS and RAF, with outputs >150% higher than the Leontief benchmark. For all other directly constrained regional sectors, deviations stayed within ±50%.

Sectoral outputs that were not directly constrained were adjusted flexibly to minimize coefficient deviations arising from the constraints on other outputs and intermediate flows, and their relative changes could exceed 50%. For example, the enforced reduction in crop and livestock outputs in IND and RAS led to the decrease of their VA, so the solver raised other agriculture outputs by 60% in IND and 84% in RAS to ensure total agriculture VA

satisfied scenario constraint, while alleviating the resulting VA-coefficient deviations (Figures S10 and S11). In a second example, enforcing energy consumption constraint in the USA pushed food-processing energy use up by 230% from the fourth optimization onward, so the solver raised food-processing output by 38%–93% to alleviate the resulting energy-coefficient deviations (Figures S6 and S7).

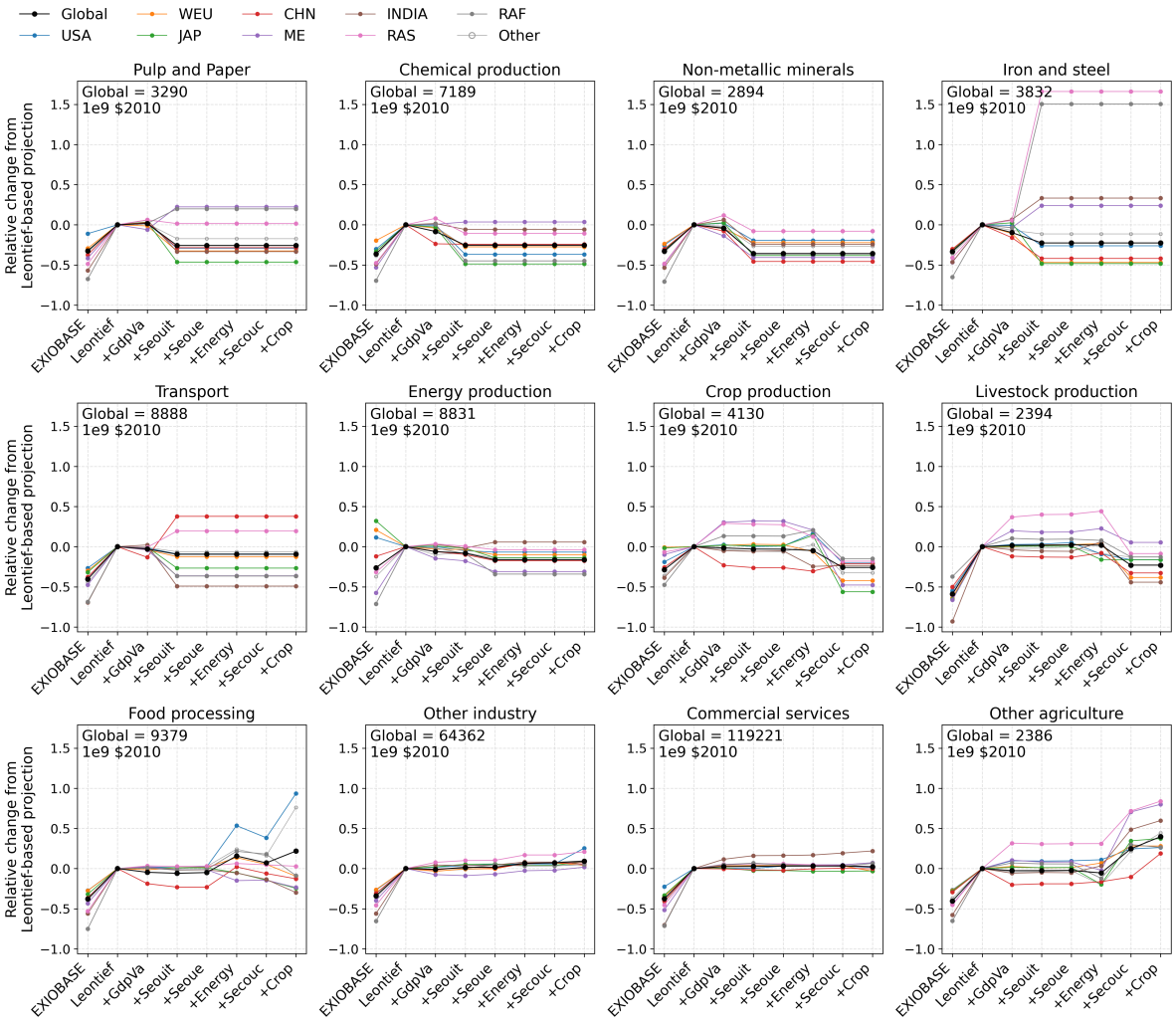

Figure S5: Relative changes of regional sector outputs in EXIOBASE 2019 and prospective MRIOs under cumulative scenario constraints from the Leontief-based projection. On the x-axis, the remaining tick labels after the tick of "Leontief" represent the progressively added scenario constraints; the order corresponds to Table 1.

Energy and agriculture consumption flows and their coefficients showed higher sensitivity than sectoral outputs and GDP&VA (Figures S6, S7, S8, S9). The response of energy and agriculture consumption flows and their coefficients depended on whether IMAGE-derived

coefficients had been integrated into the Leontief-based projection (see Table S7).

For flows whose coefficients were already taken from IMAGE, including energy consumed by heavy industry, transport, and energy production, and agriculture inputs consumed by energy production (mainly crops for biofuels), the coefficients were largely preserved through the optimization. Once the consuming sectors' outputs were enforced, the resulting energy and agriculture consumption already came close to satisfying the consumption constraints. These flows therefore deviated alongside the sectoral output constraints and remained relatively stable thereafter, with the coefficients returning to their Leontief-projection levels once the consumption constraints were enforced.

For the remaining flows, where only energy and agriculture input structure were integrated, the flows fluctuated and then deviate substantially once consumption constraints were enforced, which produces large deviations in the corresponding energy and agriculture coefficients. Energy consumption by commercial services is an exception: both its flow and its coefficient deviated most when the energy output constraint was enforced. Because commercial services has the lowest energy coefficient (energy is a small input share of its output), the solver concentrated the adjustment there to minimize the overall coefficient deviation.

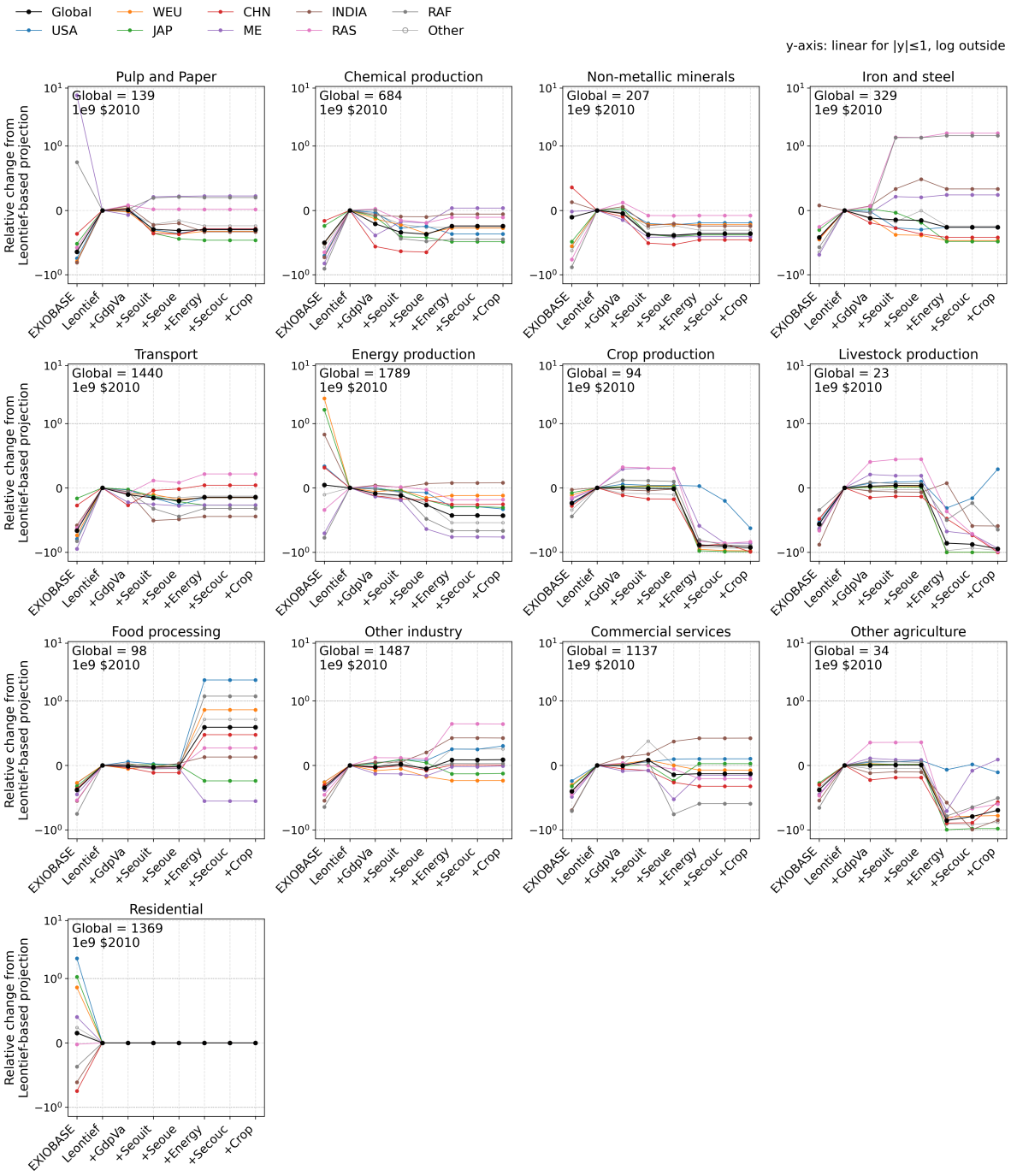

Figure S6: Relative changes of energy consumption by region-sector in EXIOBASE 2019 and prospective MRIOs under cumulative scenario constraints from the Leontief-based projection. On the x-axis, the remaining tick labels after the tick of "Leontief" represent the progressively added scenario constraints; the order corresponds to Table 1.

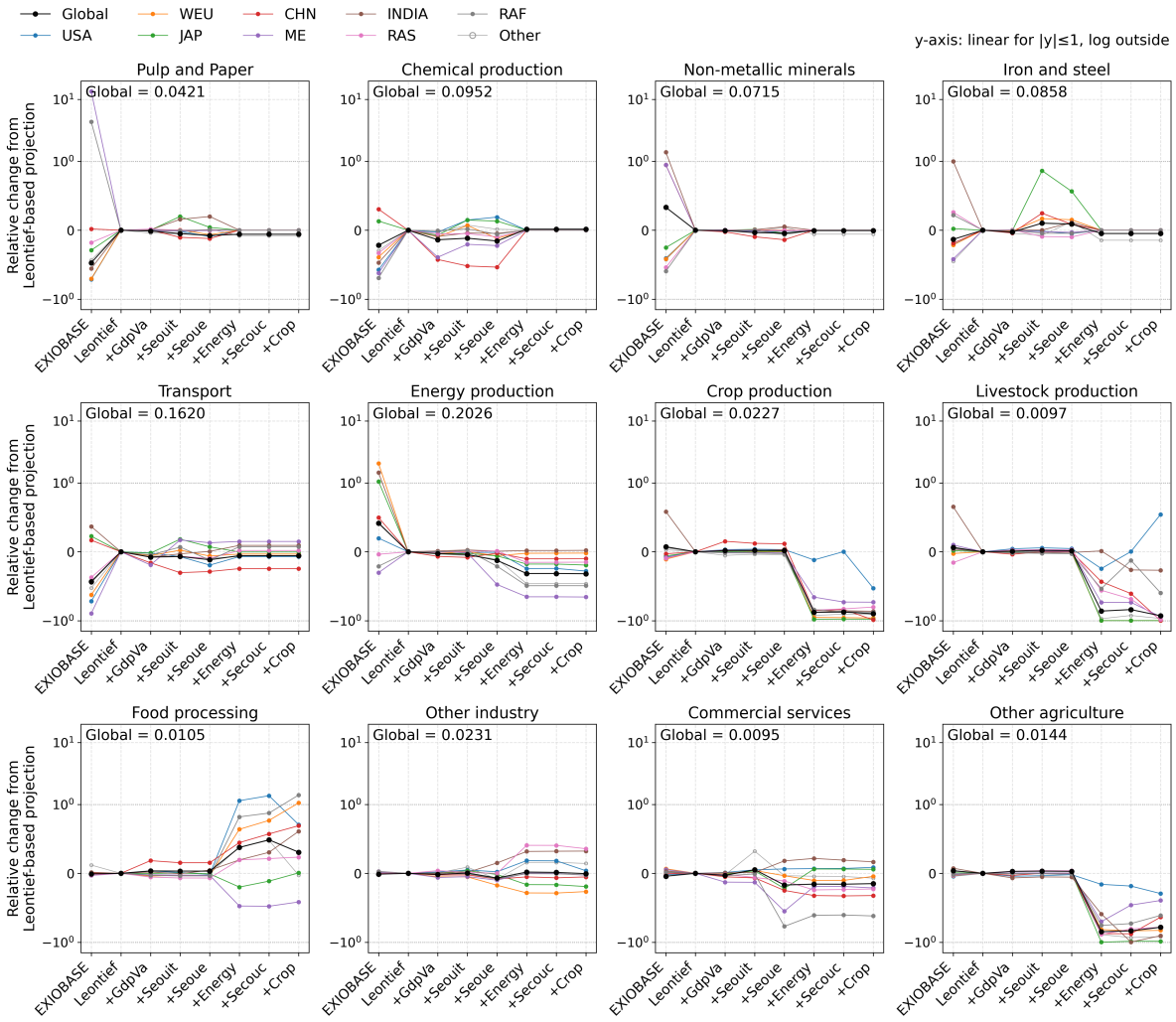

Figure S7: Relative changes of energy input coefficients by region-sector in EXIOBASE 2019 and prospective MRIOs under cumulative scenario constraints from the Leontief-based projection. On the x-axis, the remaining tick labels after the tick of "Leontief" represent the progressively added scenario constraints; the order corresponds to Table 1.

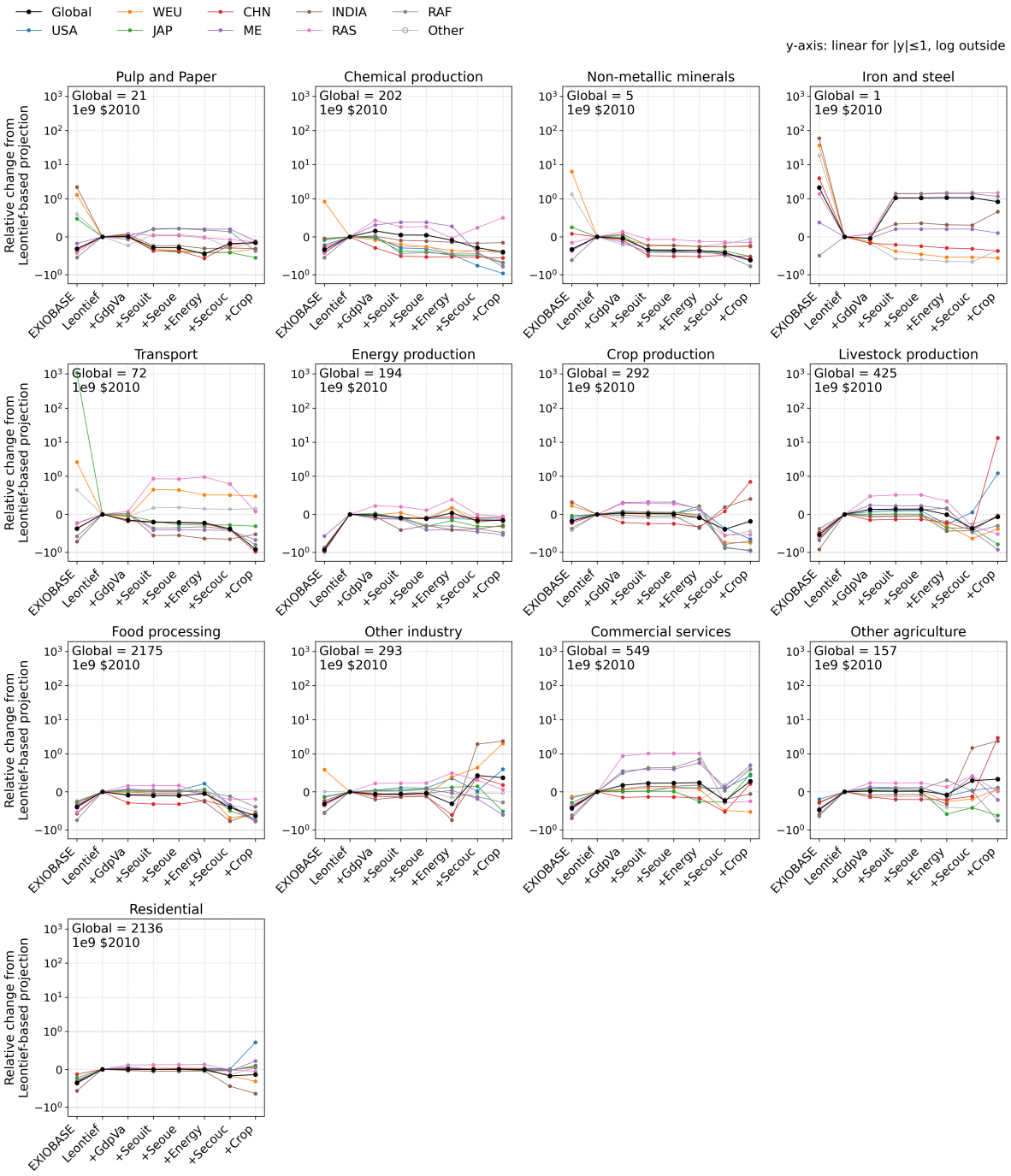

Figure S8: Relative changes of crop consumption by region-sector in EXIOBASE 2019 and prospective MRIOs under cumulative scenario constraints from the Leontief-based projection. On the x-axis, the remaining tick labels after the tick of "Leontief" represent the progressively added scenario constraints; the order corresponds to Table 1.

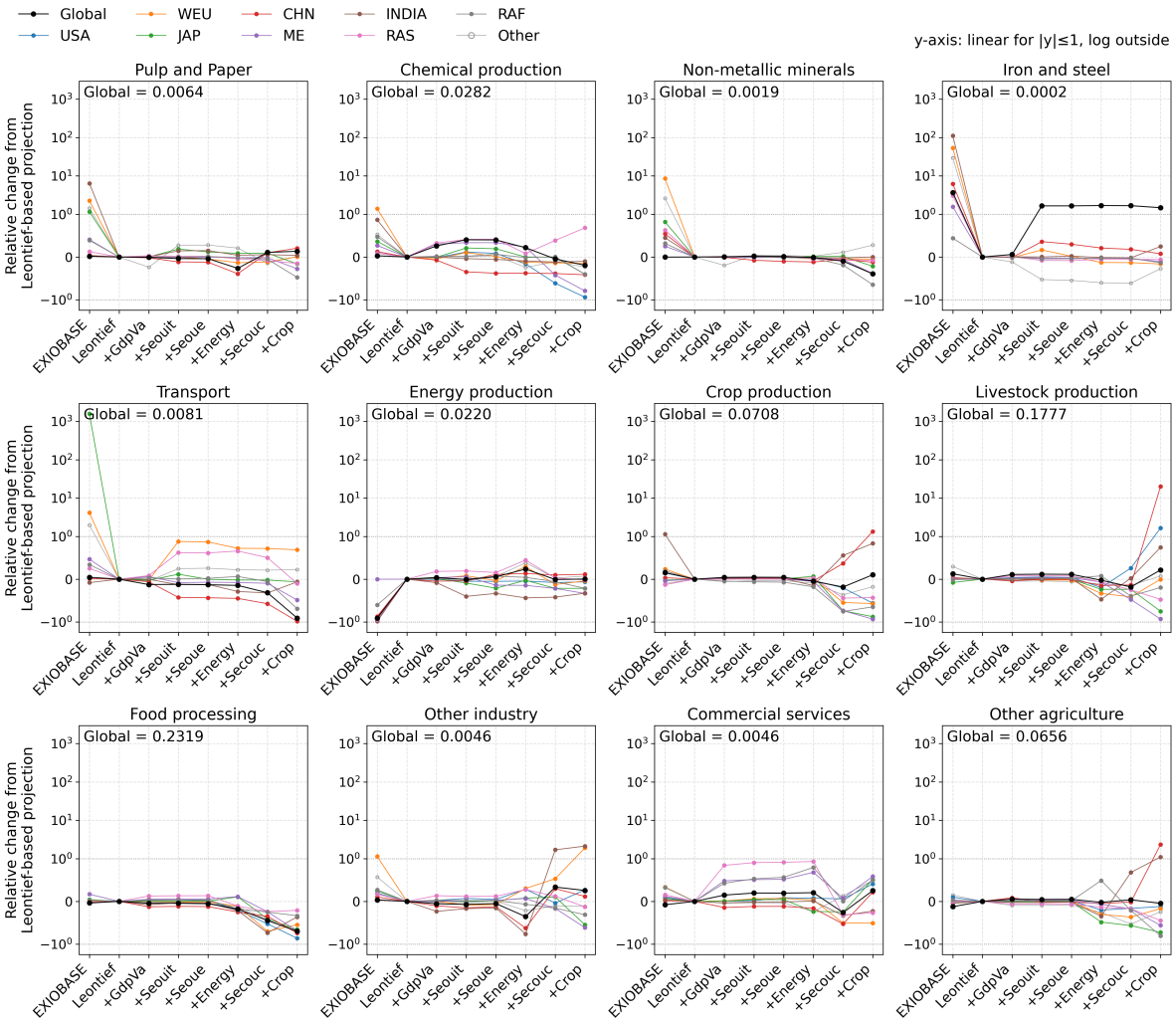

Figure S9: Relative changes of crop input coefficients by region-sector in EXIOBASE 2019 and prospective MRIOs under cumulative scenario constraints from the Leontief-based projection. On the x-axis, the remaining tick labels after the tick of "Leontief" represent the progressively added scenario constraints; the order corresponds to Table 1.

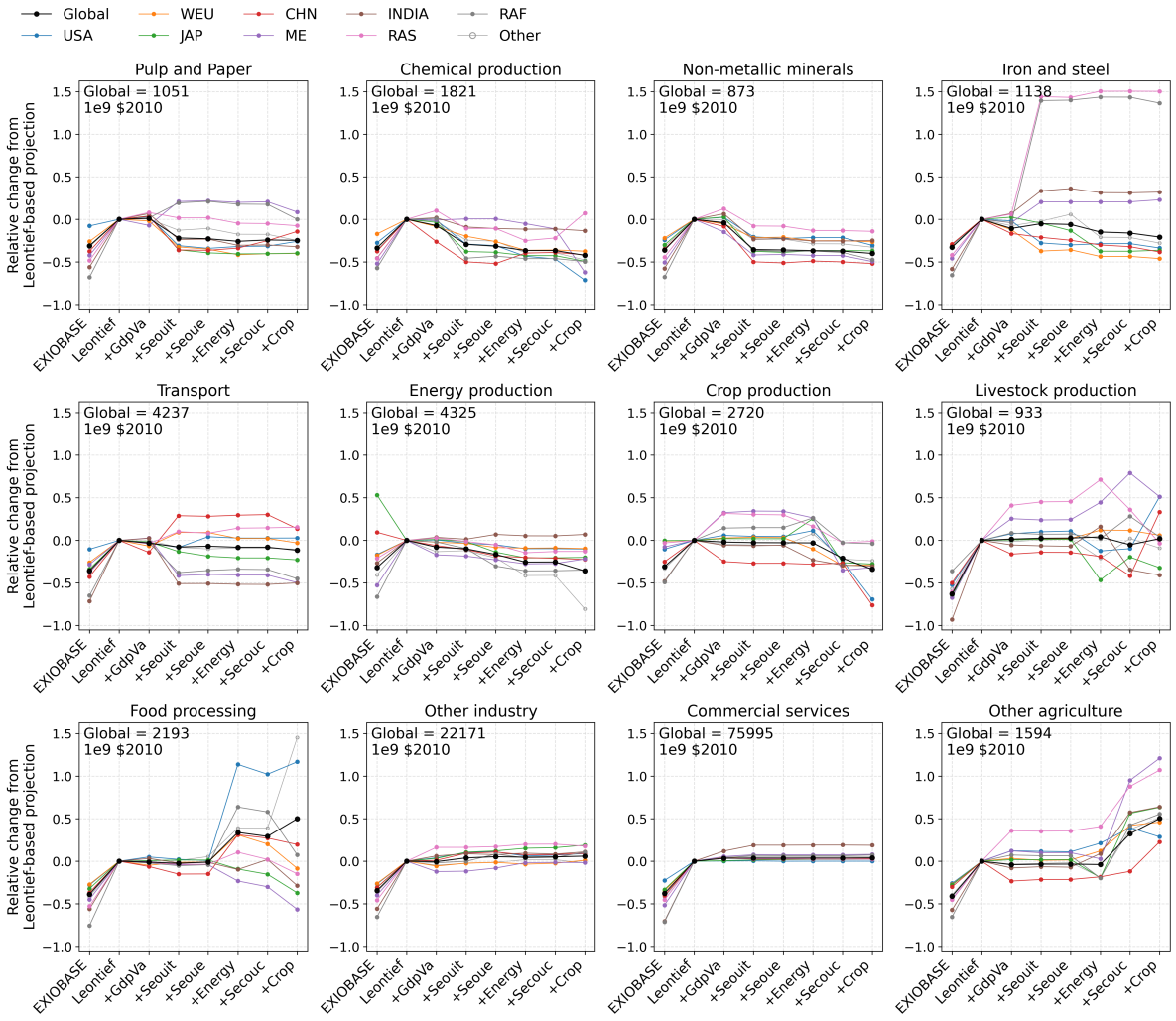

Figure S10: Relative changes of value added (VA) by region and aggregated sector in EXIOBASE 2019 and prospective MRIOs under cumulative scenario constraints from the Leontief-based projection. On the x-axis, the remaining tick labels after the tick of "Leontief" represent the progressively added scenario constraints; the order corresponds to Table 1.

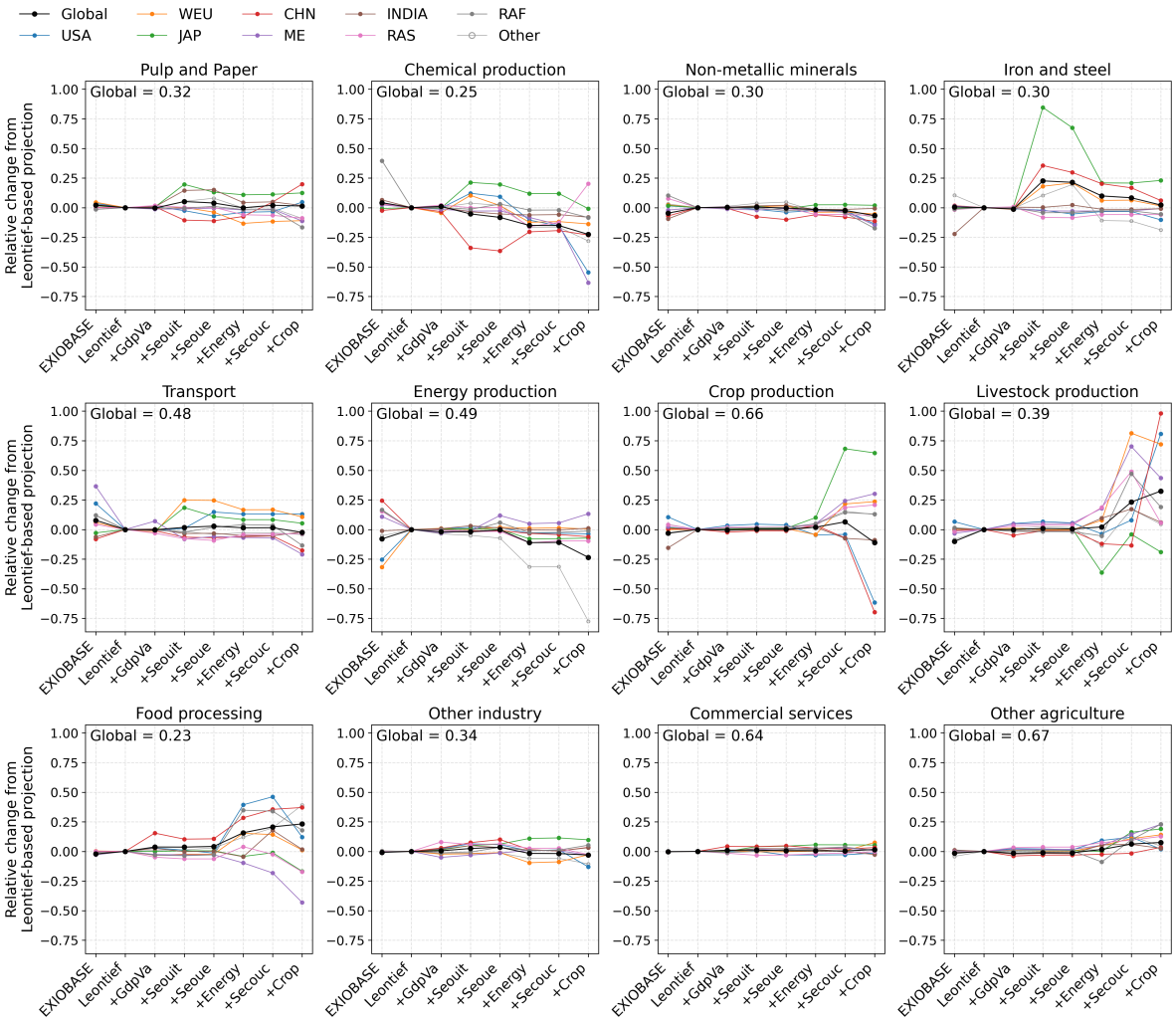

Figure S11: Relative changes of value-added (VA) shares by region and aggregated sector in EXIOBASE 2019 and prospective MRIOs under cumulative scenario constraints from the Leontief-based projection. On the x-axis, the remaining tick labels after the tick of "Leontief" represent the progressively added scenario constraints; the order corresponds to Table 1.

S2.4 Changes of regional consumption-based footprints under cumulative scenario constraints

Figure S12 illustrates the evolution of the regional carbon footprints. From 2019 to 2035, global footprints were projected to decline slightly from 44,408.2 Mt CO_2-eq to 44,046.0 Mt CO_2-eq (-0.82%) according to IMAGE data. Regionally, the Leontief-based projection showed the largest footprint increases in the Rest of Africa (+48.6%), India (+45.2%), and

the Rest of Asia (+27.6%), whereas the most significant decreases occurred in the USA (-26.6%), Western Europe (-21.4%), and Japan (-20.6%), corresponding to the relative differences in GDP growth in FigureS4.

Although the global impact was fixed across all levels of scenario compliance, the results indicate that the cumulative enforcement of scenario constraints caused varying levels of footprint changes across different regions, which induces regional reallocation compared to the Leontief-based benchmark. In particular, enforcing all scenario constraints simultaneously triggered the most significant reallocation, as the MRIO exhibited the highest level of coefficient deviations from the initial structure. Specifically, footprints for the USA and Middle East were 14.3% and 13.5% higher than those in the Leontief-based projection, respectively, while those for WEU and JAP were 12.7% and 11.0% lower. This indicates that the Leontief-based projection overestimated the footprint reduction for the USA from 2019 to 2035 and underestimated the reductions for Western Europe and Japan. However, the regional shares in the global footprint are rather stable, as shown in Figure S13.

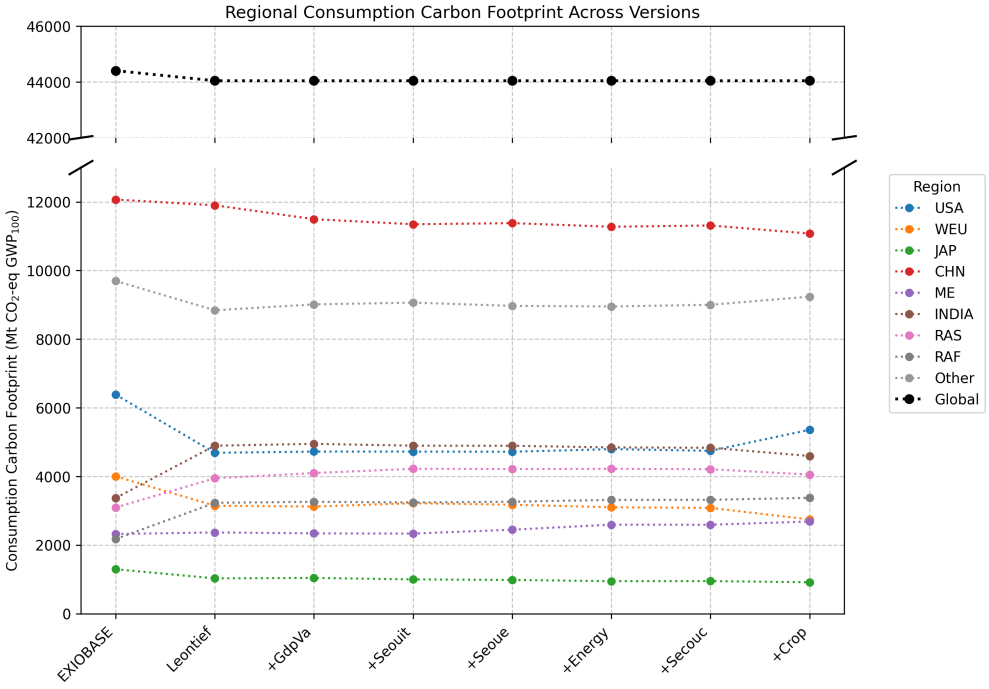

Figure S12: Regional consumption-based carbon footprints for 2019 and 2035 under different levels of scenario compliance.

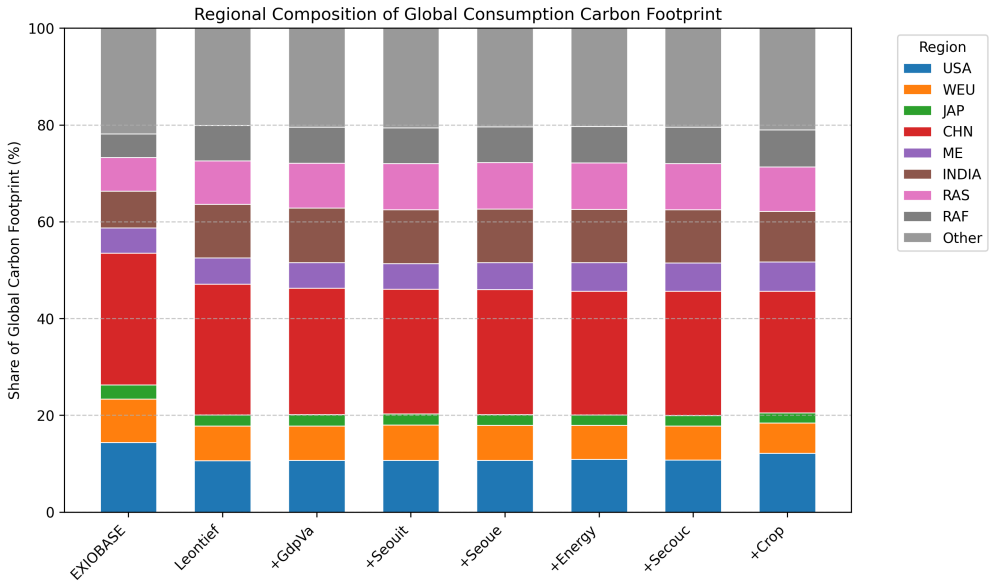

Figure S13: Regional shares in global consumption-based carbon footprints for 2019 and 2035 under different levels of scenario compliance.

S2.5 Carbon footprints from CO_2

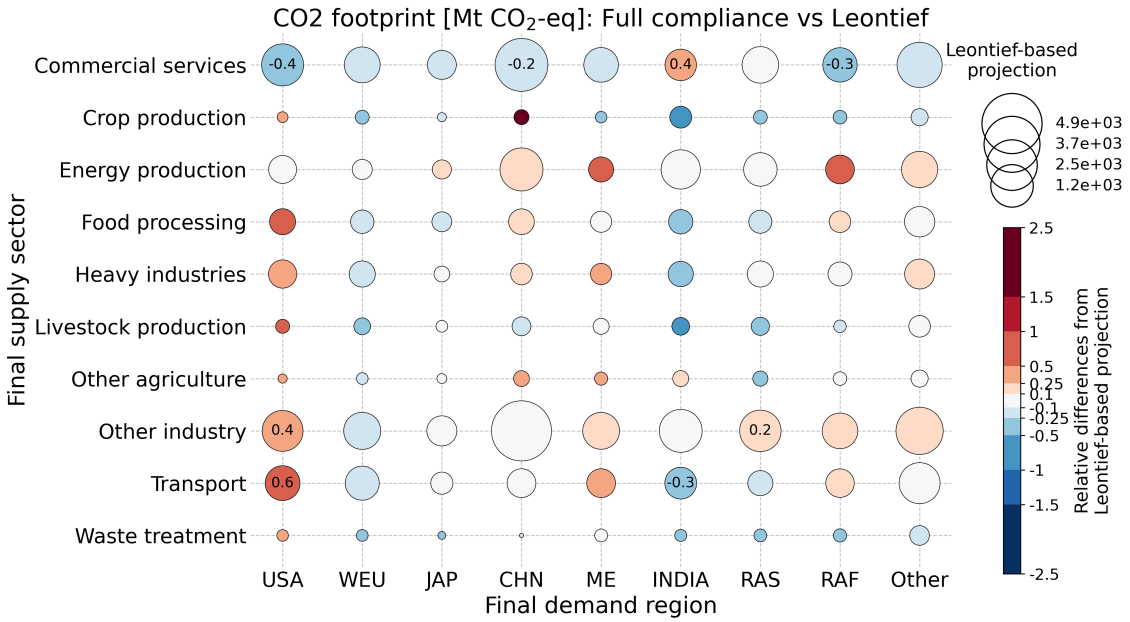

Figure S14: Carbon footprints from CO_2 emissions induced by consumption for each final supply sector and final demand region, comparing the Leontief-based projection with the fully-constrained prospective MRIO. Circle sizes indicate the footprints from the Leontief-based projection, and colors indicate the relative shifts of the footprints in the fully-constrained prospective MRIO; red and blue denote positive and negative shifts, respectively.

S2.6 Agriculture footprints and carbon footprints from N_2O and CH_4

Similar to the energy footprints, the overall agriculture footprint decreases (Figure S15a), as the enforcement of sector output constraints limits the global supply of crops and livestock (Figure S5). The most substantial reduction occurs in food processing, where direct agricultural consumption accounts for 58%–75% of the sectoral footprints across regions according to Leontief-based projection. Therefore, this decrease is primarily driven by the enforcement of agricultural consumption constraints, which reduce agriculture inputs for the sectoral production and proportionally reduce direct agriculture consumption of the food processing consumed by various regions (Figure S8). The agriculture footprints induced by livestock production consumed by the USA and other industry consumed by both the USA and India increase significantly. In the first case, 91% of the footprint is driven by livestock production as final demand of USA, which increases by 71% (SI3, residential use in Figure S8), while 2% stems from direct agriculture consumption, which surges by 328% due to the enforcement of agriculture consumption constraints (Figure S8). In the case of other industry consumed by USA and India, 25% and 36% of the footprints are driven by the direct agriculture consumption, respectively. Therefore, the footprint increases are partially attributable to the enforcement of agriculture consumption constraints, which increases agriculture inputs of these sectoral production (Figure S8).

Similar to the energy case, changes in direct agriculture consumption determined by agriculture consumption constraints, do not always correspond to agriculture footprint changes. For instance, direct agriculture consumption for livestock production consumed by China (primarily feed crops) increases significantly, but the total agriculture footprint remains relatively stable. This occurs because direct agriculture consumption contributes only 1% to the total, while the footprint is dominated by the final demand for livestock itself (76%),

which increases by 7% (SI3, residential use in Figure S8). Similarly, the total footprint of crop production consumed by USA increases, because 98% of the footprint is caused by final demand which grows by 71%, offsetting a 16% decrease in direct agricultural consumption that represents only 2% of the footprint (SI3, Figure S8). Finally, for commercial services consumed by India, the total footprint increases substantially despite a minor 8% rise in direct agriculture consumption, as 74% of the footprint originates from indirect agriculture consumption, which increases by 160% (SI3, Figure S8).

Similar to the reallocation of CO_2 impacts, the fixed global carbon impact from N_2O and CH_4 is attributed differently to the consumers between the Leontief-based projection and the fully-constrained prospective MRIO. The relative shifts in the agriculture footprint determine how these impacts are redistributed. Sectors and regions with more significant reductions in their agriculture footprints, such as food processing consumed by all regions, are allocated less carbon footprint. In these cases, the relative decreases in the carbon footprints are generally less pronounced than the reduction in the agriculture footprints themselves. Conversely, for sectors and regions where the agriculture footprints grow, such as livestock production consumed by the USA, the relative increases in carbon footprints typically exceed the growth of the agriculture footprints.

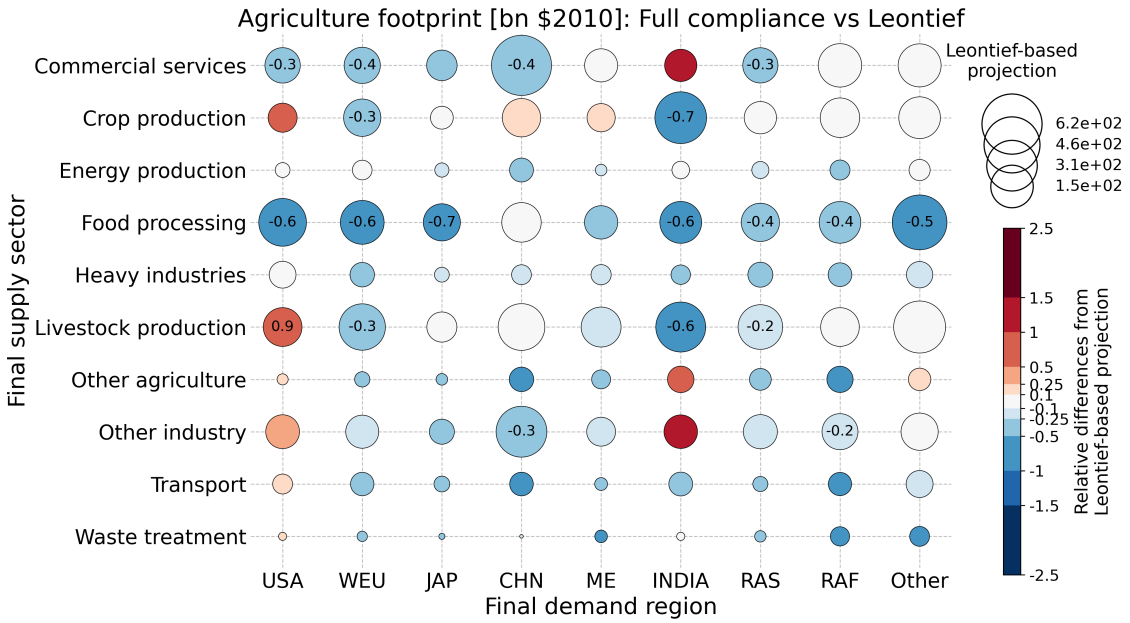

(a)

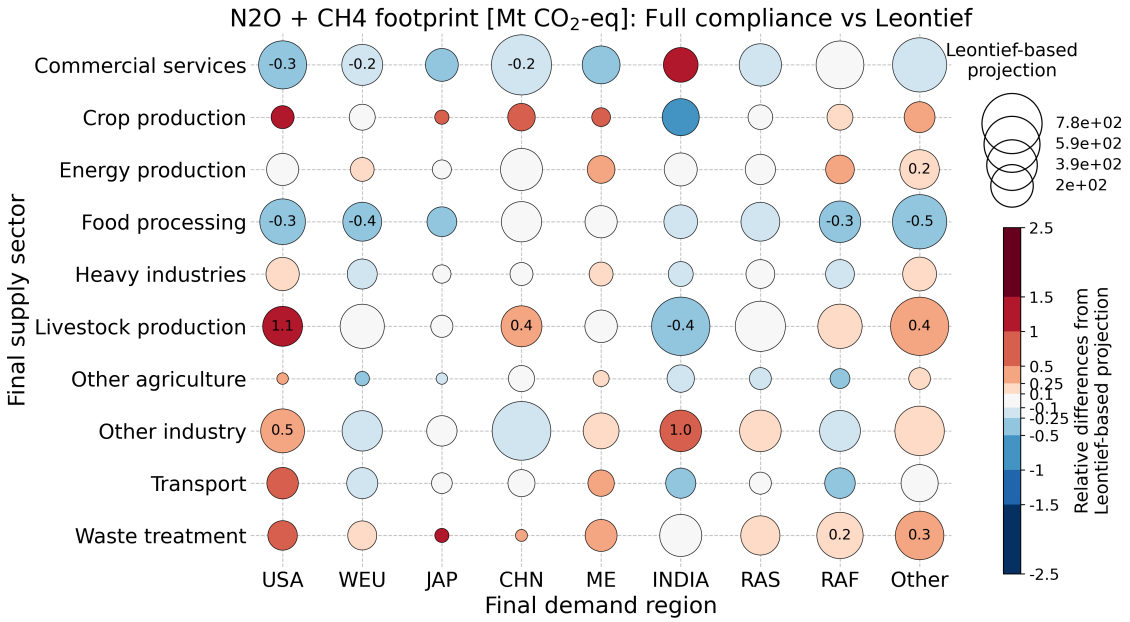

(b)

Figure S15: Environmental footprints induced by consumption for each final supply sector and final demand region, comparing the Leontief-based projection with the fully-constrained prospective MRIO. Panels show (a) agriculture footprints, and (b) carbon footprints from N_2O and CH_4 emissions. In each panel, circle sizes indicate the footprints from the Leontief-based projection, and colors indicate the relative shifts of the footprints in the fully-constrained prospective MRIO; red and blue denote positive and negative shifts, respectively.

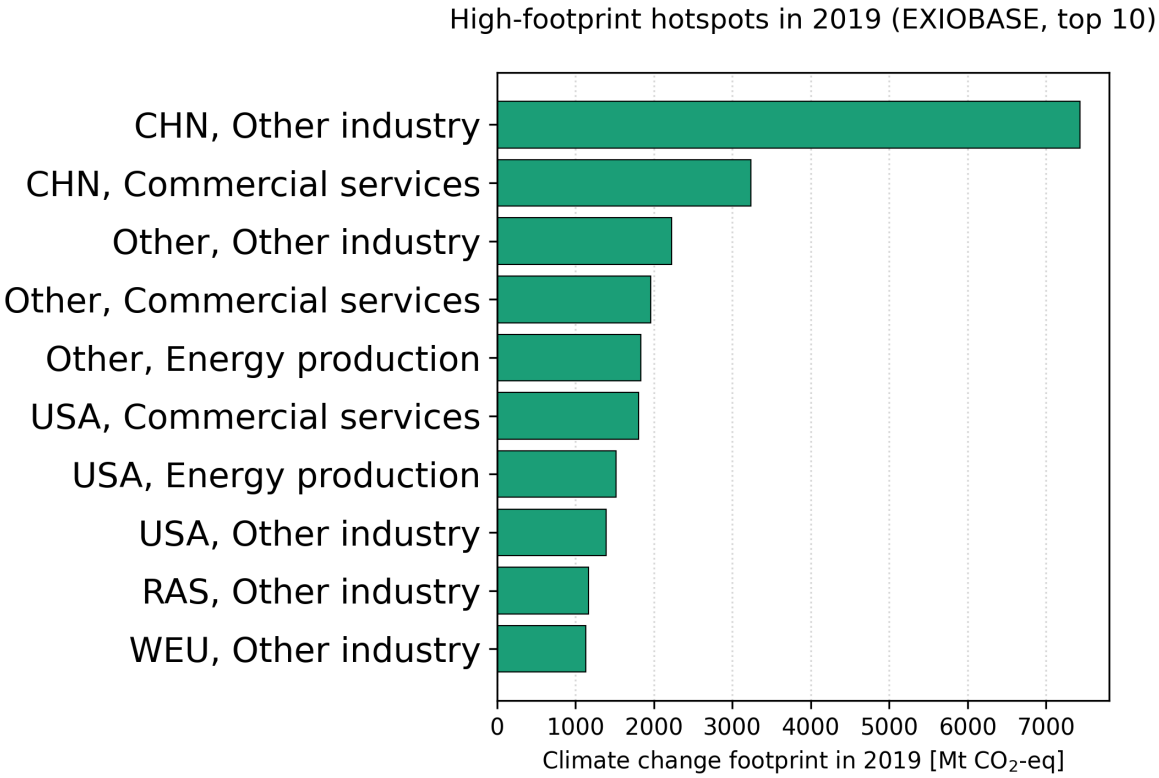

Figure S16: Top-10 region-sector pairs ranked by consumption-based GWP footprints based on EXIOBASE in 2019.

References

(1) Eurostat *NACE Rev. 2: Statistical Classification of Economic Activities in the European Community*; Office for Official Publications of the European Communities: Luxembourg, 2008; Eurostat, Methodologies and Working Papers; Catalogue No. KS-RA-07-015-EN.

(2) Eurostat *CPA 2008 Introductory Guidelines*; 2008.

(3) Stadler, K. et al. EXIOBASE 3. 2021; `https://doi.org/10.5281/zenodo.5589597`.

(4) European Central Bank Euro foreign exchange reference rates: US dollar (USD). 2019; `https://www.ecb.europa.eu/stats/policy_and_exchange_rates/euro_reference_exchange_rates/html/eurofxref-graph-usd.en.html`.

(5) U.S. Bureau of Labor Statistics CPI Inflation Calculator. 2026; `https://www.bls.gov/data/inflation_calculator.htm`.

(6) Woltjer, G. B.; Kuiper, M.; Kavallari, A.; van Meijl, H.; Powell, J. P.; Rutten, M. M.; Shutes, L. J.; Tabeau, A. A. *The MAGNET Model: Module Description*; LEI Report 14-057, 2014; p 146.

(7) Hanssen, S. V.; Daioglou, V.; Steinmann, Z. J. N.; Doelman, J. C.; Van Vuuren, D. P.; Huijbregts, M. A. J. The climate change mitigation potential of bioenergy with carbon capture and storage. *Nature Climate Change* **2020**, *10*, 1023–1029.

(8) Netherlands Organisation for Applied Scientific Research (TNO) Phyllis2: Database for the Physico-Chemical Composition of (Treated) Lignocellulosic Biomass, Micro- and Macroalgae, Various Feedstocks for Biogas Production and Biochar. `https://phyllis.nl/Browse`.

(9) Wright, L. L.; Perlack, R. D.; Turhollow, A. F.; Eaton, L. M. Switchgrass Production in the USA. IEA Bioenergy Task 43: 2011:03, Promising Resources and Sys-

tems for Producing Bioenergy Feedstocks, 2011; https://www.ieabioenergy.com/wp-content/uploads/2018/01/IEA_Bioenergy_Task43_PR2011-03.pdf.

(10) Lantz, V.; Chang, W.-Y.; Pharo, C. Benefit-cost analysis of hybrid willow crop production on agricultural land in eastern Canada: Assessing opportunities for on-farm and off-farm bioenergy use. *Biomass and Bioenergy* **2014**, *63*, 257–267.

(11) ICAR-Sugarcane Breeding Institute Biomass and energy potential of *Erianthus arundinaceus* and *Saccharum spontaneum*-derived novel sugarcane hybrids in rainfed environments. *Scientific Reports* **2024**,

(12) INRAE, CIRAD, AFZ and FAO Beet Pulp, Dried. Feedipedia/Feedtables: Animal Feed Resources Information System, https://www.feedtables.com/content/beet-pulp-dried.

(13) Razzaghi, A.; Leskinen, H.; Ahvenjärvi, S.; Aro, H.; Bayat, A. R. Energy utilization and milk fat responses to rapeseed oil when fed to lactating dairy cows receiving different dietary forage to concentrate ratio. *Animal Feed Science and Technology* **2022**, *293*, 115454.

(14) INRAE, CIRAD, AFZ and FAO Soybean, Whole, Extruded. Feedipedia/Feedtables: Animal Feed Resources Information System, https://www.feedtables.com/content/soybean-whole-extruded.

(15) INRAE, CIRAD, AFZ and FAO Maize Grain. Feedipedia/Feedtables: Animal Feed Resources Information System, https://www.feedtables.com/content/maize.

(16) Shonhiwa, C. An assessment of biomass residue sustainably available for thermochemical conversion to energy in Zimbabwe. *Biomass and Bioenergy* **2013**, *52*, 131–138.

(17) Avcıoğlu, A.; Dayıoğlu, M.; Türker, U. Assessment of the energy potential of agricultural biomass residues in Turkey. *Renewable Energy* **2019**, *138*, 610–619.

(18) Becerra-Pérez, L. A.; Rincón, L.; Posada-Duque, J. A. Logistics and Costs of Agricultural Residues for Cellulosic Ethanol Production. *Energies* **2022**, *15*, 4480.

(19) Shinners, K. J.; Binversie, B. N.; Muck, R. E.; Weimer, P. J. Comparison of wet and dry corn stover harvest and storage. *Biomass and Bioenergy* **2007**, *31*, 211–221.

(20) Karp, S. G.; others Bioeconomy and Biofuels: The Case of Sugarcane Ethanol in Brazil. *Biofuels, Bioproducts and Biorefining* **2021**, *15*, 899–912.

(21) Ngai, L. R.; Pissarides, C. A. Structural Change in a Multisector Model of Growth. *American Economic Review* **2007**, *97*, 429–443.

(22) Kongsamut, P.; Rebelo, S.; Xie, D. Beyond Balanced Growth. *Review of Economic Studies* **2001**, *68*, 869–882.

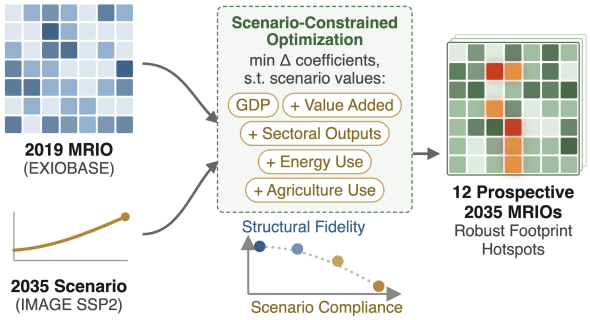
2019 MRIO
(EXIOBASE)
2035 Scenario
(IMAGE SSP2)
Scenario-Constrained Optimization
min Δ coefficients,
s.t. scenario values:
GDP
+ Value Added
+ Sectoral Outputs
+ Energy Use
+ Agriculture Use
Structural Fidelity
Scenario Compliance
12 Prospective 2035 MRIOs
Robust Footprint Hotspots